Journal of Medicinal Chemistry

pubs.acs.org/jmc

Article

Optimization of 1,2,4-Triazole-3-thiones toward Broad-Spectrum Metallo-β-lactamase Inhibitors Showing Potent Synergistic Activity on VIM- and NDM-1-Producing Clinical Isolates

Alice Legru,[¶] Federica Verdirosa,[¶] Yen Vo-Hoang, Giusy Tassone, Filippo Vascon, Caitlyn A. Thomas, Filomena Sannio, Giuseppina Corsica, Manuela Benvenuti, Georges Feller, Rémi Coulon, Francesca Marcoccia, Savannah Rowane Devente, Ezeddine Bouajila, Catherine Piveteau, Florence Leroux, Rebecca Deprez-Poulain, Benoît Deprez, Patricia Licznar-Fajardo, Michael W. Crowder, Laura Cendron, Cecilia Pozzi, Stefano Mangani, Jean-Denis Docquier,[*,#] Jean-François Hernandez,[*,#] and Laurent Gavara[*,#]

Cite This: https://doi.org/10.1021/acs.jmedchem.2c01257

Read Online

ACCESS | Metrics & More | Article Recommendations | Supporting Information

ABSTRACT: Metallo-β-lactamases (MBLs) contribute to the resistance of Gram-negative bacteria to carbapenems, last-resort antibiotics at hospital, and MBL inhibitors are urgently needed to preserve these important antibacterial drugs. Here, we describe a series of 1,2,4-triazole-3-thione-based inhibitors displaying an α-amino acid substituent, which amine was mono- or disubstituted by (hetero)aryl groups. Compounds disubstituted by certain nitrogen-containing heterocycles showed submicromolar activities against VIM-type enzymes and strong NDM-1 inhibition (K_i = 10−30 nM). Equilibrium dialysis, native mass spectrometry, isothermal calorimetry (ITC), and X-ray crystallography showed that the compounds inhibited both VIM-2 and NDM-1 at least partially by stripping the catalytic zinc ions. These inhibitors also displayed a very potent synergistic activity with meropenem (16- to 1000-fold minimum inhibitory concentration (MIC) reduction) against VIM-type- and NDM-1-producing ultraresistant clinical isolates, including *Enterobacterales* and *Pseudomonas aeruginosa*. Furthermore, selected compounds exhibited no or moderate toxicity toward HeLa cells, favorable absorption, distribution, metabolism, excretion (ADME) properties, and no or modest inhibition of several mammalian metalloenzymes.

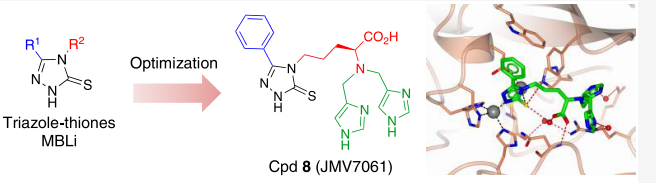

K_i (μM) of Cpd 8		Meropenem MIC (μg/mL) + - Cpd 8 (32 μg/mL)		
VIM-2	NDM-1	*K. pneumoniae* (bla_{VIM-1}^+)	*P. aeruginosa* (bla_{VIM-2}^+)	*E. coli* (bla_{NDM-1}^+)
0.41	0.03	0.03 (16)	8 (128)	0.06 (64)

1. INTRODUCTION

The WHO, among others, has relentlessly and alarmingly raised awareness of the risks associated with antimicrobial resistance (AMR). Indeed, growing bacterial resistance might represent one of the most worrying threats to Public Health worldwide.[1] In the absence of concerted international response and transdisciplinary efforts, deaths by infectious diseases may become a relevant cause of morbidity and mortality in industrialized countries by 2050.[2,3] Moreover, AMR significantly more broadly impacts modern medicine overall by limiting our capacity to successfully treat hospital-acquired infections caused by resistant bacteria following common surgical interventions.[4] A list of resistant bacteria for which new antibiotics are urgently needed was published by WHO, the critical priority concerning carbapenem-resistant Gram-negative opportunistic pathogens.[5−7] It includes *Enterobacterales* such as *Klebsiella pneumoniae* and *Escherichia coli*, frequently causing respiratory and urinary tract infections.[8] β-Lactam antibiotics (penicillins, cephalosporins, carbapenems, monobactams) sharing a four-membered β-lactam ring remain an invaluable therapeutic resource.[9] The major mechanism of β-lactam resistance is the production of one or more β-lactamases, enzymes able to hydrolyze the amide bond of the β-lactam ring. Among β-lactams, carbapenems represent an important last-resort class of antibacterials, being introduced to contrast the diffusion of MDR bacteria, commonly producing ESBLs. Unfortunately, the more recent mobilization and spread of carbapenem-hydrolyzing β-lactamases, or carbapenemases, significantly endanger the clinical efficacy of carbapenems.

β-Lactamases belong to four distinct molecular classes according to Ambler classification (A, B, C, and D),[10,11]

Received: August 2, 2022

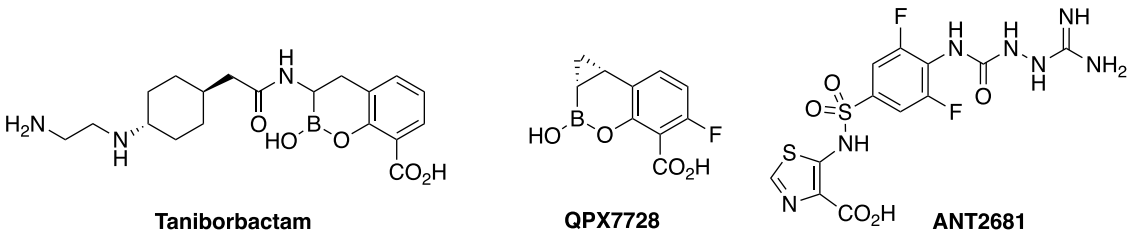

Figure 1. Structures of most advanced MBL inhibitors.

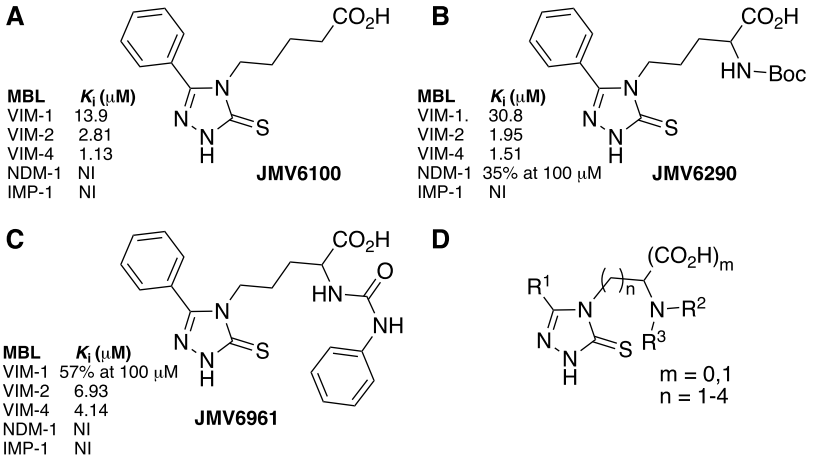

Figure 2. Structure of compounds based on the 1,2,4-triazole-3-thione scaffold and their inhibitory potency toward selected MBLs:[41] (A) 4-alkanoic analogue JMV6100; (B) Boc-protected ornithine analogue JMV6290; (C) ornithine urea analogue JMV6961; (D) general structure of synthesized compounds.

reflecting their significant structural and functional heterogeneity. Classes A, C, and D belong to the serine hydrolase family, whose catalytic mechanism involves the formation of a tetrahedral transition-state intermediate resulting from the catalytic serine residue addition on the β-lactam carbonyl.[12] Several covalent inhibitors were developed, such as clavulanic acid or, recently, avibactam or vaborbactam, which are active against serine-carbapenemases (*e.g.*, KPC-type, OXA-48), and are currently used in combination with β-lactam antibiotics to counteract bacterial resistance.[13−15] By contrast, class B β-lactamases, called metallo-β-lactamases (MBLs), first identified in 1966, are characterized by the presence of one or two zinc ions in the active site acting as Lewis acids that both increase the electrophilicity of the β-lactam ring and allow the deprotonation of a water molecule to yield the hydroxide nucleophile.[16] These enzymes, which are able to inactivate a broad spectrum of β-lactams including carbapenems, are produced by those Gram-negative bacteria identified as critical priorities by the WHO.[7] They are now recognized as one of the most worrying threats in the context of AMR. Class B β-lactamases are further subdivided into three different subclasses, B1, B2, and B3, based on the nature and position of zinc-binding residues, zinc requirement, and hydrolytic profile. Nowadays, the most clinically relevant MBLs belong to the B1 subfamily, now counting over 700 unique variants, and include the subtypes imipenemase (IMP), Verona integron-borne metallo-β-lactamase (VIM), and New Delhi metallo-β-lactamase (NDM).[17] Initially identified in 2008, NDM-1 rapidly spread worldwide thanks to horizontal gene transfer, to become presently the most common MBL in several countries.[18,19] Over 40 NDM variants were reported, whose evolution implied the selection of variants showing improved activity in zinc-depleted conditions encountered *in vivo*.[20−22] To fight the bacterial resistance mediated by MBL production, it is crucial to develop potent and selective inhibitors able to restore the susceptibility of Gram-negative pathogens to carbapenems.[23]

Today, no MBL inhibitor received FDA approval, and only a few compounds are in preclinical or clinical stages.[14,15] The discovery of cyclic boronate derivatives as serine-β-lactamase inhibitors (*e.g.*, vaborbactam) culminated with the discovery and development of pan-spectrum inhibitors active on both serine-β-lactamase (SBL) and MBL enzymes.[24,25] Examples of two bicyclic boronate compounds are taniborbactam (formerly VNRX-5133)[26,27] and QPX7728[28] (Figure 1). Microbiological evaluations showed the ability of taniborbactam to restore the susceptibility of several multidrug-resistant strains to cefepime, and this compound has recently completed a phase 3 clinical trial.[27] QPX7728 shows a similar dual profile of β-lactamase inhibition with some improvement on critical enzymes such as oxacillinase (OXA) and NDM types, and it recently entered phase 1 clinical trials. To the best of our knowledge, only one selective MBL inhibitor completed preclinical evaluations, ANT2681[29] (Figure 1). This compound was shown to restore meropenem susceptibility of clinical isolates producing different epidemiologically relevant NDM-type variants. Considering the significance of infections by MBL-producing ultra-resistant bacteria and the paucity of drugs active on such strains, it remains of primary importance to develop a selective broad-spectrum inhibitor of MBLs to offer new and innovative therapeutic solutions able to keep pace with the development of resistance in nosocomial opportunistic pathogens.

In this context, we are developing 1,2,4-triazole-3-thione-based MBL inhibitors. The potential of such compounds to

https://doi.org/10.1021/acs.jmedchem.2c01257
J. Med. Chem. XXXX, XXX, XXX−XXX

Scheme 1. Synthesis of 1,2,4-Triazole-3-thione Derivatives[a]

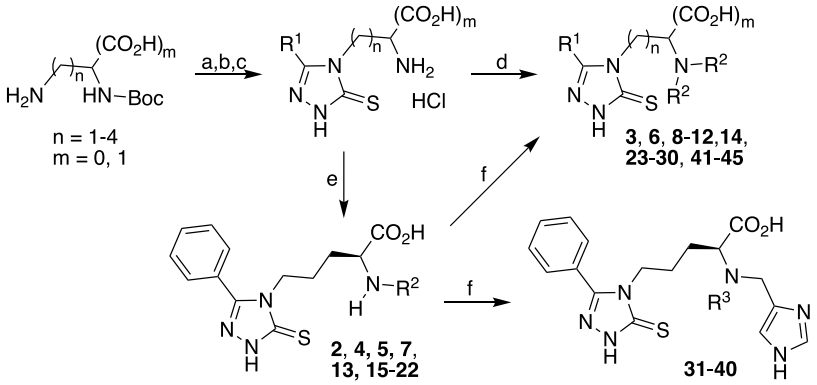

[a]Reagents and conditions: (a) i, DPT, Na_2CO_3, DMF, sealed tube, 55 °C, 3 h; ii, R^1-CONHNH$_2$, DMF, 55 °C, 3 h; (b) aqueous KOH or $NaHCO_3$, 100 °C, 3 h; (c) conc. HCl/dioxane (1:2), anisole (3 equiv), 45 °C, 1 h; (d) $R^{2\prime}$-CHO (5 equiv), triethylamine (TEA, 2 equiv), $NaBH_3CN$ (5 equiv), EtOH, rt; (e) $R^{2\prime}$-CHO (2−5 equiv), anhydrous DMF, $NaBH_4$, rt, 15 h; (f) $R^{2\prime}$-CHO or $R^{3\prime}$-CHO (3 equiv), $NaBH_3CN$ (3 equiv), DMF/AcOH (98:2) rt,15 h. R^2 = $R^{2\prime}$-CH_2-, R^3 = $R^{3\prime}$-CH_2-.

inhibit MBLs was first highlighted by an *in silico* study looking for inhibitors of L1, a subclass B3 MBL,[30] and the description of their original L1 binding mode showing an original double interaction with the two active site zincs.[31] These promising data were further reinforced by several other random *in silico* and experimental studies showing that these compounds could also inhibit B1 subclass MBLs (*i.e.*, IMP-1,[32] VIM-2,[33] and NDM-1[34]) with the same binding mode.[31,33,35−38] The heterocyclic scaffold therefore appears well adapted to the MBL di-zinc active sites and may offer a chance to spare human metalloenzymes in contrast to inhibitors containing zinc binding groups such as thiols or multiple carboxylates.

We already reported several series of 1,2,4-triazole-3-thione inhibitors varying by their substituents at positions 4 and 5 of the heterocycle.[35,37−42] In particular, we developed a series of Schiff base analogues possessing an amine group at position 4 diversely substituted by aryl aldehydes.[35] Some of these compounds were broad-spectrum MBL inhibitors active against VIM-type enzymes (*i.e.*, VIM-1/2/4), NDM-1 and IMP-1. Unfortunately, they did not show sufficient potentiation of meropenem against MBL-producing MDR clinical isolates. This was most likely due to their inefficiency to diffuse through the outer membrane and/or to their susceptibility to hydrolysis. To solve these limitations, we developed several series in which the 4-position of the heterocycle was diversely alkylated.[37,38,41] The replacement of the hydrazone-like bond by a stable CH_2−CH_2 segment led to compounds potently inhibiting VIM-type enzymes with K_i values in the micromolar to submicrolar range, but not[38,41] or to a lesser extent inhibiting NDM-1 and/or IMP-1.[37,42] In particular, compounds from both series were able to restore the susceptibility of VIM-1/4-producing *K. pneumoniae* clinical strains to meropenem, with a minimum inhibitory concentration (MIC) reduction of up to 16-fold. However, none showed synergistic activity on VIM-2-producing *Pseudomonas aeruginosa* and NDM-1-producing *E. coli* strains.

Among these series, compounds with an alkanoic chain (*e.g.*, JMV6100, Figure 2A) showed micromolar inhibitory potency against VIM-1, VIM-2, and VIM-4 and modest activity in microbiological assays.[41] In this series, we observed that, although the addition of a free amine group at the α-position of the carboxylic function abolished inhibition of VIM-type enzymes, its substitution by bulky substituents as Boc (*i.e.*, JMV6290, Figure 2B) or phenylurea (*i.e.*, JMV6961, Figure 2C) restored their activity. We further studied the substitution of this amine group and chose to introduce one or two aryl or heteroaryl moieties via reductive amination (Figure 2D). We found that the presence of two nitrogen-containing heteroaryl groups not only allowed strong inhibition of both VIM-type and NDM-1 enzymes but also high meropenem potentializing activities on various MDR clinical isolates. The inhibition mode of these compounds was investigated by equilibrium dialysis, native mass spectrometry, isothermal calorimetry, and X-ray crystallography.

2. RESULTS AND DISCUSSION

2.1. Chemistry. The intermediate 1,2,4-triazole-3-thiones were prepared from the hydrazides R^1-C(O)NHNH$_2$ and the corresponding α-Boc-protected diamine compounds according to Deprez-Poulain et al.[43] and as described in Gavara et al.[41] The hydrazides R^1-C(O)NHNH$_2$ were first obtained in two steps from the corresponding carboxylic derivatives. The commercially available α-Boc-protected diamine compounds were treated with dipyridylthionocarbonate (DPT) to yield the intermediate isothiocyanates, which were directly reacted with hydrazides to form the thiosemicarbazide derivatives. Basic treatment induced cyclization toward the expected 1,2,4-triazole-3-thione compounds. Finally, the Boc protecting group was removed in acidic conditions in the presence of anisole (Scheme 1). The deprotected amine was substituted by reductive amination using diverse (hetero)aryl-carbaldehyde compounds. Homo-disubstituted analogues were generally obtained by treatment with $NaBH_3CN$ in ethanol. However, this reaction was found more or less efficient and some carbaldehydes gave mixtures of unsubstituted and monosubstituted compounds with low amounts of expected analogues. In this case, the monosubstituted compounds could be isolated and purified for testing or treated again with the same aldehyde in the presence of $NaBH_3CN$ in a mixture of 2% AcOH in *N*,*N*-dimethylformamide (DMF) to yield the homo-disubstituted analogues. The hetero-disubstituted analogues were obtained from the monosubstituted ones following the same pathway. To obtain the monosubstituted analogues only, the reductive amination step was performed in the presence of $NaBH_4$. All compounds were purified by reversed-phase high-

https://doi.org/10.1021/acs.jmedchem.2c01257
J. Med. Chem. XXXX, XXX, XXX−XXX

Table 1. Inhibitory Activity of 1,2,4-Triazole-3-thione Analogues 1−14 against Various MBLs[a]

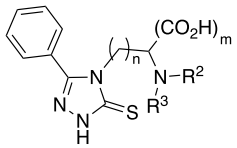

Cpd	Structure		K_i (μM) or (% inhibition at 100 μM)				
	R^2	R^3	VIM-1	VIM-2	VIM-4	NDM-1	IMP-1
JMV 6290[41]	Boc	H	30.8 ± 2.8	2.0 ± 0.1	1.5 ± 0.1	(35%)	NI
1[b] (m = 0)	Boc	H	0.75 ± 0.08	(53%)	3.1 ± 0.2	(42%)	NI
2	Bzl	H	ND	NI	NI	NI	NI
3	Bzl	Bzl	(38%)	(63%)	(64%)	(32%)	NI
4	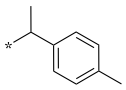	H	10.8 ± 1.5	(36%)	NI	NI	NI
5	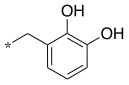	H	8.1 ± 0.5	(57%)	4.2 ± 0.2	(37%)	(32%)
6	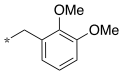	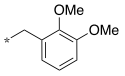	2.0 ± 0.1	0.76 ± 0.06	0.36 ± 0.04	(43%)	NI
7	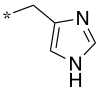	H	(53%)	NI	NI	(35%)	NI
8	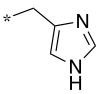	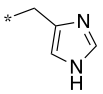	0.15 ± 0.01	0.41 ± 0.02	0.20 ± 0.01	0.030 ± 0.004	(40%)
9[c] (D)	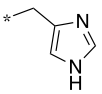	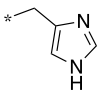	0.17 ± 0.09	0.19 ± 0.04	0.11 ± 0.01	0.014 ± 0.003	7.4 ± 0.2
10[b] (m = 0)	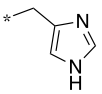	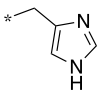	0.85 ± 0.15	1.5 ± 0.2	0.90 ± 0.06	9.2 ± 1.4	(34%)
11[d] (n = 1)	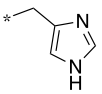	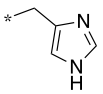	0.88 ± 0.09	1.5 ± 0.1	0.56 ± 0.06	0.040 ± 0.003	4.2 ± 0.3
12[d] (n = 2)	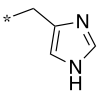	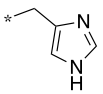	0.39 ± 0.04	0.21 ± 0.03	0.23 ± 0.03	0.040 ± 0.004	6.2 ± 0.8
13[d] (n = 4)	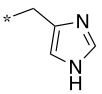	H	1.8 ± 0.2	(39%)	NI	4.0 ± 0.4	(44%)
14[d] (n = 4)	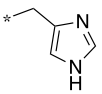	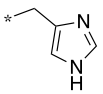	0.040 ± 0.003	0.97 ± 0.09	0.47 ± 0.03	0.36 ± 0.03	5.0 ± 0.6

[a]All compounds have CO_2H ($m = 1$), L stereochemistry, $n = 3$, excepted. [b]No CO_2H ($m = 0$). [c]D stereochemistry. [d]$n \neq 3$. Kinetics were monitored at 30 °C by following the absorbance variation observed upon substrate hydrolysis. K_i values were determined when inhibition >70%. Assays were performed in triplicate. NI: no inhibition (<30% inhibition at 100 μM). ND: not determined.

https://doi.org/10.1021/acs.jmedchem.2c01257
J. Med. Chem. XXXX, XXX, XXX−XXX

Table 2. Inhibitory Activity of Monosubstituted 1,2,4-Triazole-3-thione Analogues 15−22 with R^3 = H against Various MBLs[a]

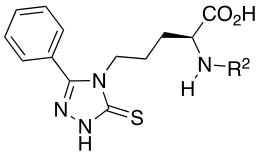

Cpd	Structure	K_i (μM) or (% inhibition at 100 μM)				
	R^2	VIM-1	VIM-2	VIM-4	NDM-1	IMP-1
7	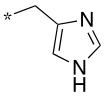	(53%)	NI	NI	(35%)	NI
15	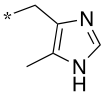	(51%)	NI	NI	NI	NI
16	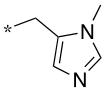	9.5 ± 1.5	(47%)	NI	(38%)	NI
17	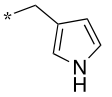	5.0 ± 0.3	NI	(32%)	NI	NI
18	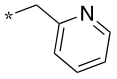	NI	(44%)	NI	2.0 ± 0.2	(34%)
19	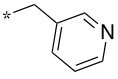	(48%)	(47%)	NI	NI	NI
20	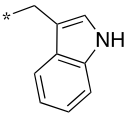	ND	NI	NI	NI	NI
21	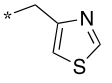	(55%)	NI	(43%)	NI	(47%)
22	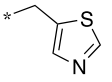	(60%)	(58%)	3.4 ± 0.2	NI	NI

[a]NI: no inhibition (<30% inhibition at 100 μM). ND: not determined. Kinetics were monitored at 30 °C by following the absorbance variation observed upon substrate hydrolysis. K_i values were determined when inhibition > 70%. Assays were performed in triplicate.

performance liquid chromatography (HPLC) and isolated with >95% purity.

2.2. Evaluation of Inhibitory Potency toward Purified MBLs. The inhibitory activity of the compounds was evaluated using a panel of five representative acquired subclass B1 MBLs: VIM-1, VIM-2, VIM-4, NDM-1, and IMP-1.

2.2.1. First Series (Table 1). According to the hypothesis that the presence of a bulky substituent on the amine of JMV6290 (*i.e.*, Boc group, Figure 2B) was favorable to VIM-type MBL inhibition, we prepared a first series of compounds, which were mono- or homo-disubstituted via reductive amination yielding a secondary or tertiary amine, respectively (compounds **2**−**14**, Table 1). We also checked the importance of the carboxylic group by synthesizing the decarboxylated analogue of JMV6290, **1**, which was found to maintain potent activity against VIM-1 and VIM-4 but not VIM-2.

The mono-benzyl **2** was inactive while adding a second benzyl group yielded compound **3** with higher but still moderate inhibitory potency. Compared to **2**, the mono-substituted **4** (1-*p*-toluyl-ethyl) and **5** (1,2-dihydroxy-phen-3-ylmethyl) were also found more potent on VIM-1 and/or VIM-4. However, the close disubstituted compound **6** (1,2-dimethoxy-phen-3-ylmethyl) was a potent inhibitor of both VIM-type enzymes. These first results confirmed the interest to explore this position.

We then introduced a heteroaryl group (*i.e.*, imidazole) and whereas the monosubstituted **7** was only a poor inhibitor, the presence of a second imidazole led to a remarkable improvement in inhibitory activity. Indeed, compound **8** (JMV7061[44]) was a submicromolar inhibitor of both VIM-type MBLs and showed an exceptional inhibitory potency against NDM-1 (K_i value of 30 nM). Therefore, we further

https://doi.org/10.1021/acs.jmedchem.2c01257
J. Med. Chem. XXXX, XXX, XXX−XXX

Table 3. Inhibitory Activity of Homo-Disubstituted 1,2,4-Triazole-3-thione Analogues 23−30 with $R^2 = R^3$ against Various MBLs[a]

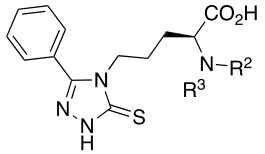

Cpd	Structure	K_i (μM) or (% inhibition at 100 μM)				
	$R^2 = R^3$	VIM-1	VIM-2	VIM-4	NDM-1	IMP-1
8	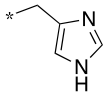	0.15 ± 0.01	0.41 ± 0.02	0.20 ± 0.01	0.030 ± 0.004	(40%)
23	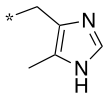	0.31 ± 0.03	0.22 ± 0.01	0.35 ± 0.04	0.023 ± 0.004	(57%)
24	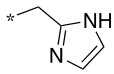	0.69 ± 0.08	0.90 ± 0.09	0.66 ± 0.05	0.020 ± 0.004	(61%)
25	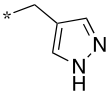	3.7 ± 0.3	2.5 ± 0.1	0.29 ± 0.01	NI	NI
26	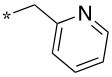	1.7 ± 0.2	0.96 ± 0.12	0.76 ± 0.05	0.57 ± 0.08	NI
27	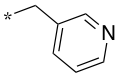	2.6 ± 0.1	0.42 ± 0.03	0.52 ± 0.02	(67%)	NI
28	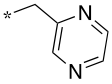	2.5 ± 0.3	1.2 ± 0.1	0.63 ± 0.04	17.9 ± 1.1	(51%)
29	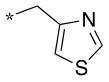	2.4 ± 0.2	2.5 ± 0.1	2.0 ± 0.2	6.5 ± 0.7	(48%)
30	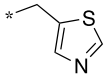	0.30 ± 0.02	0.10 ± 0.01	0.14 ± 0.01	28.0 ± 2.3	NI

[a]NI: no inhibition (<30% inhibition at 100 μM). Kinetics were monitored at 30 °C by following the absorbance variation observed upon substrate hydrolysis. K_i values were determined when inhibition > 70%. Assays were performed in triplicate.

explored this compound configuration by modifying its stereochemistry (**9**), removing the carboxylic group (**10**), varying the alkyl length between the triazole ring and the amino acid moiety (**11**, **12**, **14** with n = 1, 2, and 4, respectively). Overall, all compounds exhibited similar inhibitory potencies against VIM-type enzymes with a maximum of 6-fold difference compared to compound **8** (in the case of **11** against VIM-1, K_i values of 0.88 *vs* 0.15 μM). The activity against NDM-1 was also generally kept with two notable exceptions. In contrast to VIM-type enzymes, the absence of the α-carboxylic group (*i.e.*, compound **10**) led to a 450-fold decrease in NDM-1 inhibition. Also, adding a methylene group (n = 4, compound **14**) led to a more moderate 18-fold decrease. It is interesting to note that the mono-imidazole analogue **13** (n = 4) showed a similar restricted spectrum to **7** (n = 3) but with higher potencies against VIM-1 and NDM-1 (K_i values in the micromolar range). It is remarkable that the D isomer **9** behaved very similarly to compound **8** but also inhibited IMP-1, as compounds **11**, **12**, and **14**, with K_i value in the micromolar range. This result suggested significantly different structural requirements for IMP-1 inhibition than for other tested MBLs.

2.2.2. Nα-Monosubstituted and Homo-Disubstituted Analogues (Tables 2 and 3). As the imidazole group gave very interesting results, we wondered if introducing other nitrogen-containing heteroaryl groups would yield similarly or even more potent inhibitors. We therefore prepared two series of monosubstituted (**15**−**22**, Table 2) and homo-disubstituted (**23**−**30**, Table 3) analogues, derived from compounds **7** and **8**, respectively.

Overall, in the case of the monosubstituted analogues, which contained either methylated imidazole (**15**, **16**), pyrrole (**17**),

https://doi.org/10.1021/acs.jmedchem.2c01257
J. Med. Chem. XXXX, XXX, XXX−XXX

Table 4. Inhibitory Activity of Hetero-Disubstituted 1,2,4-Triazole-3-thione Analogues 31−40 with R^2 = (1*H*-Imidazol-4-yl)methyl against Various MBLs[a]

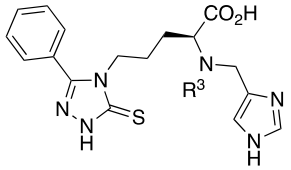

Cpd	Structure	K_i (μM) or (% inhibition at 100 μM)				
	R^3	VIM-1	VIM-2	VIM-4	NDM-1	IMP-1
8	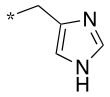	0.15 ± 0.01	0.41 ± 0.02	0.20 ± 0.01	0.030 ± 0.004	(40%)
31	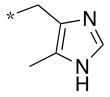	0.38 ± 0.05	0.35 ± 0.03	0.42 ± 0.04	0.038 ± 0.004	4.5 ± 0.6
32	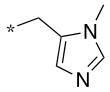	4.4 ± 0.5	3.2 ± 0.5	3.8 ± 0.6	(66%)	(50%)
33	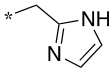	0.45 ± 0.04	3.3 ± 0.1	0.35 ± 0.02	2.7 ± 0.5	(49%)
34	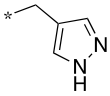	4.6 ± 0.4	(53%)	2.0 ± 0.2	(37%)	(34%)
35	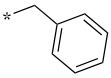	4.1 ± 0.2	2.1 ± 0.2	1.0 ± 0.1	(60%)	(45%)
36	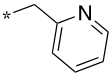	0.95 ± 0.11	0.64 ± 0.08	0.56 ± 0.08	0.38 ± 0.05	NI
37	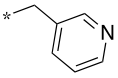	5.2 ± 0.5	1.8 ± 0.2	1.7 ± 0.2	34.8 ± 7.9	NI
38	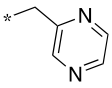	3.3 ± 0.2	2.4 ± 0.2	1.9 ± 0.2	0.89 ± 0.11	(43%)
39	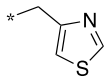	0.82 ± 0.06	0.35 ± 0.07	0.35 ± 0.03	0.030 ± 0.002	(59%)
40	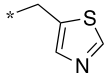	2.5 ± 0.1	1.1 ± 0.1	0.77 ± 0.05	13.1 ± 2.0	(39%)

[a]NI: no inhibition (<30% inhibition at 100 μM). ND: not determined. Kinetics were monitored at 30 °C by following the absorbance variation observed upon substrate hydrolysis. K_i values were determined when inhibition > 70%. Assays were performed in triplicate.

pyridine (**18**, **19**), indole (**20**), or thiazole (**21**, **22**), most compounds were poor inhibitor of any tested MBL, as expected from results obtained with **7**. A few exceptions were compounds **17** (mono-pyrrol-3-yl), **18** (mono-pyridin-2-yl), and **22** (mono-thiazol-5-yl), which inhibited VIM-1, NDM-1, and VIM-4, respectively, with a K_i value close to 2 μM. Interestingly, the isomer of **18**, **19** (mono-pyridin-3-yl), was inactive.

In the case of the homo-disubstituted compounds (Table 3), results showed that it was possible to replace the two imidazoles of **8** without losing global activity. Rather expectedly, it is the case of compounds **23** and **24** (isomer of **8**), which contained two 5-methylated imidazoles branched as in **8** (*i.e.*, at position 4) or two imidazoles branched at position 2, respectively. These compounds showed similarly high inhibitory potencies against VIM-type MBLs and NDM-1. Moving one nitrogen of the imidazole ring (*i.e.*, pyrazole ring in

https://doi.org/10.1021/acs.jmedchem.2c01257
J. Med. Chem. XXXX, XXX, XXX−XXX

compound **25**) led to a decrease in inhibitory potency against VIM-type enzymes with the exception of VIM-4. In contrast, compound **25** did not inhibit NDM-1, indicating a clear difference between VIM-type enzymes and NDM-1 in this series. Such difference was also observed when comparing compounds **26** and **27**, which possess pyrid-2-yl and pyrid-3-yl groups, respectively. Although **26** and **27** were similarly good to potent inhibitors of VIM-type MBLs as compound **8**, a difference was observed in the case of NDM-1. Indeed, **26** was a potent NDM-1 inhibitor despite a K_i value 20-fold higher than that of **8**, but **27** was significantly less potent. Compound **28** with pyrazin-2-yl groups behaved as the close pyridine analogue **26** except that **28** was about 30 times less potent than **26** against NDM-1. This unexpected result might come from the pK_a difference between the two heterocycles (*vide infra*).

The two thiazole-containing compounds **29** and **30** showed a different behavior toward VIM-type MBLs and NDM-1. Indeed, while **29** (thiazol-4-yl) was a moderate to good inhibitor of VIM-type enzymes and NDM-1, **30** (thiazol-5-yl) potently inhibited both VIM-type enzymes with K_i values in the low submicromolar range, but was less efficient against NDM-1. Finally, all compounds were modest or not inhibitors of IMP-1.

Overall, VIM-type enzymes were quite tolerant to heterocycle replacement as K_i values were in the micromolar to submicromolar range for all compounds. By contrast, NDM-1 was more sensitive to these modifications. The results suggested that the position of one nitrogen relative to the branching carbon of the heterocycle was important. When comparing the three imidazole analogues **8**, **23**, and **24** with the pyrazole **25**, and the pyrid-2-yl analogue **26** with the pyrid-3-yl **27**, potent NDM-1 inhibition was observed for compounds where a cyclic nitrogen was at the ortho position of the methylene link. By contrast, although this feature was shared by the pyrazine and thiazole moieties in **28** and **29**, respectively, these compounds were less potent NDM-1 inhibitors (K_i values, 18 and 6.5 μM, respectively). This discrepancy could be due to the different physicochemical properties of the heterocycles. For instance, the pK_a values of the nonprotonated nitrogen (corresponding to deprotonation of conjugate acid) of unsubstituted imidazole, pyridine, thiazole and pyrazine were 6.9, 5.2, 2.5, and 0.6, respectively.[45] Therefore, a nitrogen at the ortho position and its basic character seem to be important for NDM-1 inhibition.

In this series of homo-disubstituted analogues, **8** remained the most interesting compound, being characterized by a potent and broad-spectrum inhibition of both VIM-type MBLs and NDM-1. Although less potent toward NDM-1, the structurally different dipyrid-2-yl analogue **26** also showed promising properties.

2.2.3. Nα-Hetero-Disubstituted Analogues (Table 4). We further explored the substitution of the α-amine group by preparing a series of hetero-disubstituted analogues. One heterocycle was the imidazol-4-yl group for all compounds, while the second was variable and chosen among those used in the preceding series (Table 4). Overall, when the comparison was possible, the inhibition behavior of the hetero-disubstituted analogues was similar to that of the corresponding homo-disubstituted compounds containing the variable heterocycle, with a few exceptions.

As expected, the analogues **31** (5-methyl-imidazol-4-yl) and **33** (imidazol-2-yl) showed similar activities against both VIM-type enzymes as compound **8** and their corresponding homo-disubstituted analogues **23** and **24** (Table 3). Curiously, although **31** and **23** comparably inhibited NDM-1 as expected, a significant drop in potency was observed for **33** compared to **24** (K_i value increased >130-fold). This case is an exception to the rule previously proposed for potent NDM-1 inhibition. Combining the imidazol-4-yl heterocycle with its *N*-methylated derivative, 1-methyl-imidazol-5-yl (for which no homo-disubstituted analogue could be synthesized) in compound **32** led to a decrease in potency. However, while its K_i values against VIM-type MBLs were 8- to 30-fold higher than for **8**, the decrease in potency was much more pronounced against NDM-1. Compound **34** behaved as its dipyrazol-4-yl analogue **25** with moderate to good inhibitory potencies against VIM-type enzymes and low activity against NDM-1. Interestingly, although the dibenzyl analogue **3** was poorly active against all tested enzymes, the corresponding hetero-disubstituted compound **35** displayed K_i values in the micromolar range against both VIM-type enzymes (5- to 28-fold higher than for **8**), indicating that two nitrogen-containing heterocycles are not strictly required to inhibit these enzymes. However, again, NDM-1 inhibition was moderate. Compared to **35**, combining a pyridyl group led to higher or similar activities if the nitrogen was at position ortho (**36**) or meta (**37**), respectively. Indeed, compound **37** (pyrid-2-yl) exhibited K_i values in the submicromolar range against both VIM-type enzymes and NDM-1 and therefore very close to those of the corresponding dipyrid-2-yl analogue **26**. Then, while **37** (pyrid-3-yl) was only slightly less potent against VIM-type MBLs compared to **36** (3- to 5-fold), a close to 100-fold decrease in potency was observed in the case of NDM-1. The pyrazin-2-yl analogue **38** was similarly potent as the corresponding dipyrazin-2-yl **28** against VIM-type enzymes, but was about 20-fold more potent against NDM-1, suggesting a favorable effect of the imidazole ring. Finally, the two thiazole compounds **39** (thiazol-4-yl) and **40** (thiazol-5-yl) showed reverse behaviors compared to their respective homo-dithiazolyl analogues **29** and **30**. In addition, while **39** displayed K_i values in the submicromolar range against both VIM-type enzymes, it was also a highly potent NDM-1 inhibitor with a K_i value of 30 nM as compound **8**. Interestingly, **40** was more than 400-fold less potent against this enzyme.

Overall, as observed in the homo-disubstituted series, most hetero-disubstituted analogues showed micromolar to submicromolar inhibitory potencies against VIM-type enzymes. It is in particular the case of compound **35**, which contains a simple phenyl ring combined to the imidazol-4-yl group. As the dibenzyl **3** and the mono-imidazol-4-yl **7** were poor inhibitors, these results indicated that a single imidazole was determining for activity but only if combined to another aromatic ring. Obviously, the fact that this aromatic ring contains a nitrogen further improves VIM inhibition. The structural requirements for NDM-1 inhibition were even more evident in this series. Indeed, only compounds possessing two heterocycles with an unsubstituted nitrogen at the ortho position of the branching carbon potently inhibited NDM-1. It is the case of analogues **31**, **36**, **38**, and **39**, while **33** was an exception to this rule. In particular, **36** was 100 times more potent than **37**. More strikingly, combination of the imidazol-4-yl with a thiazol-4-yl ring in compound **39** led to very potent NDM-1 inhibition, while the thiazol-5-yl isomer was only moderately active. Finally, the *N*-methylation of one of the two imidazol-4-yl groups of compound **8** (*i.e.*, **32**) led to a very large decrease in

https://doi.org/10.1021/acs.jmedchem.2c01257
J. Med. Chem. XXXX, XXX, XXX−XXX

Table 5. Inhibitory Activity of 1,2,4-Triazole-3-thione Analogues 41−45 with Variable R^1, and R^2 = R^3 = (1*H*-Imidazol-4-yl)methyl, against Various MBLs[a]

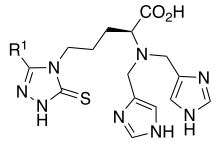

Cpd	Structure	K_i (μM) or (% inhibition at 100 μM)				
	R^1	VIM-1	VIM-2	VIM-4	NDM-1	IMP-1
8		0.15 ± 0.01	0.41 ± 0.02	0.20 ± 0.01	0.030 ± 0.004	(40%)
41	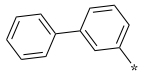	0.13 ± 0.01	0.09 ± 0.01	0.07 ± 0.01	0.013 ± 0.002	(69%)
42	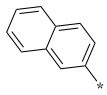	0.52 ± 0.06	0.11 ± 0.02	0.34 ± 0.04	0.030 ± 0.004	4.7 ± 0.5
43	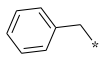	0.12 ± 0.02	0.41 ± 0.02	0.12 ± 0.01	0.09 ± 0.01	(54%)
44	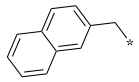	0.08 ± 0.01	0.27 ± 0.02	0.19 ± 0.01	0.03 ± 0.01	11.2 ± 0.9
45		0.28 ± 0.02	0.11 ± 0.01	0.09 ± 0.01	0.0035 ± 0.0006	(48%)

[a]NI: no inhibition (<30% inhibition at 100 μM). ND: not determined. Kinetics were monitored at 30 °C by following the absorbance variation observed upon substrate hydrolysis. K_i values were determined when inhibition > 70%. Assays were performed in triplicate.

potency, strongly supporting that the two ortho-nitrogens should be unsubstituted to inhibit NDM-1.

2.2.4. Nα-Diimidazole Analogues Modified at Position 5 (Table 5). Finally, we developed a series based on compound **8** where the phenyl ring at position 5 of the triazole ring was replaced by various groups (Table 5). In previous series,[35,38,39,41] we explored many different R^1 groups. While we found that the 5-substituent was less impacting the inhibitory potencies than the 4-substituent, probably because the first points to a wider and more solvent-exposed cavity than the second,[38,39] we identified a few favorable groups common to all series. For instance, the replacement of the phenyl ring by a biaryl (*e.g.*, *m*-biphenyl as in **41**, naphthyl as in **42** and **44**) generally led to increased potencies. In the present series, compounds **41**, **42**, and **44** showed quite similar activities as **8**, although slight improvements could be observed in particular for compound **41**. It is noteworthy that **41** contains an *m*-biphenyl substituent, which was previously shown as the most favorable for inhibiting VIM-type enzymes. Interestingly, compound **42** with a naphth-2-yl group inhibited IMP-1 with K_i value in the micromolar range, making it the best broad-spectrum inhibitor in the full series of 1,2,4-triazole-3-thione-based analogues. Finally, with a K_i value in the low nanomolar range, compound **45** is the best NDM-1 inhibitor presented in this study. Overall, changing the 5-phenyl substituent toward more hydrophobic groups had little but favorable influence on inhibitory potencies as observed in previous series.

In an effort to explain the structural requirements here defined for highly potent NDM-1 inhibition, it is noteworthy that a motif combining a carboxylate, a tertiary α-amine and two nitrogen-containing heterocycles in close positions may behave as a tripodal tetradentate ligand able to establish metal complexes with metallic ions such as Zn^{2+} as shown for HemiGly, a derivative of *N*,*N*-(diimidazol-4-ylmethyl)glycine (Figure 3A).[46] A similar configuration based on

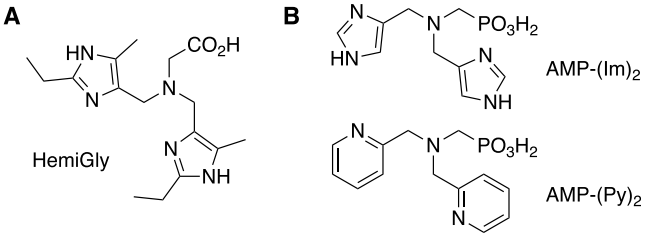

Figure 3. Structures of (A) HemiGly[46] and (B) (aminomethylene)-phosphonate (AMP) derivatives[47] studied as tripodal tetradentate ligands for divalent cations.

(aminomethylene)phosphonate (*i.e.*, CO_2H replaced by PO_3H_2) substituted by two imidazol-4-ylmethyl (AMP-$(Im)_2$) or two pyridin-2-ylmethyl (AMP-$(Py)_2$) groups led to two highly stable Zn^{2+} complexes, the former being the most stable (Figure 3B).[47] In these complexes, the zinc ion is coordinated by the two heterocycle nitrogens, which are at the ortho position of the branching carbon as required for complex formation. The dipyrid-2-ylmethyl derivative AMP-$(Py)_2$ as well as the corresponding compound **26** of the present study are of course analogues of dipicolylamine (DPAm) and *N*-

https://doi.org/10.1021/acs.jmedchem.2c01257
J. Med. Chem. XXXX, XXX, XXX−XXX

acetic/acetamide derivatives, which were shown to inactivate NDM-1 by sequestering the metals of the enzymes.[48−51] Therefore, compound **8** and other potent NDM-1 inhibitors in this series were suspected to inhibit NDM-1 by stripping its zinc cations. In the case of VIM-type enzymes, the inhibition mode appeared different as these MBLs did not display such restricted structural requirements as NDM-1.

Further studies were conducted to better characterize NDM-1 and VIM-type MBL inhibition by compound **8** and its analogues.

2.3. Equilibrium Dialysis and Native State Electrospray Ionization Mass Spectrometry (Native MS). We evaluated the mechanism of inhibition of this series of compounds by studying the effect of compounds **8**, **26**, **27**, and **30** on the metal content of VIM-2 and NDM-1 using equilibrium dialysis and by native MS. In these experiments, the compounds were incubated with the enzymes for 1 h followed by overnight dialysis and analysis.

2.3.1. Zinc Content of VIM-2 and NDM-1. The effect of compounds on the metal content of the MBLs was assessed using equilibrium dialysis followed by metal analysis with atomic absorption spectroscopy.[52,53] The inhibitors investigated fall into two groups (Figure 4). Group 1 contained compounds **27** and **30**. These inhibitors tended to act on VIM-2 and NDM-1 similarly by not removing Zn^{II} from the MBLs.

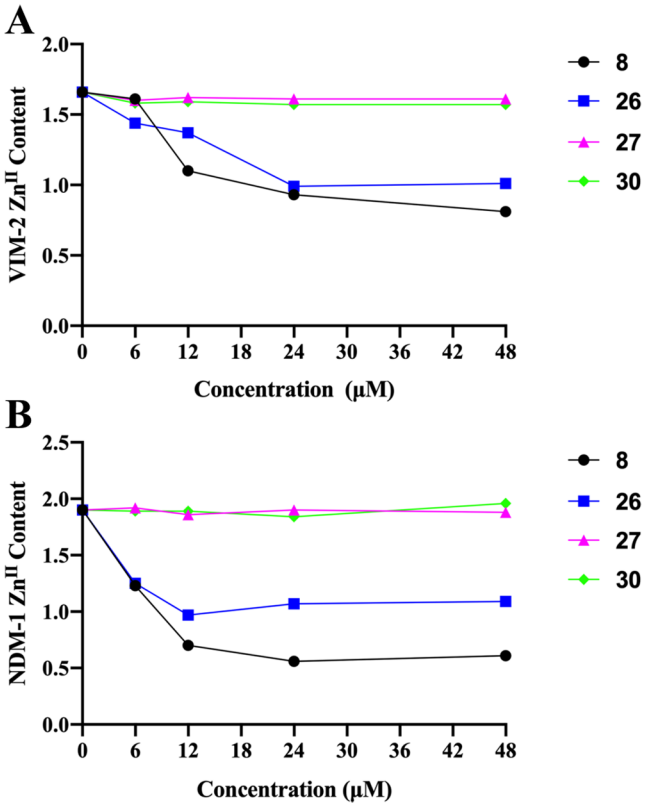

Figure 4. Equilibrium dialysis study with VIM-2 (A) and NDM-1 (B) in the presence of compounds **8**, **26**, **27**, and **30**. The metal content of VIM-2 (3 μM) and NDM-1 (3 μM) was measured after overnight dialysis with various inhibitor concentrations ranging from 0 to 48 μM. The buffer used was 50 mM 4-(2-hydroxyethyl)-1-piperazine-ethanesulfonic acid (HEPES), pH 7.5. It is important to note that the starting Zn^{II} content of VIM-2 of 1.6 equiv is due to the extensive dialyses conducted prior to analysis, as previously reported.[53,54] Each data point is an average of three samples during the analysis process.

These data suggest that compounds **27** and **30** form a ternary complex with the enzymes and act as purely competitive inhibitors. The group 2 inhibitors included **8** and **26**. These compounds resulted in less Zn^{II} bound to both MBL enzymes, the effect being less pronounced for **26** compared to **8** in the case of NDM-1 (1.09 equiv Zn^{II} vs 0.61 at 48 μM compound). These data suggest that the group 2 compounds exhibit a metal stripping mechanism of inhibition with VIM-2 and NDM-1, at least at concentrations above 5 μM in the case of VIM-2.

2.3.2. Native MS. Native MS allows probing the mechanism of inhibition at low enzyme/inhibitor concentrations. The experiments were performed using 10 μM VIM-2 or NDM-1 and 5 equiv of inhibitor. Before studying the inhibitors, native VIM-2 and NDM-1 were analyzed to ensure proper metal content (Table 6). The native MS of 10 μM VIM-2 showed dominant +8 and +9 peaks at 3247 and 2886 m/z, corresponding to the mass of VIM-2 with 2 equiv Zn^{II} bound (native VIM-2, 25,972 Da) (Figure S1A). The native MS of 10 μM NDM-1 revealed dominant +9 and +10 peaks at 2821 and 2539 m/z, respectively, corresponding to the mass of NDM-1 with 2 equiv Zn^{II} bound (native NDM-1 25,385 Da) (Figure S1B).

The mechanism of inhibition for the same four inhibitors was studied with recombinant VIM-2 (with the exception of compound **30**) and NDM-1. The expected masses of VIM-2 and NDM-1 with each of the tested inhibitors are shown in Table 6. Overall, the results obtained using native MS confirmed the equilibrium dialysis experiments and placed the tested compounds into the same two groups.

The native MS of VIM-2 and compound **8** showed the dominant +8 peak at 3295 m/z, corresponding to the mass of one Zn^{II} bound VIM-2 + 1 equiv of compound **8** (26,359 Da) (Figure 5A). Combined, the equilibrium dialysis and native MS data suggest a mixed mechanism of VIM-2 inhibition as compound **8** strips 1 equiv of Zn^{II} from VIM-2 prior to binding to the mono-Zn^{II} form of VIM-2. Alternatively, this result could mean that compound **8** only coordinates one Zn^{II} in the active site of VIM-2. This result was partially contradicted by the resolution of the crystallographic structure of the complex VIM-2/**8** (see below). The native MS of NDM-1 with compound **8** showed the dominant +8 peak at 3158 m/z, which corresponds to the mass of NDM-1 with no bound Zn^{II} (25,255 Da) (Figure S2B). This result confirms the metal stripping mechanism of NDM-1 inhibition by **8**.

The native MS of VIM-2 and compound **26** showed a dominant +8 peak at 3231 m/z, corresponding to the mass of VIM-2 with no bound Zn^{II} (25,842 Da) (Figure S3A). In agreement with the equilibrium dialysis data, the native MS suggests compound **26** exhibits a metal stripping mechanism of inhibition with VIM-2. The native MS of NDM-1 and compound **26** showed the dominant +8 peak at 3174 m/z, which corresponds to the mass of native NDM-1 (25,835 Da). The nondominant +8 peak at 3233 m/z corresponds to the mass of native NDM-1 with 1 equiv of compound **26** (25,859 Da) (Figure 5B). Both native MS and equilibrium dialysis data suggest a mixed mechanism of NDM-1 inhibition by compound **26**.

The native MS of VIM-2 with compound **27** revealed a dominant +7 peak at 3711 m/z, which corresponds to the mass of native VIM-2 (25,972 Da). The nondominant +7 peak at 3781 m/z corresponds to the mass of native VIM-2 with 1 equiv of compound **27** (26,446 Da) (Figure S4A). The native MS of NDM-1 and compound **27** showed the dominant +7

https://doi.org/10.1021/acs.jmedchem.2c01257
J. Med. Chem. XXXX, XXX, XXX−XXX

Table 6. Summary of the ESI-MS Experimental Results for VIM-2 (10 μM) and NDM-1 (10 μM) in the Presence of Compounds 8, 26, 27, and 30 (50 μM in All Samples)

sample	cpd MW (g/mol)	actual peak(s)[a] (charge)	protein MW[b] (Da)	suspected species[c]
VIM-2	NA	3247 (8+), 2886 (9+)	25,972	VIM-2
VIM-2 + **8**	452	3295 (8+)	26,359	VIM-2 with 1 equiv Zn^{II} + 1 equiv **8**
VIM-2 + **26**	474	3231 (8+)	25,842	apo-VIM-2
VIM-2 + **27**	474	3711 (7+)	25,972	VIM-2
		3779 (7+)	26,446	VIM-2 + 1 equiv **27**
NDM-1	NA	2821 (9+), 2539 (10+)	25,385	NDM-1
NDM-1 + **8**	452	3158 (8+)	25,255	apo-NDM-1
NDM-1 + **26**	474	3174 (8+)	25,385	NDM-1
		3233 (8+)	25,859	NDM-1 + 1 equiv **26**
NDM-1 + **27**	474	3627 (7+)	25,385	NDM-1
		3697 (7+)	25,859	NDM-1 + 1 equiv **27**
NDM-1 + **30**	486	3174 (8+)	25,385	NDM-1
		3236 (8+)	25,871	NDM-1 + 1 equiv **30**

[a]Main multicharged species observed in mass spectra. [b]MW values calculated from mass spectrum deconvolution. [c]VIM-2 and NDM-1: native enzymes containing 2 equiv Zn^{II}; apo-VIM-2 and apo-NDM-1 are enzymes without Zn^{II}.

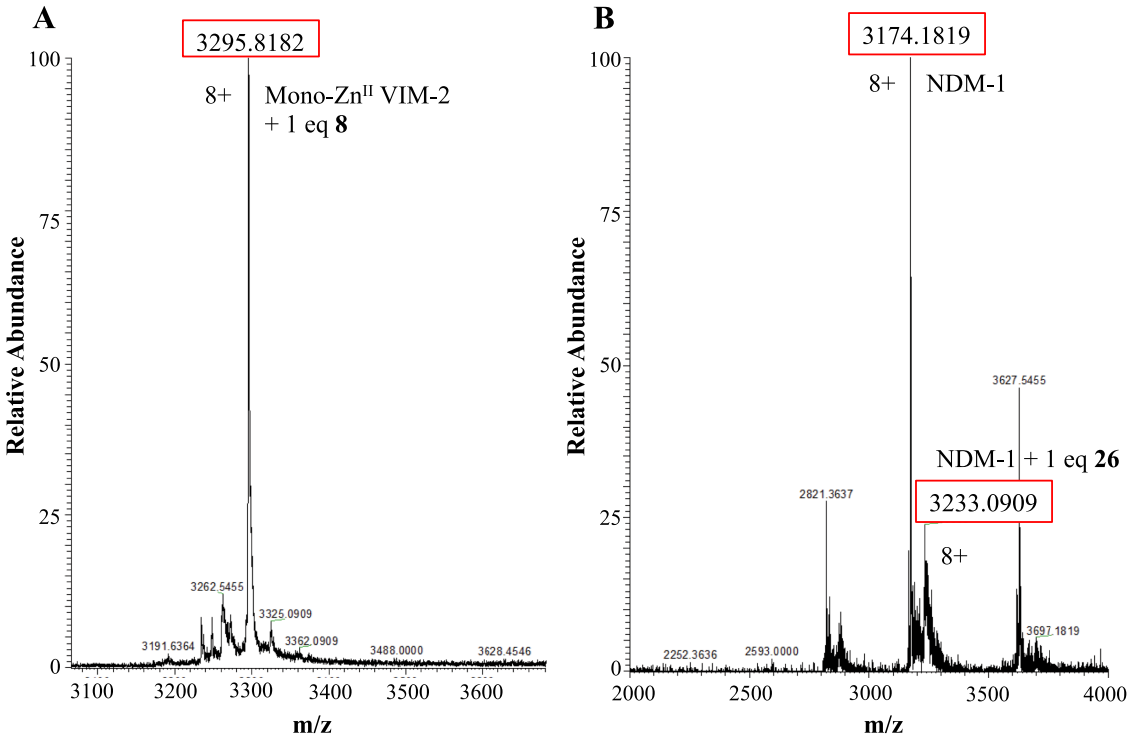

Figure 5. Native mass spectra of 10 μM VIM-2 (A) and 10 μM NDM-1 (B) with compounds **8** and **26**, respectively. The protein samples were diluted using 100 mM ammonium acetate, pH 7.5, and incubated with 50 μM of the compound for 5 min prior to analysis. The dominant +8 peak, at 3295 m/z (A), corresponds to mono-Zn^{II} VIM-2 + 1 equiv of compound **8**. The dominant +8 peak, at 3174 m/z (B), corresponds to native NDM-1 (2 Zn^{II} bound). The nondominant +8 peak, at 3233 m/z, corresponds to native NDM-1 + 1 equiv of compound **26**.

peak at 3627 m/z, which corresponds to the mass of native NDM-1 (25,385 Da). The nondominant +7 peak at 3697 m/z corresponds to the mass of native NDM-1 binding 1 equiv of compound **27** (25,859 Da) (Figure S4B). In agreement with the equilibrium dialysis data, the native MS suggests that compound **27** forms a ternary complex with both VIM-2 and NDM-1.

Finally, when studied with compound **30**, the native MS of NDM-1 showed a nondominant +8 peak at 3174 m/z corresponding to native NDM-1 (25,385 Da). The dominant +8 peak at 3236 m/z corresponds to the mass of native NDM-1 with 1 equiv of compound **30** (25,871 Da) (Figure S5). The native MS and equilibrium dialysis data show that compound **30** forms a ternary complex with NDM-1.

Overall, these results are consistent with the inhibition data reported for compounds **8**, **26**, **27**, and **30**. Only compounds **8** and **26**, which possess heterocycles (imidazo-4-yl and pyridin-2-yl, respectively) with a nitrogen at the ortho position of the methylene link, are able to diminish the zinc content of both VIM-2 and NDM-1, while it should be noted that this phenomenon is observed after a significant time of incubation of the enzyme in the presence of the inhibitor. It suggests that these compounds at least partially inhibited one or both MBLs by zinc stripping. Compound **8** partially removed Zn^{II} from VIM-2, while forming a ternary complex with the enzyme. But

https://doi.org/10.1021/acs.jmedchem.2c01257
J. Med. Chem. XXXX, XXX, XXX−XXX

it fully inhibited NDM-1 by zinc stripping. Compound **26** showed a reverse behavior as it fully removed Zn^{II} from VIM-2, while it showed a mixed inhibition mode against NDM-1. The lower capacity of **26** to decrease the zinc content of NDM-1 compared to **8** may explain its about 20-fold lower inhibitory potency (0.57 vs 0.03 μM K_i values). In contrast, compounds **27** and **30**, which do not possess heterocycles with a nitrogen at the ortho position of the methylene link, do not decrease the MBL zinc content as expected. These moderate NDM-1 inhibitors form ternary complexes with tested MBLs. It confirms that potent NDM-1 inhibition in this series at least relates to zinc stripping.

2.4. Isothermal Calorimetry Experiments (ITC). To further explore the binding mode to VIM-2 and NDM-1, ITC experiments were performed with compounds **8** and **26**.

2.4.1. Interaction of Compounds with Zinc. First, we measured the affinity of **8** and **26** for Zn^{II}. An equilibrium between free and Zn^{II}-bound compounds was well characterized by ITC, with K_d values of about 10 nM and a stoichiometry of 1 (Figure S6). These K_d values were at the resolution limit of ITC and the resulting uncertainty prevented calculating $\Delta G°$. The enthalpic $\Delta H°$ values were about 5 and 6 kcal/mol for compounds **8** and **26**, respectively, suggesting that **26** would perform more favorable interactions with the zinc ion.

Accordingly, all titrations with enzymes were performed without $ZnSO_4$ in the same buffer.

2.4.2. Interaction of Compounds with VIM-2. In the case of VIM-2 in the presence of compound **8**, an equilibrium was detected by ITC as shown by the sigmoidal shape of the corresponding Wiseman graph presented in Figure 6A (bottom).

The thermodynamic parameters of binding of **8** with VIM-2 are given in Table 7, and the experiment showed a stoichiometric relationship between VIM-2 and **8**, which clearly indicated a 1:1 association. However, the linear decrease of the injection amplitudes seen in the ITC thermogram (Figure 6A, top) suggested the existence of a concomitant event, which could be the chelation of 1 equiv Zn^{II} as suggested by native MS experiments. Accordingly, calculated values should be regarded as apparent values.

In the case of VIM-2 in the presence of compound **26**, no equilibrium was detected by ITC as shown by the almost linear Wiseman graph presented in Figure 6B (bottom). According to results obtained with the native MS study, the ITC experiment would reflect zinc chelation. The biphasic form of the chart may correspond to the chelation of the two zinc ions with distinct affinities. No quantification was possible in this case.

2.4.3. Interaction of Compounds with NDM-1. In the case of NDM-1, no equilibrium was detected with both compounds. The Wiseman graph showed a biphasic curve for compound **8** (Figure S7A, bottom), also suggesting distinct affinities for Zn^{II}, while it was not sigmoidal for compound **26** (Figure S7B, bottom). These results suggested that **8** chelated both enzyme zinc ions as found in the native MS study, while it was less clear for **26**. In both cases, no quantification was possible.

Overall, results obtained with ITC for compounds **8** and **26** reflected those obtained with native MS experiments, with the exception of **26** interaction with NDM-1.

2.5. Crystallography. *2.5.1. Crystal Structure of the Complex between VIM-2 and Compound 8.* The structure of

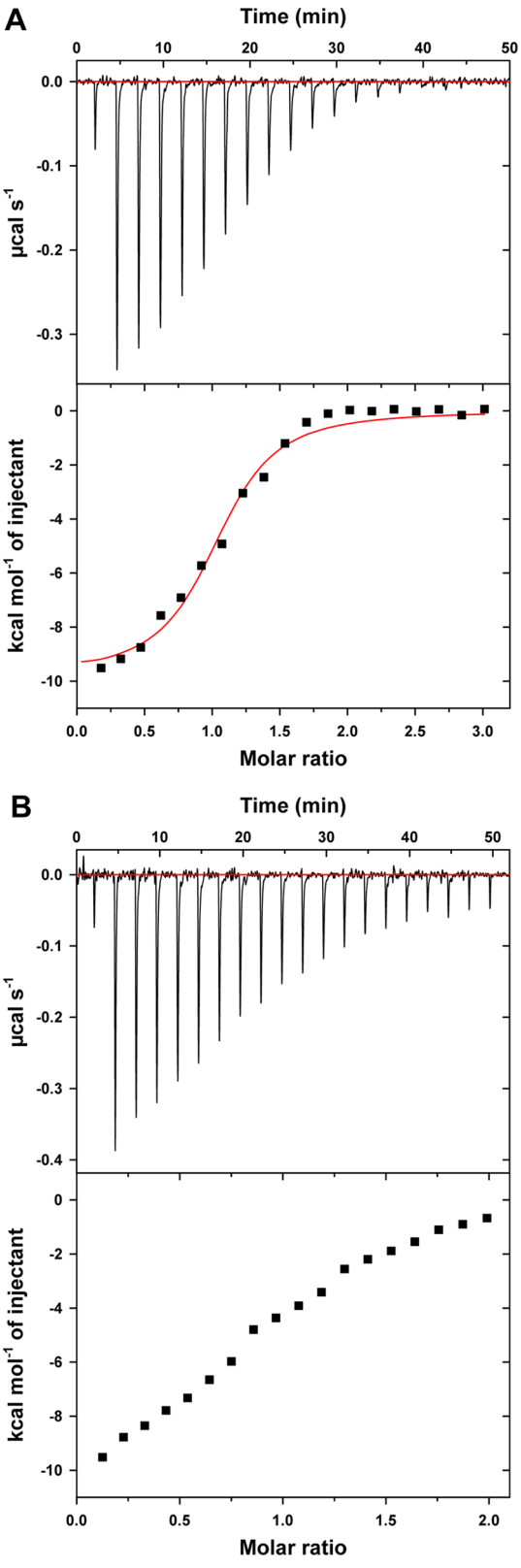

Figure 6. Isothermal titration calorimetry of VIM-2 by compounds **8** (A) and **26** (B) at 25 °C. (Top) Exothermic microcalorimetric trace of compound injections into VIM-2 solution (19.0 μM). (Bottom) Wiseman plot of heat releases versus molar ratio of injectant/protein in the cell and nonlinear fit of the binding isotherm for *n* equivalent binding sites. The binding enthalpy corresponds to the amplitude of the transition curve, K_a is derived from the slope of the transition, and the stoichiometry n is determined at the transition midpoint.

https://doi.org/10.1021/acs.jmedchem.2c01257
J. Med. Chem. XXXX, XXX, XXX−XXX

Table 7. Apparent Thermodynamic Parameters of Compound 8 Binding to VIM-2 at 25 °C without Zn^{II}

cpd	n	K_a (M^{-1})	K_d (μM)	$\Delta G°$ (kcal/mol)	$\Delta H°$ (kcal/mol)	$T\Delta S°$ (kcal/mol)
8	1.01 ± 0.02	1.4 ± 0.3 10^6	0.7	−8.4	−9.8 ± 0.3	−1.4

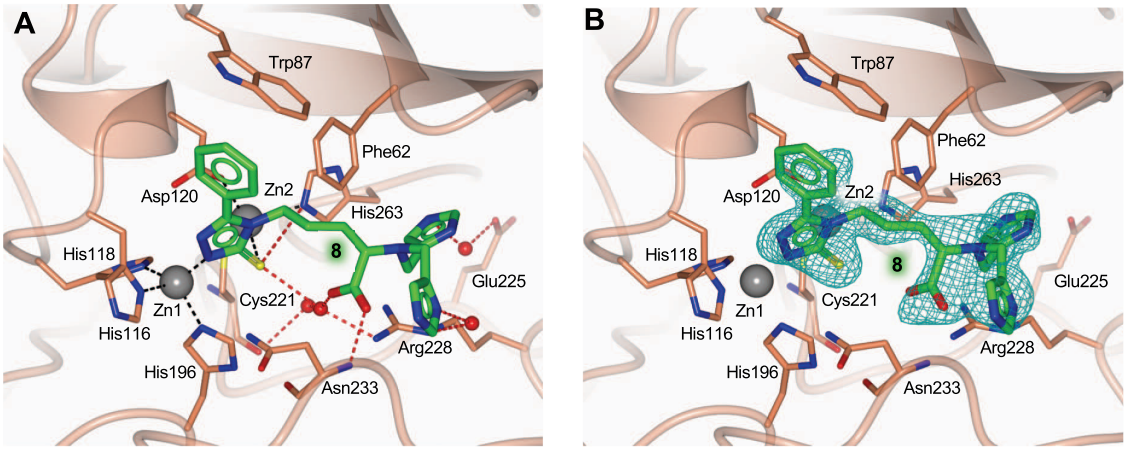

Figure 7. Active-site view of VIM-2 (coral cartoon and carbon atoms; residues in sticks) in complex with **8** (in sticks, green carbons) (PDB code 8A4M). (A) Hydrogen and coordination bonds are represented as tan and black dashed lines, respectively; (B) the inhibitor is surrounded by the omit map (petrol mesh) contoured at the 3-σ level. Zn ions and water molecules are displayed as gray and red spheres (arbitrary radius), respectively. Oxygen atoms are colored red, nitrogen blue, and sulfur yellow.

VIM-2 in complex with compound **8** was obtained at 1.98 Å resolution (Figure 7, PDB code 8A4M, Table S1).

In contrast to the native MS experiments, the crystal structure showed the presence of both zinc ions in the VIM-2 active site. This discrepancy very probably comes from different experimental conditions. For instance, enzymes and compounds are preincubated 1 h in the native MS study. It is also the case in the equilibrium dialysis experiment.

The structure provided a clear view of the main interactions entailed by the inhibitor within the enzyme catalytic cavity. The triazole-thione core of the compound coordinates both zinc ions (Figure 7A), displacing the catalytic hydroxide anion. The Zn1 ion populates the 3H site where it is coordinated by the nitrogen 2 of **8** and the three histidine residues His116, His118, and His196. The second zinc ion, Zn2, occupies the DCH site where it is coordinated by the thione of **8** and the residues Asp120, Cys221, and His263. This binding mode is peculiar of triazole-thione inhibitors; indeed, it was formerly observed in the complexes of compounds sharing this Zn-binding motif with L1,[30] VIM-2,[33,35,37,38] and NDM-1.[36] The thione group of **8** entails water-mediated interactions with the inhibitor carboxylate moiety (intramolecular interaction) and with the Cys221 backbone carbonyl and the Arg228 guanidinium group (Figure 7A). The 5-phenyl moiety of **8** is within van der Waals contact with the Trp87 indole and forms a T-shaped interaction with Phe62. The carboxylate of **8** is H-bonded to the Asn233 backbone nitrogen, and the two imidazole rings form water-mediated interactions with the Arg228 guanidinium and the Glu225 carboxylate moieties (Figure 7A). The occupancy of both zinc ions and of inhibitor **8** inside the VIM-2 catalytic cavity has been estimated to be 80%.

We formerly investigated other triazole-thione compounds, reporting the characterization of the structural complexes of VIM-2 with the inhibitors JMV4690 (PDB code 6YRP[35]), 8 (numbering in ref 37, PDB code 7OVF, named here **8b** for clarity), and 28 (numbering in ref 38, PDB code 7PP0, named here **28b** for clarity). All compounds have a common, variably substituted 5-phenyl moiety on the triazole-thione core, sharing the same orientation in their respective complexes (Figure 8), whereas different substituents are present in position 4.

At variance with **8** that has an alkanoic α-amine chain homo-disubstituted with two imidazole rings, compound **8b** has a *p*-fluoro-phenyl moiety connected to the triazole-thione core by a thioether-containing 4-atom linker. On the other hand, both compounds JMV4690 and **28b** have in this position an *o*-benzoic moiety connected through a two-atom linker (N═CH for JMV4690, $(CH_2)_2$ for **28b**). A comparison among these complexes shows that the 4-substituted phenyl moiety of compound **8b** is accommodated in the active site pocket lined by Tyr67, Arg228, and His263, matching the position of one imidazole ring of **8** (Figure 8A). The latter compound has a second imidazole, pointing toward the active site wall formed by Gly232, Asn233, and Arg228 (Figure 8A). The shorter linker presents in compounds JMV4690 and **28b** allows the positioning of the benzoic ring stacked to His263 (Figure 8B,C).

It is noteworthy that the carboxylate group of compounds **8**, JMV4690, and **28b** establish a H-bond with the Asn233 backbone NH (Figure 8B,C). It was previously hypothesized that this residue would stabilize either a substrate or an inhibitor in VIM-2 active site.[55] However, it is not clear if Asn233 similarly interacts with the C-3/C-4 carboxylate of β-lactams as no structure of complex with intact substrates is available. Only structures with hydrolyzed β-lactams were published but comparison has to be analyzed with caution as it might not exactly reflect the binding contribution of the substrate. The structural information available on VIM-2 in complex with hydrolyzed β-lactam antibiotics is limited. Only three structures have been recently released and they delivered distinct information on the role of Asn233 in the binding of hydrolyzed β-lactam antibiotics. The first two ones display VIM-2 in complex with two forms of the hydrolyzed

https://doi.org/10.1021/acs.jmedchem.2c01257
J. Med. Chem. XXXX, XXX, XXX−XXX

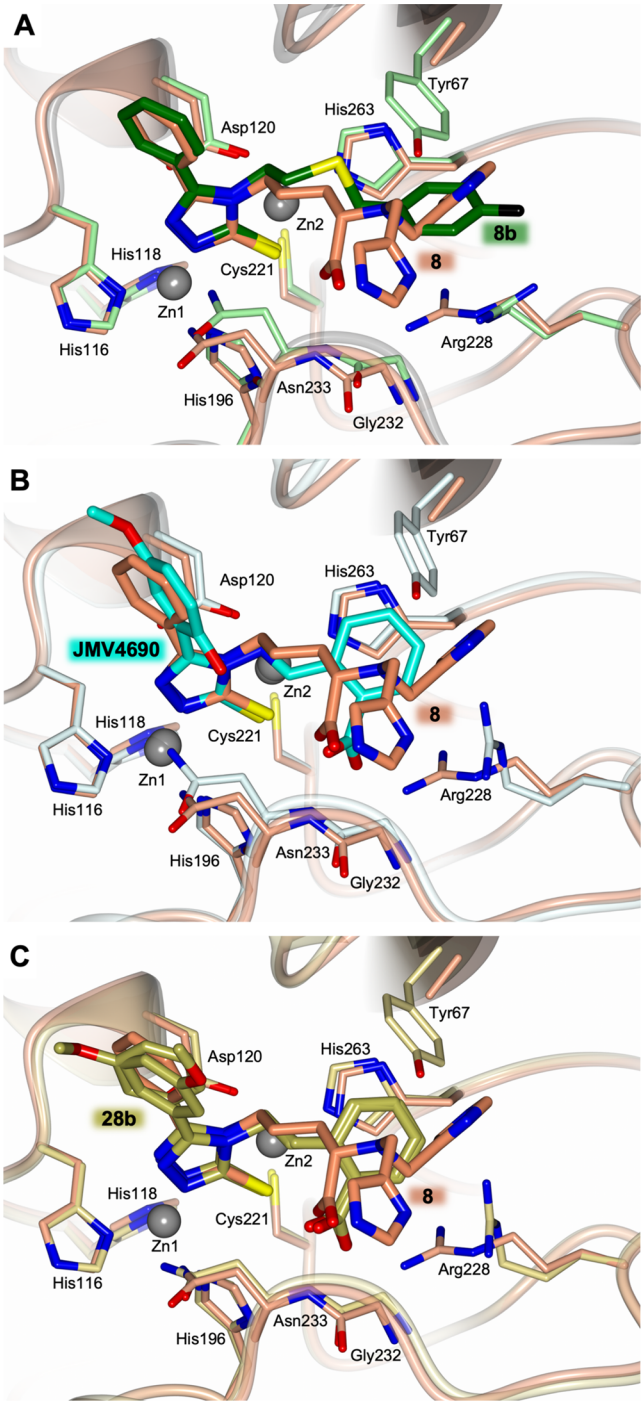

Figure 8. Active-site view of the superimposition between the structures of VIM-2 in complex with **8** (VIM-2 light coral cartoon, carbons and waters; **8** in sticks, coral carbons) and (A) **8b** (PDB code 7OVF;[37] VIM-2 light green cartoon and carbons; **8b** in sticks, dark green carbons, and black fluorine); (B) JMV4690 (PDB code 6YRP;[35] VIM-2 light cyan cartoon, carbons and waters; JMV4690 in sticks, cyan carbons); (C) **28b** (PDB code 7PP0;[38] VIM-2 light gold cartoon and carbons; **28b** in sticks, gold carbons).

faropenem, a penem (PDB codes 7A60 and 7A5Z) and the carboxylic group establishes an H-bond with Asn233 similar to compound **8** (Figure S8A).[56] In the third structure showing VIM-2 in complex with hydrolyzed biapenem, a carbapenem (PDB code 6Y6J, Figure S8B), the carboxylate group of the hydrolyzed substrate makes an H-bond with Arg228, not with Asn233.[57] In this complex, the Asn233 side chain adopts a different orientation because of a different arrangement of the Gly232-Asn233 segment, and the backbone NH of the residue is here not available for interaction with the biapenem carboxylate.

*2.5.2. Crystal Structure of NDM-1 in the Presence of Compounds **8** and **26**. 2.5.2.1. Compound **8**.* The incubation of NDM-1 crystals with compound **8** as well as any other trial to trap a complex describing their interaction invariably produced apo crystals, as a consequence of zinc stripping from both metal-binding sites of the two molecules present in the a.s.u. Indeed, anomalous maps showed a signal for zinc ions higher than 20 sigma in the case of NDM-1 in complex with **26** (see below and Figure S9A), while no Zn^{II} signal was detectable in the structure of NDM-1 treated with **8** (1.58 Å resolution; Figure S9B). Moreover, incubation of NDM-1 with compound **8** resulted in shifting or even disordering of highly conserved residues defining the zinc coordination site (Figure S9C). Despite a generally high structural homology (r.m.s.d. over backbone Cα of 0.5 Å), active-site loops in our apo structure are slightly to markedly rearranged even in comparison to previously solved apo-NDM-1 (PDB 3RKJ[58]), as shown in Figure S9D. In particular, the loop 120−127 (including His122 and Asp124 involved in Zn^{II} coordination) shows a very high flexibility, loses its helical pattern, and moves toward the solvent in the apo structure obtained from treatment with compound **8**. This result is in agreement with native MS experiments.

*2.5.2.2. Compound **26**.* The structure of NDM-1 in complex with compound **26** has been determined at 1.5 Å resolution. Two monomers of NDM-1 (chain A visible from residue Glu40 to Arg270, chain B clearly defined from residue Glu40 to Met67 and from Gly71 to Arg270) are present in the asymmetric unit (a.s.u.), but **26** is clearly detectable only in the active site pocket of chain A (Figure 9A), as revealed by omit maps at 3-σ shown in Figure 9B.

Crystallographic occupancy of **26** as well as Zn atoms has been refined to 80% in both A and B chains. The 5-phenyl-1,2,4-triazole-3-thione core of compound **26** is clearly resolved in the electron density map and its position perfectly superposes to that of an analogous ligand coordinating the catalytic metal ions through a common motif (Figure 9C), as shown in a previously solved structure (PDB 6TGD[36]). In both cases, the thione group and one of the triazole nitrogen atoms coordinate the two zinc cations in the NDM-1 active site while the phenyl group interacts by π-stacking with the side chain of Trp93 (Figure 9A).

Conversely, the electron density becomes less clearly defined moving along the aliphatic portion connecting the triazole-3-thione core to the carboxylic moiety and the two 2-methylpyridine branches.

The carboxylic moiety of compound **26** is partially stabilized by a salt bridge with Lys211 side chain and a hydrogen bond with Asn220 backbone nitrogen. This interaction is analogous to that of the carboxylate group of compound **8** with the VIM-2 Asn233 backbone nitrogen. Several hydrophobic interactions can occur between **26** aliphatic scaffold and the side chains of Leu65, Met67, Phe70, Val73, and Trp93. The pyridine substituents point toward the solvent and are not involved in specific interactions stabilizing a peculiar state. Since they can experience multiple conformations within NDM-1 active site, the corresponding electron density is poorly defined for this portion of the ligand. As observed in other NDM-1 structures,

https://doi.org/10.1021/acs.jmedchem.2c01257
J. Med. Chem. XXXX, XXX, XXX−XXX

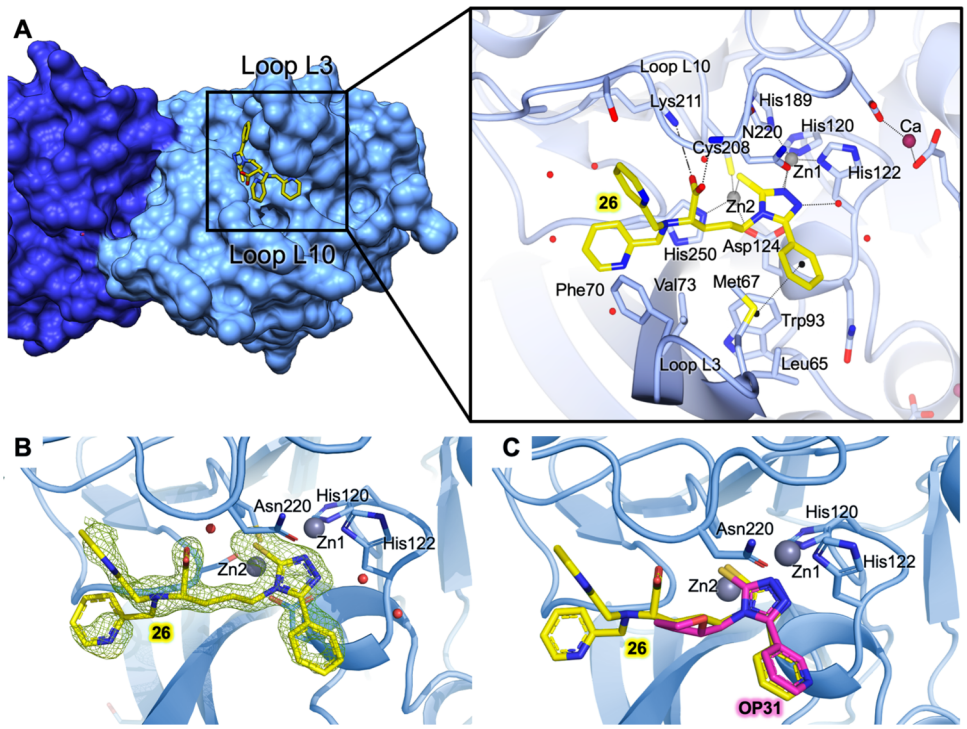

Figure 9. (A) NDM-1 (blue cartoon and carbon atoms; residues in sticks) in complex with compound **26** (in sticks, yellow carbons, PDB code 8A76), with a detailed view of the interactions with NDM-1 residues (A, zoomed inset). (B) Omit map contoured at the 3-σ level. (C) Superposition of **26** (in sticks, yellow carbons) and the triazole-thione-based inhibitor OP31 (in sticks, fuchsia carbons) from PDB 6TGD. Zn ions and water molecules are displayed as gray and red spheres (arbitrary radius), respectively. In all figures, oxygen atoms are colored red, nitrogen blue, and sulfur yellow.

the loop between residues Asp66 and Gly71 (Loop L3) is slightly less defined than the rest of the protein, especially in the case of Asp66 and Phe70 side chains.

2.6. *In Vitro* Antibacterial Synergistic Activity. Considering the high inhibitory potency of numerous compounds toward VIM-type and NDM-1 enzymes, the potential synergistic activity of 32 compounds was tested using a broth microdilution method on several MBL-producing multidrug-resistant clinical isolates. Tested at a fixed concentration of 32 μg/mL, many compounds were able to reduce the minimum inhibitory concentration (MIC) of meropenem toward VIM-1- or VIM-4-producing *K. pneumoniae* bacteria, VIM-2-producing *P. aeruginosa*, and NDM-1-producing *E. coli* clinical isolates, although the results were not totally correlated with the inhibitory potencies against the corresponding MBLs (Table 8). Compounds **3**, **6**, and **7** were similarly unable to significantly reduce meropenem MICs against both isolates. While it was expected for **3** and **7** because of their low activity against all enzymes, **6** displayed submicromolar to micromolar inhibitory potencies against VIM-1 and VIM-4 enzymes. Its inactivity might be the result of poor bacteria wall penetration. By contrast, compound **8**, which similarly inhibited VIM-4 (10-fold more potent on VIM-1 than **6**), fully restored the susceptibility of *K. pneumoniae* isolates to meropenem (about 250- and 500-fold reduction of MIC for VIM-1- and VIM-4-producing bacteria, *i.e.*, 8 and 9 dilutions, respectively). Remarkably, **8** was also highly potent on the NDM-1-producing *E. coli* clinical isolate (1000-fold reduction of meropenem MIC), and showed a significant potentiation (16-fold) of meropenem activity on a VIM-2-producing *P. aeruginosa* clinical isolate, with a resulting MIC below the EUCAST resistance breakpoint. Close analogues, which displayed comparable inhibitory potencies, showed similar potentiation activities. It is the case of the D isomer **9** and all compounds differing by the alkyl length (**11**, **12**, **14**) or the substituent at position 5 of the triazole (**41**−**45**). However, compound **10**, which inhibited both VIM-type enzymes in the low micromolar to submicromolar range, was inactive in this microbiological assay, suggesting that the α-carboxylic group of **8** was essential to reach sufficient concentration in the bacteria periplasm.

In the case of the homo- ($R^2 = R^3$) **23** and **25**−**30**, and hetero-disubstituted (R^2 = imidazol-4-yl (4Im), $R^3 \neq$ imidazol-4-yl) **31**−**40** compounds, their potentiation activity against VIM-producing clinical isolates was highly dependent on the structure of R^2/R^3 substituents. Indeed, while the homo-disubstituted **23** (di-5-methylimidazol-4-yl) and **26** (dipyrid-2-yl) and their corresponding hetero-disubstituted **31** and **36** behaved as **8** as expected (also the case of **33** and the slightly less potent **39**), the low micromolar to submicromolar VIM inhibitors **25** and **27**−**30** and the hetero-disubstituted **37**, **38**, and **40** were moderately (up to 16-fold MIC reduction on VIM-producing *K. pneumoniae* isolates) or not active (on VIM-2-producing *P. aeruginosa* isolates). The hetero-disubstituted **32** and **35** were also poorly active on VIM-producing *K. pneumoniae* isolates despite they were micromolar VIM inhibitors. In contrast, the results correlated well with the corresponding inhibitory potencies in the case of the NDM-1-producing isolate, except for compounds **23**, **38**, and **39**, which were unexpectedly moderately active (respectively, 32-, 8-, and 16-fold MIC decrease) despite inhibitory potencies similar to **8** or **26**. In these two series, compounds **26**, **31**, **33**, and **36** were as active as **8**.

https://doi.org/10.1021/acs.jmedchem.2c01257
J. Med. Chem. XXXX, XXX, XXX−XXX

Table 8. Antibacterial Synergistic Activity of Compounds on VIM-1, VIM-2, VIM-4,-and NDM-1 Producing Clinical Isolates with Meropenem Determined by the Broth Microdilution Method

	meropenem MIC[a] (μg/mL)			
cpd (32 μg/mL)	*K. pneumoniae* 7023 (bla_{VIM-1}^{+})	*K. pneumoniae* VA-416/02 (bla_{VIM-4}^{+})	*P. aeruginosa* VA-182/00 (bla_{VIM-2}^{+})	*E. coli* SI-004 (bla_{NDM-1}^{+})
none	16	16	128	64
3	2	4	128	64
6	2	4	128	64
7	2	4	128	64
8	0.03	0.03	8	0.06
9	0.03	0.03	8	0.06
10	4	1	128	32
11	0.03	0.03	16	0.06
12	0.06	0.03	8	0.06
14	0.03	0.03	16	0.06
23	0.03	0.03	16	2
25	2	1	128	64
26	0.06	0.03	16	0.06
27	4	1	128	64
28	4	2	128	32
29	1	1	128	32
30	1	1	128	32
31	0.06	0.03	8	0.06
32	2	4	128	32
33	0.06	0.06	8	0.06
35	2	2	128	32
36	0.06	0.03	8	0.06
37	4	1	128	64
38	4	1	128	8
39	0.12	0.06	16	4
40	1	2	128	32
41	0.03	0.03	8	0.06
42	0.03	0.03	8	0.06
43	0.03	0.03	8	0.06
44	0.03	0.06	8	0.06
45	0.06	0.12	8	0.06

[a]Minimal inhibitory concentration. ND, not determined.

Overall, the results suggested that the potentiation activity of the compounds exhibited a structure dependence similar to that highlighted for NDM-1 inhibition, *i.e.*, the importance of a carboxylate group and of two heterocycles possessing an unsubstituted nitrogen at position adjacent to the branching atom. Indeed, only compounds **23** (di-5-methyl-4Im), **26**, (di-pyrid-2-yl), **31** (4Im/5-methyl-4Im), **33** (4Im/2Im), and **36** (4Im/pyrid-2-yl) showed similar activities as **8** and di-4Im analogues (with the exception of **23** in the case of the NDM-1-producing bacteria). Exceptions to this rule were the homo-disubstituted **28** (di-pyrazinyl), **29** (di-thiazol-4-yl), and the corresponding hetero-disubstituted **38** (4Im/pyrazinyl) and **39** (4Im/thiazol-4-yl). As suggested for NDM-1 inhibition, this different behavior might be due to significantly divergent physicochemical properties between imidazole or pyridine and other heterocycles (i.e., pyrazine and thiazole), possibly associated with differences in zinc chelation strength.

It generally appeared that the structural features favorable to high synergistic activity are the same as for potent NDM-1 inhibition, which relate, at least in part, to the compound's capacity to bind metal ions.

Furthermore, as compound **8** was identified as a very interesting inhibitor, its synergistic activity was also evaluated on VIM-1-producing clinical *P. aeruginosa* isolate (ARS243 strain) and a VIM-4-producing environmental *P. aeruginosa* strain (FAPL-B64) collected in an urban river.[59] In the presence of compound **8** at 32 μg/mL, the MIC of meropenem decreased from 128 to 8 μg/mL toward both VIM-producing isolates, therefore showing similar efficiency as observed with the VIM-2 producing *P. aeruginosa* clinical isolate (Table 8). Overall, these data support the ability of such compounds (**8** and close analogues showing synergistic activity) to readily accumulate in the periplasm of Gram-negative bacteria, including that of bacteria known to have a particularly selective outer membrane (*e.g. P. aeruginosa*), representing a major progress compared to previously published series of triazole-thione inhibitors.[37,41]

Finally, and to further establish true synergism between compound **8** and meropenem, a chequerboard analysis was carried out with the NDM-1-, VIM-1-, and VIM-4-producing *Enterobacterales* strains (Table 9). Using cation-adjusted

Table 9. Chequerboard Analysis Showing the Drug−Drug Interaction between Compound 8 and Meropenem

	meropenem MIC[a] (μg/mL)		
[**8**] (μg/mL)	*K. pneumoniae* 7023 (bla_{VIM-1}^{+})	*K. pneumoniae* VA-416/02 (bla_{VIM-4}^{+})	*E. coli* SI-004 (bla_{NDM-1}^{+})
0	16	16	64
32	0.03	0.03	0.03
16	0.06	0.06	0.06
8	1	1	32
4	2	2	32
2	4	4	64
1	8	8	64
0.5	16	16	64

[a]Experiments were performed in duplicate.

Mueller−Hinton broth as the culture medium, a striking difference in the activity of the combination emerged between strains producing either NDM-1 or VIM-type enzymes. With the former, the synergistic activity of **8** was only observed at concentrations ≥16 μg/mL, but completely vanished at lower concentrations. By contrast, the MIC of meropenem varied in a dose-dependent manner with the concentration of **8** with both VIM-1- and VIM-4-producing strains, allowing to compute an average FICI of 0.34 in both cases, reflecting true synergism rather than an additive effect. Interestingly, meropenem MIC values corresponding to susceptible phenotypes were measured with these strains at concentrations as low as 4 μg/mL (for comparison, vaborbactam is tested at a fixed concentration of 8 μg/mL).

Although it is tempting to correlate the different behavior of the combination on NDM-1-producing strain with its peculiar mechanism of inhibition (in which the zinc stripping effect and subsequent formation of the inactive apo-enzyme seem more important than with the VIM-type enzymes), we cannot exclude the impact of other strain-related factors, such as increased efflux or permeability-related resistance mechanisms, in that peculiar isolate. Microbiological testing on a larger set of MBL-producing isolates is needed to better understand these aspects, *i.e.*, to identify the best partner antibiotic and potential cross-resistance mechanisms, to determine the

https://doi.org/10.1021/acs.jmedchem.2c01257
J. Med. Chem. XXXX, XXX, XXX−XXX

optimal concentration of the inhibitor and to compare its activity with that of comparators (*e.g.* taniborbactam, ANT2681). Nonetheless, this is the first demonstration that meropenem resistance could be reversed *in vitro* with extensively drug resistance MBL-producing *K. pneumoniae* isolates by 1,2,4-triazole-3-thione inhibitors at clinically useful concentrations.

2.7. Cytotoxicity Assays on Mammalian Cells. The potential cytotoxic activity of five compounds was evaluated using a membrane integrity assay (CytoTox 96, Non-Radioactive Cytotoxicity Assay, Promega). They were tested for their ability to induce the lysis of HeLa cells at concentrations up to 250 μM (Table 10).

Table 10. Cytotoxic Activity against HeLa Cells

cpd	HeLa cells IC_{50} (μM)
8	>250
12	>250
23	141 ± 25
31	105 ± 35
36	175 ± 18

Half of the tested compounds (**8**, **12**) showed IC_{50} values > 250 μM, indicating that they do not induce cell lysis. Others displayed moderate toxicity with IC_{50} values > 100 μM (*i.e.*, **23**, **31**, **36**). Interestingly, the less toxic compounds **8** and **12** are diimidazole analogues, while the more toxic **23** and **31** are very close in structure and contained at least one 5-methylimidazole.

A further evaluation of their potential cytotoxicity was performed using the RealTime-Glo MT Viability Assay, which substantially confirmed these results.

2.8. Study of ADME and Selectivity Profiles *In Vitro*. Five compounds were evaluated for their absorption, distribution, metabolism, excretion (ADME) and selectivity profiles toward human metalloenzymes. All were potent inhibitors of VIM-type enzymes and NDM-1 and showed similar activities in microbiological assays, but displayed significant structural differences, which may influence their bioavailability and selectivity. Compounds **12** (one methylene less in the alkyl chain), **26** (di-pyrid-2-yl), **31** (4Im/5Me4Im), and **42** (naphth-2-yl at position 5) have been compared to the reference analogue **8**.

2.8.1. ADME Profile. Data are presented in Table 11.

Both compounds were highly soluble in aqueous buffer. They also showed Log *D* values around −2, except, as expected, the more hydrophobic **26** and **42**. They were all fully stable in mouse plasma for at least 6 h. Compounds **8**, **31**, and **42** were also fully or almost fully stable in the presence of mouse microsomes for at least 40 min, while **12** and more particularly **26** with two pyridyl groups showed slightly lower stability. Finally, binding to proteins of mouse plasma was measured to about 55−70% for all compounds except **42**, which bound to plasma proteins more strongly (95%) probably because of its naphthyl group. Overall, these data were very favorable.

2.8.2. Selectivity Profile. The same compounds were tested against four mammalian metalloenzymes to evaluate their selectivity and therefore possible off-target effect related to their metal-binding properties (Table 12). These enzymes were metallopeptidases from the M1 and M16 families (human IDE, (Insulin Degrading Enzyme), porcine APN (Aminopeptidase *N*), mouse ERAAP (Endoplasmic Reticulum Aminopeptidase associated with antigen Processing)) or hydrolases (human HDAC6 (Histone DeAcetylase 6)).

Table 12. Selectivity Profile toward Mammalian Metalloenzymes.

	IC_{50} [CI 95%][a] (μM) or (% inhibition at 100 μM)			
cpd	IDE[b]	APN[c]	ERAAP[d]	HDAC6[e]
8	20 [16−25]	30 [20−40]	(51%)	NI[f]
12	17 [12−20]	27 [10−79]	(51%)	NI
26	41 [32−63]	(30%)	(13%)	NI
31	35 [31−40]	(58%)	(42%)	NI
42	9.1 [7.9−10.0]	16 [13−20]	(63%)	NI

[a]IC_{50} values are reported with their 95% confidence intervals in brackets (one experiment in duplicate). [b]IDE, Insulin Degrading Enzyme, the enzymatic assay was performed with ATTO 655-Cys-Lys-Leu-Val-Phe-Phe-Ala-Glu-Asp-Trp as a substrate and BDM44768 as a control inhibitor (65% inhibition at 0.4 μM). [c]APN, Aminopeptidase *N*, the enzymatic assay was performed with H-Leu-AMC as a substrate and bestatin as a control inhibitor (48.6% inhibition at 3.0 μM). [d]ERAAP, Endoplasmic Reticulum Aminopeptidase associated with Antigen Processing, the enzymatic assay was performed with H-Leu-AMC as a substrate and a not disclosed in-house inhibitor as a control (55.7% inhibition at 4.0 μM). [e]HDAC6, Histone DeAcetylase 6, the enzymatic assay was performed using the kit HDAC6 Fluorimetric Assay from Enzo Life Sciences with Fluor de Lys as a substrate and panobinostat as a control inhibitor (96.3% inhibition at 5.0 μM). [f]NI, No Inhibition (≤10% at 100 μM).

All compounds were poor or not inhibitors of ERAAP and HDAC6, respectively. Significant inhibitory activity was

Table 11. ADME Profile *In Vitro*

				microsomes[d]		
cpd	solubility (μM)[a]	Log *D*[b]	plasma[c] $t_{1/2}$ (h)	$t_{1/2}$ (min)	Cl_{int} (μL/min/mg)	plasma proteins binding (%)[e]
8	≥200	−2.117 ± 0.107	>6	>40	stable	67.6
12	≥200	−2.201 ± 0.030	>6	>40 (91.2%)	10.6	55.0
26	≥200	0.243 ± 0.003	>6	>40 (80.5%)	16.5	68.7
31	≥200	−1.925 ± 0.029	>6	>40 (98.1%)	5.5	62.3
42	≥200	−0.823 ± 0.012	>6	>40	stable	95.2

[a]Solubility was evaluated in 10 mM phosphate buffer saline (PBS), pH 7.4. [b]Log *D* was measured by mixing in 10 mM PBS pH 7.4/*n*-octanol (1:1). [c]Stability in plasma was evaluated at 37 °C using mouse plasma, mix gender, with enalapril as control ($t_{1/2}$ = 1h03). [d]Microsomal stability was evaluated at 37 °C using mouse microsomes, mix gender, with propranolol as control (31% remaining after 40 min), remaining intact compound after 40 min is indicated between parentheses. [e]Binding to plasma proteins was evaluated using mouse plasma, mix gender, with diclofenac as control (>95% binding).

https://doi.org/10.1021/acs.jmedchem.2c01257
J. Med. Chem. XXXX, XXX, XXX−XXX

measured against IDE and APN. Compound **42** (5-naphth-2-yl) displayed IC_{50} values of 9.1 and 16 μM against IDE and APN, respectively, being the less selective in the series. Most compounds displayed at least 2-log selectivities on MBLs in comparison to enzymes in the selectivity panel.

3. CONCLUSIONS

In previously published 1,2,4-triazole-3-thione-based series, we identified potent MBL inhibitors with either broad spectrum (*i.e.*, VIM-type enzymes, NDM-1 and IMP-1)[35,37,40,42] or narrower spectrum (*i.e.*, VIM-type MBLs) of inhibition.[38,41] The most potent analogues generally showed submicromolar inhibitory potencies against VIM-type enzymes, and for a few of them, micromolar activity against NDM-1 and IMP-1. Despite their high inhibitory potencies, one limitation was often their ability to restore the susceptibility of multiresistant MBL-producing clinical isolates to meropenem. Indeed, compounds of the "hydrazone" series were devoid of synergistic activity despite potent inhibitory potencies.[35] Some activity could be obtained in the presence of a sub-toxic concentration of colistin indicating that their inactivity may originate from poor outer membrane penetration. But replacing the hydrolysis susceptible N=CH link by a CH_2–CH_2 segment and further exploring various substituents at position 4 of the triazole ring allowed the identification of several compounds able to decrease the MIC of meropenem toward MBL-producing clinical isolates up to 16-fold, although limited to VIM-producing *Enterobacterales*.[37,38,41,42]

Compared to these previous series, the present one displayed two major improvements. First, while most potent compounds inhibited VIM-type enzymes with K_i values in the same submicromolar range as compounds of previous series, a strong increase in inhibitory potency against NDM-1 (K_i values of 10–40 nM, about 100-fold more potent than best compounds in previous series) was observed. In particular, it is noteworthy that the close analogue JMV6290 (Table 1) only poorly inhibited this enzyme. Second, the synergistic activity of the most potent compounds was much significantly improved and was for the first time observed on Gram-negative nonfermenters (i.e., *P. aeruginosa*). The MIC of meropenem was decreased in the presence of compound **8** and few others by 266-, 533-, and 1066-fold toward VIM-1- and VIM-4-producing *K. pneumoniae* (compared to up to 16-fold only with the best compounds of the previous series) and NDM-1-producing *E. coli* (no synergistic activity in the previous series), respectively. In addition, compound **8** and others also decreased the MIC of meropenem below the resistance breakpoint (according to EUCAST) toward a VIM-2-producing extremely drug-resistant (XDR) *P. aeruginosa* clinical isolate (no activity in previous series). This result was confirmed for **8** with VIM-1- and VIM-4-producing *P. aeruginosa*. Although the decrease was more modest (16-fold), this result was quite encouraging because the outer membrane of *Pseudomonas* bacteria is known to be more impervious to drugs.

Both improvements (*i.e.*, high NDM-1 inhibitory potency and potent activity in microbiological assays) were generally dependent on the presence at the 4-position of the triazole heterocycle of a zinc-chelating moiety formed by an α-amino acid residue Nα-disubstituted by two heteroaryl groups bearing a nitrogen adjacent to the branching link, providing that they are imidazole and/or pyridine heterocycles but not the more acidic pyrazine and thiazole groups. According to structure–activity relationships, such structural property did not seem to have much influence on VIM-type enzyme inhibition compared to NDM-1. However, it is crucial for full synergistic activity on both VIM- and NDM-1-producing clinical isolates. For instance, compounds **27** (di-pyridin-3-yl) and **30** (di-thiazol-5-yl), which do not obey this rule are only active on VIM-producing *K. pneumoniae* isolates reducing meropenem MIC by up to 16-fold, despite similar VIM inhibitory potencies as compound **8**. Therefore, they behave similarly to the best compounds of the previous series.

Experiments including equilibrium dialysis, native MS, and ITC showed that tested compounds inhibited both VIM-2 and NDM-1 at least partially by zinc stripping. This mixed mode of inhibition was confirmed by X-ray crystallography as compound **8** was found to interact in VIM-2 active site in the same manner as in previously reported complexes involving 1,2,4-triazole-3-thione inhibitors,[35,37,38] while it was not able to form a stable complex with NDM-1 but completely removed its zinc ions. In contrast, compound **26** could form a ternary complex with NDM-1. Finally, IMP-1 activity was not as disturbed by such motif. The reason might be a lower accessibility of its zinc ions and/or a higher affinity for these metals.[60] However, some of the best compounds identified in the present series also inhibited IMP-1 with K_i values in the low micromolar range.

The potent and broad-spectrum MBL inhibition by compound **8** and analogues, their remarkable synergistic activity, and their favorable properties in terms of ADME, toxicity, and selectivity profiles make these compounds highly promising. Furthermore, their spectrum of MBL inhibition is somewhat broader than that of ANT2681,[29] which is prevalently active on NDM-1-producing *Enterobacterales* in combination with meropenem, and the synergistic activity of our best compounds, when tested in combination with meropenem, seems at least comparable to that of cefepime-taniborbactam.[27] However, a large-scale microbiological study, currently underway, is required to better position our compounds in the competitive landscape (besides identifying the best partner antibiotic, optimal inhibitor concentration, and potential resistance mechanisms). They are also currently further investigated to evaluate their potency toward other VIM and NDM variants, other acquired MBLs (*e.g.* SIM-1, SPM-1), and their *in vivo* activity.

Overall, this article highlights the validity of this new class whose optimization led to potent MBL inhibitors, which are shown to reverse carbapenem resistance on XDR MBL-producing *Enterobacterales* clinical isolates at clinically achievable concentrations.

4. EXPERIMENTAL SECTION

4.1. Chemistry. *4.1.1. General Procedures. 4.1.1.1. NMR.* ^{1}H NMR and ^{13}C NMR spectra were recorded at room temperature on a 300, 400, or 500 MHz instrument in [D_6]DMSO solutions (unless otherwise indicated). Chemical shifts are reported in parts per million (ppm) relative to residual solvent signals (DMSO: 2.50 ppm for ^{1}H and 39.52 for ^{13}C). Splitting patterns in ^{1}H NMR spectra were designated as follows: s, singlet; d, doublet; t, triplet; q, quartet; m, multiplet; br, broad.

4.1.1.2. Thin-Layer Chromatography (TLC). Thin-layer chromatographies were performed on aluminum-backed sheets of silica gel F_{254} (0.2 mm), which were visualized under 254 nm light, and by spraying with a 2% ninhydrin solution in ethanol followed by heating, or by charring with an aqueous solution of ammonium sulfate and

https://doi.org/10.1021/acs.jmedchem.2c01257
J. Med. Chem. XXXX, XXX, XXX–XXX

sulfuric acid (200 g $(NH_4)_2SO_4$ and 40 mL concentrated sulfuric acid in 1 L of water).

4.1.1.3. Analytical Reversed-Phase HPLC. Samples were prepared in an acetonitrile/water (50/50 v/v) mixture. RP-HPLC analyses were performed on a Chromolith SpeedRod C18 column (0.46 × 5 cm) by means of a linear gradient (0−100%) of 0.1% TFA/acetonitrile in 0.1% aqueous TFA over 5 min, and at a flow rate of 3 mL/min.

4.1.1.4. Liquid Chromatography−Mass Spectrometry (LC−MS). The LC/MS system consisted of a Waters Alliance 2690 HPLC, coupled to a Waters Micromass ZQ spectrometer (electrospray ionization mode, ESI+). All analyses were carried out using a C18 monolithic Onyx Phenomenex 2.5 × 0.46 cm column. The flow rate was set to 3 mL/min with eluent A (water/0.1% formic acid) and a gradient of 0 → 100% of eluent B (acetonitrile/0.1% formic acid) over 3 min was then used. Positive-ion electrospray mass spectra were acquired at a solvent flow rate of 100−500 μL/min. Nitrogen was used as both the nebulizing and drying gas. The data were obtained in a scan mode in 0.1 s intervals; 10 scans were added up to get the final spectrum. High-resolution mass spectrometry (HRMS) were registered on a JEOL JMS−SX-102A mass spectrometer.

4.1.1.5. Purification. (i) Column chromatography was performed using Merck silica gel 60 of particle size 40−63 mm. (ii) Reversed-phase preparative HPLC purification of final compounds was performed on a Waters Delta Pak C18 column (40 mm × 100 mm, 15 μm, 100 Å) by means of a linear gradient of eluent B in A at a 1%/min rate (flow rate: 28 mL/min). Eluent A: water, 0.1% TFA; eluent B: acetonitrile, 0.1% TFA.

All final compounds (except **1**) were obtained as TFA salts after freeze-drying. All are ≥95% pure as determined by RP-HPLC.

ADME and selectivity profiles were established as described in the Supporting Information.

4.1.2. General Procedure for the Preparation of 1,2,4-Triazole-3-thiones. The 1,2,4-triazole-3-thione heterocycle was built according to Deprez-Poulain et al.[43] and as described[41] from various hydrazides R^1-$CONHNH_2$ and amines (Boc-Orn-OH (n = 3), Boc-*D*-Orn-OH, Boc-Lys-OH (n = 4), Boc-Dab-OH (n = 2), Boc-Dap-OH (n = 1), *N*-Boc-1,4-diaminobutane).

4.1.2.1. Thiosemicarbazide Intermediates. The amine compound (0.5 mmol, 1 equiv), Na_2CO_3 (1 mmol, 2 equiv, added if hydrochloride salt), and DPT (117 mg, 0.5 mmol, 1 equiv) were solubilized in anhydrous DMF (5 mL). The mixture was stirred at 55 °C for 1.5 h. The hydrazide R^1-$CONHNH_2$ (0.55 mmol, 1.1 equiv) was then added, and the mixture was again heated at 55 °C for 1.5 h. After cooling to room temperature, AcOEt and water were added and the organic phase was washed fivefold with water, dried over $MgSO_4$, filtered, and concentrated under vacuum. The product was used in the next step without purification.

4.1.2.2. Cyclization. The thiosemicarbazide intermediates were solubilized in a mixture of water and ethanol (2:3, 1 mL/20 mg) and Na_2CO_3 (4 equiv) was added. The reaction was refluxed for 2−4 h. The mixture was then neutralized with a saturated aqueous $KHSO_4$ solution, and the aqueous phase was extracted twice with AcOEt. The organic phases were mixed and dried over $MgSO_4$, filtered, and evaporated under vacuum. The residues were purified by gel column chromatography (AcOEt/Hexane).

4.1.3. General Procedure for Boc Removal. The Boc protecting group was removed by treatment with a mixture dioxane and conc. HCl (2:1, 10 mL/100 mg) in the presence of anisole (3 equiv). The reaction was stirred at 45 °C for 1 h. The solvents were then evaporated to yield the hydrochloride salts of the deprotected amine compounds as powders.

4.1.4. General Procedures for Reductive Amination. 4.1.4.1. Synthesis of Homo-Disubstituted Compounds. Protocol A. To a solution of the hydrochloride salt of a deprotected amine compound (1 equiv) in absolute ethanol (1 mL/30 mg) were added triethylamine (2 equiv) and an aldehyde (5 equiv). The reaction mixture was stirred for 10 min under inert atmosphere, and $NaBH_3CN$ (5 equiv) was added portion-wise. The mixture was further stirred until reaction completion and evaporated. The residue was purified by preparative RP-HPLC to yield the homo-disubstituted compound as a TFA salt. According to the aldehyde compound, completion was not attained and a significant amount of monosubstituted compound was recovered during purification. This monosubstituted analogue could be further submitted to protocol C (see below) to give either homo- or hetero-disubstituted analogues.

4.1.4.2. Synthesis of Monosubstituted Compounds. Protocol B. The hydrochloride salt of an amine compound (1 equiv) was solubilized in anhydrous DMF and a few 4 Å molecular sieves were added. The mixture was cooled to 0 °C, and an aldehyde (2−5 equiv) was added. The reaction was stirred at 0 °C for 15 min and at rt for 3 h. The mixture was again cooled to 0 °C, and $NaBH_4$ (3 equiv) was added portion-wise. After one night at rt, water was added and the reaction mixture was evaporated to yield the expected monosubstituted analogue, which was purified by preparative RP-HPLC or directly use in protocol C.

4.1.4.3. Synthesis of Homo- and Hetero-Disubstituted Compounds from the Corresponding Monosubstituted Ones. Protocol C. A monosubstituted analogue (1 equiv) was dissolved in a mixture of anhydrous DMF/AcOH (98:2, 1 mL/30 mg), and an aldehyde (3 equiv) was added. The reaction was stirred at rt for 15 min, and $NaBH_3CN$ (3 equiv) was added portion-wise. After stirring at rt overnight, the mixture was evaporated, and the residue was purified by preparative RP-HPLC.

*4.1.5. Characterization of Final Compounds. 4.1.5.1. tert-Butyl N-[4-(3-Phenyl-5-sulfanylidene-4,5-dihydro-1H-1,2,4-triazol-4-yl)-butyl]-carbamate (**1**).* Purified on silica gel column (Hex/EtOAc, 9:1 to 1:1). Colorless oil, 216 mg (72%); UPLC-MS t_R: 3.01 min; m/z (ES+) 349.3 ($M + H^+$); ^1H NMR (600 MHz, DMSO-d_6): 13.96 (s, 1H), 7.67−7.55 (m, 5H), 6.73 (t, J = 5.6 Hz, 1H), 4.05−4.01 (m, 2H), 2.78−2.75 (m, 2H), 1.52−1.47 (m, 2H), 1.34 (s, 9H), 1.23−1.19 (m, 2H); ^{13}C NMR (151 MHz, DMSO-d_6): 167.1, 155.5, 151.2, 130.8, 129.1, 128.6, 126.2, 77.4, 43.5, 28.3, 26.5, 25.2; HRMS (ESI+) calcd for $C_{17}H_{25}N_4O_2S$ ($M + H$)$^+$ 349.1698, found 349.1705.

*4.1.5.2. (2S)-2-(Benzylamino)-5-(3-phenyl-5-sulfanylidene-4,5-dihydro-1H-1,2,4-triazol-4-yl)pentanoic Acid (**2**).* Purification by RP-HPLC (0.1% TFA in water/MeCN, 100:0 to 70:30 in 30 min). White powder, 25 mg (17%); UPLC-MS t_R: 1.92 min; m/z (ES+) 383.3 ($M + H^+$); ^1H NMR (600 MHz, DMSO-d_6): 13.98 (s, 1H), 9.19 (bs, 1H), 7.67−7.55 (m, 5H), 7.41−7.38 (m, 5H), 4.10−4.08 (m, 2H), 4.02−4.00 (m, 2H), 3.65 (bs, 1H), 1.75−1.58 (m, 4H); ^{13}C NMR (151 MHz, DMSO-d_6): 170.6, 167.2, 151.1, 130.8, 129.7, 129.1, 128.7, 128.6, 126.0, 58.8, 49.6, 43.2, 26.5, 23.8; HRMS (ESI+) calcd for $C_{20}H_{23}N_4O_2S$ ($M + H$)$^+$ 383.1542, found 383.1537.

*4.1.5.3. (2S)-2-(Dibenzylamino)-5-(3-phenyl-5-sulfanylidene-4,5-dihydro-1H-1,2,4-triazol-4-yl)pentanoic Acid (**3**).* Purification by RP-HPLC (0.1% TFA in water/MeCN, 100:0 to 70:30 in 30 min). White powder, 30 mg (29%); UPLC-MS t_R: 3.15 min; m/z (ES+) 473.4 ($M + H^+$); ^1H NMR (500 MHz, DMSO-d_6): 13.97 (s, 1H), 12.35 (bs, 1H), 7.61−7.49 (m, 5H), 7.31−7.24 (m, 10H), 4.03−3.90 (m, 2H), 3.74−3.60 (m, 4H), 3.01 (s, 1H), 1.69−1.42 (m, 4H); ^{13}C NMR (126 MHz, DMSO-d_6): 172.9, 167.2, 151.2, 138.5, 130.8, 129.1, 129.0, 128.6, 128.4, 127.4, 126.2 (2C), 60.2, 54.1 (2C), 43.4, 25.4, 25.0; HRMS (ESI+) calcd for $C_{27}H_{29}N_4O_2S$ ($M + H$)$^+$ 473.2011, found 473.2009.

*4.1.5.4. (2S)-2-{[2-(p-Toluyl)eth-2-yl]amino}-5-(3-phenyl-5-sulfanylidene-4,5-dihydro-1H-1,2,4-triazol-4-yl)pentanoic Acid (**4**).* Purification by RP-HPLC (0.1% TFA in water/MeCN, 90:10 to 60:40 in 30 min). Diastereomeric mixture. White powder, 65 mg (26%), LC-MS t_R: 2.17 and 2.19 min; m/z (ES+) 411.1 ($M + H^+$); ^1H NMR (500 MHz, DMSO-d_6): 14.04, 14.02 (2s, 1H), 9.16 (bs, 1H), 7.67−7.52 (m, 5H), 7.33−7.25 (m, 2H), 7.24−7.18 (m, 3H), 4.30−4.20 (m, 1H), 4.11−3.99 (m, 2H), 3.55−3.51 (m, 0.5H), 3.27−3.22 (m, 0.5H), 2.30 (s, 3H), 1.74−1.38 (m, 7H); ^{13}C NMR (126 MHz, DMSO-d_6): 169.9 and 169.7, 167.3, 151.2 and 151.1, 138.8 and 138.7, 133.5 and 133.3, 130.9, 129.7 and 129.5, 129.2, 128.62 and 128.60, 127.9 and 127.8, 126.04 and 126.01, 56.8 and 56.7, 56.5 and 56.1, 43.0, 26.63 and 26.60, 23.61 and 23.56, 20.8, 19.2 and 19.0; HRMS (ESI+) calcd for $C_{22}H_{27}N_4O_2S$ ($M + H$)$^+$ 411.1855, found 411.1859.

4.1.5.5. (2S)-2-{[(2,3-Dihydroxyphenyl)methyl]amino}-5-(3-phenyl-5-sulfanylidene-4,5-dihydro-1H-1,2,4-triazol-4-yl)pentanoic

https://doi.org/10.1021/acs.jmedchem.2c01257
J. Med. Chem. XXXX, XXX, XXX−XXX

*Acid (**5**).* Purification by RP-HPLC (0.1% TFA in water/MeCN, 100:0 to 70:30 in 30 min). White powder, 63 mg (44%); LC-MS t_R: 0.90 min; *m/z* (ES+) 415.0 (M + H$^+$); ^{1}H NMR (400 MHz, DMSO-d_6): 13.97 (s, 1H), 9.52, (s, 1H), 7.67−7.56 (m, 5H), 6.80 (dd, *J* = 1.4, 7.7 Hz, 2H), 6.69 (dd, *J* = 1.4, 7.7 Hz, 2H), 6.66−6.62 (m, 1H), 4.08−4.04 (m, 2H), 4.01−3.94 (m, 2H), 3.62−3.60 (m, 1H), 1.76−1.55 (m, 4H); ^{13}C NMR (101 MHz, DMSO-d_6): 170.1, 167.2, 151.1, 145.3, 144.5, 130.8, 129.1, 128.6, 126.0, 121.2, 119.2, 118.9, 116.0, 58.6, 45.1, 43.2, 26.5, 23.9; HRMS (ESI+) calcd for $C_{20}H_{23}N_4O_4S$ (M + H)$^+$ 415.1440, found 415.1447.

*4.1.5.6. (2S)-2-{Bis[(2,3-dimethoxyphenyl)methyl]amino}-5-(3-phenyl-5-sulfanylidene-4,5-dihydro-1H-1,2,4-triazol-4-yl)pentanoic Acid (**6**).* Purification by RP-HPLC (0.1% TFA in water/MeCN, 70:30 to 40:60 in 30 min). White powder, 54 mg (17%); UPLC-MS t_R: 2.81 min; *m/z* (ES+) 593.3 (M + H$^+$); ^{1}H NMR (600 MHz, DMSO-d_6): 13.90 (s, 1H), 12.36 (bs, 1H), 7.59−7.56 (m, 3H), 7.49 (t, *J* = 7.6 Hz, 2H), 6.98 (t, *J* = 7.9 Hz, 2H), 6.92−6.89 (m, 4H), 4.04−3.94 (m, 2H), 3.77 (s, 6H), 3.61 (s, 6H), 2.61 (dt, *J* = 3.7, 1.9 Hz, 2H), 2.52−2.51 (m, 1H), 2.38 (dt, *J* = 3.7, 1.8 Hz, 2H), 1.63−1.45 (m, 4H); ^{13}C NMR (126 MHz, DMSO-d_6): 167.2, 152.3, 151.2, 147.2, 130.8, 129.1, 128.5, 126.1, 123.9, 121.8, 61.0, 60.1, 55.7, 48.4, 43.4, 25.3 (2C); HRMS (ESI+) calcd for $C_{31}H_{37}N_4O_6S$ (M + H)$^+$ 593.2428, found 593.2436.

*4.1.5.7. (2S)-2-{[(1H-Imidazol-4-yl)methyl]amino}-5-(3-phenyl-5-sulfanylidene-4,5-dihydro-1H-1,2,4-triazol-4-yl)pentanoic Acid (**7**).* Purification by RP-HPLC (0.1% TFA in water/MeCN, 100:0 to 70:30 in 30 min). White powder, 230 mg (30%); UPLC-MS t_R: 1.20 min; *m/z* (ES+) 373.2 (M + H$^+$); ^{1}H NMR (500 MHz, DMSO-d_6): 14.03 (s, 1H), 11.39 (bs, 1H), 8.68 (s, 1H), 7.6−7.54 (m, 6H), 4.17−4.06 (m, 4H), 3.85−3.84 (m, 1H), 1.70−1.52 (m, 4H); ^{13}C NMR (126 MHz, DMSO-d_6): 173.4, 167.3, 151.2, 135.5, 130.9, 129.2, 128.6, 127.9, 126.2, 119.5, 58.1, 43.2, 40.6, 26.4, 23.6; HRMS (ESI+) calcd for $C_{17}H_{21}N_6O_2S$ (M + H)$^+$ 373.1447, found 373.1452.

*4.1.5.8. (2S)-2-{Bis[(1H-imidazol-4-yl)methyl]amino}-5-(3-phenyl-5-sulfanylidene-4,5-dihydro-1H-1,2,4-triazol-4-yl)pentanoic Acid (**8**, JMV7061).* Purification by RP-HPLC (0.1% TFA in water/MeCN, 100:0 to 70:30 in 30 min). White powder, 260 mg (21%); UPLC-MS t_R: 1.32 min; *m/z* (ES+) 453.3 (M + H$^+$); ^{1}H NMR (500 MHz, DMSO-d_6): 13.98 (s, 1H), 12.08 (s, 1H), 9.00 (s, 2H), 7.62−7.46 (m, 7H), 4.05−3.93 (m, 2H), 3.79 (s, 4H) 3.17−3.14 (m, 1H), 1.68−1.48 (m, 4H); ^{1}H NMR (500 MHz, D_2O): 8.45 (s, 2H), 7.46−7.36 (m, 5H), 7.14 (s, 2H), 4.04−3.89 (m, 2H), 3.71 (s, 4H), 3.08−3.06 (m, 1H), 1.57−1.34 (m, 4H); ^{13}C NMR (126 MHz, DMSO-d_6): 173.4, 167.2, 151.2, 134.5, 131.0, 130.1, 129.1, 128.5, 126.2, 117.5, 61.3, 44.7, 43.3, 26.0, 24.7; HRMS (ESI+) calcd for $C_{21}H_{25}N_8O_2S$ (M + H)$^+$ 453.1821, found 453.1821.

*4.1.5.9. (2R)-2-{Bis[(1H-imidazol-4-yl)methyl]amino}-5-(3-phenyl-5-sulfanylidene-4,5-dihydro-1H-1,2,4-triazol-4-yl)pentanoic Acid (**9**).* Purification by RP-HPLC (0.1% TFA in water/MeCN, 100:0 to 70:30 in 30 min). White powder, 68 mg (28%); UPLC-MS t_R: 1.33 min; *m/z* (ES+) 453.1 (M + H$^+$); ^{1}H NMR (500 MHz, DMSO-d_6): 13.98 (s, 1H), 13.00 (bs, 1H), 9.01 (s, 2H), 7.62−7.60 (m, 2H), 7.56−7.46 (m, 5H), 4.05−3.90 (m, 2H), 4.09−4.06 (m, 2H), 3.79 (s, 4H), 3.15 (t, *J* = 7.2, 14.5 Hz, 1H), 1.64−1.47 (m, 4H); ^{13}C NMR (126 MHz, DMSO-d_6): 173.4, 167.2, 151.2, 134.5, 131.0, 130.8, 129.1, 128.5, 126.2, 117.5, 61.2, 44.6, 43.3, 26.0, 24.7; HRMS (ESI+) calcd for $C_{21}H_{25}N_8O_2S$ (M + H)$^+$ 453.1821, found 453.1820.

*4.1.5.10. 4-(4-{Bis[(1H-imidazol-4-yl)methyl]amino}butyl)-5-phenyl-4,5-dihydro-1H-1,2,4-triazole-3-thione (**10**).* Purification by RP-HPLC (0.1% TFA in water/MeCN, 95:5 to 65:35 in 30 min). White powder, 204 mg (59%); UPLC-MS t_R: 1.36 min; *m/z* (ES+) 409.3 (M + H$^+$); ^{1}H NMR (600 MHz, DMSO-d_6): 14.32 (bs, 2H), 13.93 (s, 1H), 8.97 (s, 2H), 7.65−7.52 (m, 7H), 4.01−3.98 (m, 2H), 3.69 (s, 4H), 2.38−2.34 (m, 2H), 1.50−1.45 (m, 2H), 1.39−1.32 (m, 2H); ^{13}C NMR (151 MHz, DMSO-d_6): 167.1, 151.1, 134.7, 130.7, 129.4, 129.0, 128.5, 126.2, 118.0, 51.5, 46.6, 43.2, 25.1, 22.6; HRMS (ESI+) calcd for $C_{20}H_{25}N_8S$ (M + H)$^+$ 409.1923, found 409.1923.

*4.1.5.11. (2S)-2-{Bis[(1H-imidazol-4-yl)methyl]amino}-3-(3-phenyl-5-sulfanylidene-4,5-dihydro-1H-1,2,4-triazol-4-yl)propanoic Acid (**11**).* Purification by RP-HPLC (0.1% TFA in water/MeCN, 100:0 to 70:30 in 30 min). White powder, 37 mg (31%); UPLC-MS t_R: 1.12 min; *m/z* (ES+) 425.2 (M + H$^+$); ^{1}H NMR (500 MHz, DMSO-d_6): 14.24 (bs, 2H), 13.98 (s, 1H), 13.25 (bs, 1H), 9.01 (s, 2H), 7.58−7.44 (m, 5H), 7.39 (s, 2H), 4.55−4.44 (m, 2H), 3.86−3.83 (m, 1H), 3.74 (s, 4H); ^{13}C NMR (126 MHz, DMSO-d_6): 171.1, 167.1, 151.3, 134.5, 130.6, 130.0, 128.8, 128.4, 125.8, 117.8, 57.5, 44.7, 42.7; HRMS (ESI+) calcd for $C_{19}H_{21}N_8O_2S$ (M + H)$^+$ 425.1489, found 425.1511.

*4.1.5.12. (2S)-2-{Bis[(1H-imidazol-4-yl)methyl]amino}-4-(3-phenyl-5-sulfanylidene-4,5-dihydro-1H-1,2,4-triazol-4-yl)butanoic Acid (**12**).* Purification by RP-HPLC (0.1% TFA in water/MeCN, 100:0 to 70:30 in 30 min). White powder, 59 mg (26%); UPLC-MS t_R: 1.15 min; *m/z* (ES+) 439.3 (M + H$^+$); ^{1}H NMR (500 MHz, DMSO-d_6): 14.41 (bs, 2H), 14.02 (s, 1H), 13.00 (bs, 1H), 9.06 (s, 2H), 7.64−7.62 (m, 2H), 7.56−7.43 (m, 5H), 4.16 (dt, *J* = 8.0, 15.7 Hz, 1H), 3.95 (dt, *J* = 8.0, 15.7 Hz, 1H), 3.88−3.81 (m, 4H), 3.38 (t, *J* = 7.6 Hz, 1H), 2.11 (dd, *J* = 7.7, 15.9 Hz, 2H); ^{13}C NMR (126 MHz, DMSO-d_6): 172.7, 166.9, 151.4, 134.4, 130.9, 130.7, 128.9, 128.8, 125.9, 117.5, 59.9, 44.6, 42.3, 27.7; HRMS (ESI+) calcd for $C_{20}H_{23}N_8O_2S$ (M + H)$^+$ 439.1665, found 439.1665.

*4.1.5.13. (2S)-2-{[(1H-Imidazol-4-yl)methyl]amino}-6-(3-phenyl-5-sulfanylidene-4,5-dihydro-1H-1,2,4-triazol-4-yl)hexanoic Acid (**13**).* Purification by RP-HPLC (0.1% TFA in water/MeCN, 100:0 to 70:30 in 30 min). White powder, 31 mg (21%); UPLC-MS t_R: 1.32 min; *m/z* (ES+) 387.3 (M + H$^+$); ^{1}H NMR (600 MHz, DMSO-d_6): 13.94 (s, 1H), 13.05 (bs, 1H), 8.28 (s, 1H), 7.67−7.55 (m, 5H), 7.39 (s, 1H), 4.09−3.99 (m, 4H), 3.73−3.71 (m, 1H), 1.72−1.67 (m, 2H), 1.56−1.52 (m, 2H), 1.30−1.15 (m, 2H); ^{13}C NMR (151 MHz, DMSO-d_6): 170.9, 167.0, 151.1, 135.6, 130.8, 129.1, 128.6, 126.1, 118.2, 58.1, 43.4, 41.4, 28.8, 27.2, 21.4; HRMS (ESI+) calcd for $C_{18}H_{23}N_6O_2S$ (M + H)$^+$ 387.1603, found 387.1609.

*4.1.5.14. (2S)-2-{Bis[(1H-imidazol-4-yl)methyl]amino}-6-(3-phenyl-5-sulfanylidene-4,5-dihydro-1H-1,2,4-triazol-4-yl)hexanoic Acid (**14**).* Purification by RP-HPLC (0.1% TFA in water/MeCN, 100:0 to 70:30 in 30 min). White powder, 25 mg (14%); UPLC-MS t_R: 1.45 min; *m/z* (ES+) 467.3 (M + H$^+$); ^{1}H NMR (600 MHz, DMSO-d_6): 14.24 (bs, 2H), 13.91 (s, 1H), 12.57 (bs, 1H), 8.98 (s, 2H), 7.64−7.51 (m, 7H), 4.01−3.98 (m, 2H), 3.88−3.79 (m, 4H), 3.09 (t, *J* = 7.6 Hz, 1H), 1.58−1.44 (m, 4H), 1.25−1.06 (m, 2H); ^{13}C NMR (151 MHz, DMSO-d_6): 173.5, 167.0, 151.1, 134.4, 131.2, 130.0, 129.0, 128.5, 126.2, 117.3, 61.8, 44.8, 43.3, 28.5, 27.2, 22.7; HRMS (ESI+) calcd for $C_{22}H_{27}N_8O_2S$ (M + H)$^+$ 467.1978, found 467.1980.

*4.1.5.15. (2S)-2-{[(5-Methyl-1H-imidazol-4-yl)methyl]amino}-5-(3-phenyl-5-sulfanylidene-4,5-dihydro-1H-1,2,4-triazol-4-yl)-pentanoic Acid (**15**).* Purification by RP-HPLC (0.1% TFA in water/MeCN, 100:0 to 70:30 in 30 min). White powder, 9 mg (3%); UPLC-MS t_R: 1.22 min; *m/z* (ES+) 387.0 (M + H$^+$); ^{1}H NMR (500 MHz, DMSO-d_6): 14.02 (s, 1H), 13.69 (bs, 1H), 8.54 (s, 1H), 7.67−7.55 (m, 5H), 4.09−3.99 (m, 4H), 3.69 (bs, 1H), 2.20 (s, 3H), 1.71−1.52 (m, 4H); ^{13}C NMR (126 MHz, DMSO-d_6): 171.2, 167.2, 151.2, 134.0 (2C), 130.9, 129.2, 128.6, 126.1, 123.5, 58.1, 43.2, 27.5, 26.8, 23.8, 9.0; HRMS (ESI+) calcd for $C_{18}H_{23}N_6O_2S$ (M + H)$^+$ 387.1598, found 387.1587.

*4.1.5.16. (2S)-2-{[(1-Methyl-1H-imidazol-5-yl)methyl]amino}-5-(3-phenyl-5-sulfanylidene-4,5-dihydro-1H-1,2,4-triazol-4-yl)-pentanoic Acid (**16**).* Purification by RP-HPLC (0.1% TFA in water/MeCN, 95:5 to 65:35 in 30 min). White powder, 13 mg (22%); UPLC-MS t_R: 1.24 min; *m/z* (ES+) 387.1 (M + H$^+$); ^{1}H NMR (500 MHz, DMSO-d_6): 14.01 (s, 1H), 8.87 (s, 1H), 7.67−7.54 (m, 5H), 7.49 (s, 1H), 4.09−3.87 (m, 4H), 3.77 (s, 3H), 3.29−3.26 (m, 1H), 1.68−1.45 (m, 4H); ^{13}C NMR (126 MHz, DMSO-d_6): 167.2, 151.2, 136.8 (2C), 130.9, 129.2, 128.6, 126.1, 118.3, 116.0, 63.1, 58.8, 43.3, 33.1, 27.9, 24.1; HRMS (ESI+) calcd for $C_{18}H_{23}N_6O_2S$ (M + H)$^+$ 387.1598, found 387.1611.

*4.1.5.17. (2S)-5-(3-Phenyl-5-sulfanylidene-4,5-dihydro-1H-1,2,4-triazol-4-yl)-2-{[(1H-pyrrol-3-yl)methyl]amino}pentanoic Acid (**17**).* White powder, 29 mg (12%); UPLC-MS t_R: 1.58 min; *m/z* (ES+) 372.2 (M + H$^+$); ^{1}H NMR (500 MHz, DMSO-d_6): 14.03 (s, 1H), 10.96 (bs, 1H), 7.67−7.57 (m, 5H), 6.82 (s, 1H), 6.77−6.75 (m, 1H), 6.10−6.09 (m, 1H), 4.07−4.05 (m, 2H), 3.93−3.86 (m, 2H), 3.62 (s, 1H), 1.72−1.51 (m, 4H); ^{13}C NMR (126 MHz, DMSO-d_6): 169.8,

https://doi.org/10.1021/acs.jmedchem.2c01257
J. Med. Chem. XXXX, XXX, XXX−XXX

167.2, 151.2, 130.9, 129.2, 128.7, 126.0, 119.2, 118.8, 112.1, 108.8, 57.3, 43.2, 42.5, 26.0, 23.7; HRMS (ESI+) calcd for $C_{18}H_{22}N_5O_2S$ (M + H)$^+$ 372.1494, found 372.1503.

*4.1.5.18. (2S)-5-(3-Phenyl-5-sulfanylidene-4,5-dihydro-1H-1,2,4-triazol-4-yl)-2-{[(pyridin-2-yl)methyl]amino}pentanoic Acid (**18**).* Purification by RP-HPLC (0.1% TFA in water/MeCN, 95:5 to 65:35 in 30 min). White powder, 20 mg (25%); UPLC-MS t_R: 1.65 min; *m/z* (ES+) 384.3 (M + H$^+$); ^{1}H NMR (500 MHz, DMSO-d_6): 14.03 (s, 1H), 9.45 (bs, 1H), 8.62−8.61 (m, 1H), 7.89−7.88 (m, 1H), 7.68−7.55 (m, 5H), 7.48−7.43 (m, 2H), 4.33−4.27 (m, 2H), 4.13−4.11 (m, 2H), 4.01−3.98 (m, 1H), 1.82−1.58 (m, 4H); ^{13}C NMR (126 MHz, DMSO-d_6): 169.9, 167.3, 151.7, 151.2, 149.0, 137.5, 130.9, 129.2, 128.7, 126.1, 123.9, 123.5, 58.4, 49.1, 43.1, 25.8, 25.0; HRMS (ESI+) calcd for $C_{19}H_{22}N_5O_2S$ (M + H)$^+$ 384.1494, found 384.1491.

*4.1.5.19. (2S)-5-(3-Phenyl-5-sulfanylidene-4,5-dihydro-1H-1,2,4-triazol-4-yl)-2-{[(pyridin-3-yl)methyl]amino}pentanoic Acid (**19**).* Purification by RP-HPLC (0.1% TFA in water/MeCN, 95:5 to 65:35 in 30 min). White powder, 48 mg (16%); UPLC-MS t_R: 1.36 min; *m/z* (ES+) 384.2 (M + H$^+$); ^{1}H NMR (500 MHz, DMSO-d_6): 14.05 (s, 1H), 9.48 (bs, 1H), 8.68−8.67 (m, 2H), 8.00−7.98 (m, 1H), 7.70−7.57 (m, 6H), 4.22−4.11 (m, 4H), 4.03−4.01 (m, 1H), 1.83−1.56 (m, 4H); ^{13}C NMR (126 MHz, DMSO-d_6): 169.9, 167.3, 151.2, 150.2, 149.1, 139.5, 130.9, 129.2, 128.7, 128.1, 126.0, 124.1, 58.6, 46.8, 43.1, 26.0, 23.6; HRMS (ESI+) calcd for $C_{19}H_{22}N_5O_2S$ (M + H)$^+$ 384.1494, found 384.1501.

*4.1.5.20. (2S)-2-{[(1H-Indol-3-yl)methyl]amino}-5-(3-phenyl-5-sulfanylidene-4,5-dihydro-1H-1,2,4-triazol-4-yl)pentanoic Acid (**20**).* Purification by RP-HPLC (0.1% TFA in water/MeCN, 100:0 to 70:30 in 30 min). White powder, 21.6 mg (9%); UPLC/MS t_R: 1.96 min; *m/z* (ES+) 422.2 (M + H$^+$); ^{1}H NMR (500 MHz, DMSO-d_6): 14.03 (s, 1H), 12. 12 (bs, 1H), 9.45 (bs, 1H), 8.62−8.61 (m, 1H), 7.89−7.88 (m, 1H), 7.68−7.55 (m, 5H), 7.48−7.43 (m, 2H), 4.33−4.27 (m, 2H), 4.13−4.11 (m, 2H), 4.01−3.98 (m, 1H), 1.82−1.58 (m, 4H); ^{13}C NMR (126 MHz, DMSO-d_6): 169.9, 167.2, 151.2, 135.9, 130.9, 129.2, 128.6, 127.4, 126.7, 126.0, 121.7, 119.2, 118.6, 111.8, 104.7, 58.1, 43.2, 40.9, 26.3, 23.9; HRMS (ESI+) calcd for $C_{22}H_{24}N_5O_2S$ (M + H)$^+$ 422.1651, found 422.1645.

*4.1.5.21. (2S)-5-(3-Phenyl-5-sulfanylidene-4,5-dihydro-1H-1,2,4-triazol-4-yl)-2-{[(1,3-thiazol-4-yl)methyl]amino}pentanoic Acid (**21**).* Purification by RP-HPLC (0.1% TFA in water/MeCN, 90:10 to 60:40 in 30 min). White powder, 40 mg (15%); UPLC-MS t_R: 1.58 min; *m/z* (ES+) 390.0 (M + H$^+$); ^{1}H NMR (500 MHz, DMSO-d_6): 14.04 (s, 1H), 9.54 (bs, 1H), 9.19 (s, 1H), 7.84 (s, 1H), 7.67−7.55 (m, 5H), 4.27 (s, 2H), 4.09−4.07 (m, 2H), 3.93−3.91 (m, 1H), 1.73−1.51 (m, 4H); ^{13}C NMR (126 MHz, DMSO-d_6): 169.9, 167.3, 155.6, 151.3, 147.3, 131.0, 129.3, 128.7, 126.1, 121.1, 58.1, 44.4, 43.2, 26.0, 23.7; HRMS (ESI+) calcd for $C_{17}H_{20}N_5O_2S_2$ (M + H)$^+$ 390.1053, found 390.1054.

*4.1.5.22. (2S)-5-(3-Phenyl-5-sulfanylidene-4,5-dihydro-1H-1,2,4-triazol-4-yl)-2-{[(1,3-thiazol-5-yl)methyl]amino}pentanoic Acid (**22**).* Purification by RP-HPLC (0.1% TFA in water/MeCN, 95:5 to 65:35 in 30 min). White powder, 6 mg (12%); UPLC-MS t_R: 1.49 min; *m/z* (ES+) 389.9 (M + H$^+$); ^{1}H NMR (500 MHz, DMSO-d_6): 14.03 (s, 1H), 9.50 (bs, 1H), 9.16 (s, 1H), 7.93 (s, 1H), 7.67−7.56 (m, 5H), 4.38 (s, 2H), 4.09−4.08 (m, 2H), 3.86 (bs, 1H), 1.70−1.50 (m, 4H); ^{13}C NMR (126 MHz, DMSO-d_6): 170.3, 167.3, 156.8, 151.2, 145.7, 136.0, 131.0, 129.2, 128.7, 126.1, 58.2, 43.1, 40.9, 26.2, 23.7; HRMS (ESI+) calcd for $C_{17}H_{20}N_5O_2S_2$ (M + H)$^+$ 390.1053, found 390.1047.

*4.1.5.23. (2S)-2-{Bis[(5-methyl-1H-imidazol-4-yl)methyl]amino}-5-(3-phenyl-5-sulfanylidene-4,5-dihydro-1H-1,2,4-triazol-4-yl)-pentanoic Acid (**23**).* Purification by RP-HPLC (0.1% TFA in water/MeCN, 100:0 to 70:30 in 30 min). White powder, 165 mg (59%); UPLC-MS t_R: 1.39 min; *m/z* (ES+) 481.2 (M + H$^+$); ^{1}H NMR (500 MHz, DMSO-d_6): 14.24 (bs, 2H), 13.97 (s, 1H), 8.90 (s, 2H), 7.63−7.50 (m, 5H), 4.00−3.87 (m, 2H), 3.70−3.62 (m, 4H), 3.06−3.03 (m, 1H), 2.14 (s, 6H), 1.54−1.37 (m, 4H); ^{13}C NMR (126 MHz, DMSO-d_6): 173.1, 167.2, 151.2, 133.0, 130.9, 129.1, 128.6, 126.9, 126.2, 125.3, 60.8, 43.5, 43.0, 25.4, 24.7, 8.8; HRMS (ESI+) calcd for $C_{23}H_{29}N_8O_2S$ (M + H)$^+$ 481.2129, found 481.2130.

*4.1.5.24. (2S)-2-{Bis[(1H-imidazol-2-yl)methyl]amino}-5-(3-phenyl-5-sulfanylidene-4,5-dihydro-1H-1,2,4-triazol-4-yl)pentanoic Acid (**24**).* Purification by RP-HPLC (0.1% TFA in water/MeCN, 95:5 to 65:35 in 30 min). White powder, 39 mg (16%); UPLC-MS t_R: 1.32 min; *m/z* (ES+) 453.2 (M + H$^+$); ^{1}H NMR (500 MHz, DMSO-d_6): 14.20 (bs, 2H), 13.98 (s, 1H), 13.07 (bs, 1H), 7.64−7.48 (m, 9H), 4.17 (s, 4H), 3.99−3.94 (m, 2H), 3.25−3.22 (m, 1H), 1.64−1.50 (m, 2H); ^{13}C NMR (126 MHz, DMSO-d_6): 173.3, 167.1, 151.2, 144.9, 130.8, 129.1, 128.5, 126.1, 125.9, 119.5, 63.0, 46.4, 43.3, 26.4, 25.0; HRMS (ESI+) calcd for $C_{21}H_{25}N_8O_2S$ (M + H)$^+$ 453.1816, found 453.1821.

*4.1.5.25. (2S)-2-{Bis[(1H-pyrazol-4-yl)methyl]amino}-5-(3-phenyl-5-sulfanylidene-4,5-dihydro-1H-1,2,4-triazol-4-yl)pentanoic Acid (**25**).* Purification by RP-HPLC (0.1% TFA in water/MeCN, 95:5 to 65:35 in 30 min). White powder, 192 mg (51%); UPLC-MS t_R: 1.61 min; *m/z* (ES+) 453.1 (M + H$^+$); ^{1}H NMR (500 MHz, DMSO-d_6): 14.02 (s, 1H), 13.02 (bs, 1H), 9.88 (bs, 2H), 7.70−7.66 (m, 6H), 7.62−7.55 (m, 3H), 4.27−4.11 (m, 4H), 4.09−4.06 (m, 2H), 3.64−3.62 (m, 1H), 1.91−1.86 (m, 2H), 1.83−1.56 (m, 2H); ^{13}C NMR (126 MHz, DMSO-d_6): 169.7, 167.1, 151.2, 135.2 (2C), 130.9, 129.2, 128.7, 126.1, 108.1, 61.0, 45.1, 43.3, 24.9, 23.4; HRMS (ESI+) calcd for $C_{21}H_{25}N_8O_2S$ (M + H)$^+$ 453.1816, found 453.1816.

*4.1.5.26. (2S)-2-{Bis[(pyridin-2-yl)methyl]amino}-5-(3-phenyl-5-sulfanylidene-4,5-dihydro-1H-1,2,4-triazol-4-yl)pentanoic Acid (**26**).* Purification by RP-HPLC (0.1% TFA in water/MeCN, 95:5 to 65:35 in 30 min). White powder, 63 mg (64%); UPLC-MS t_R: 1.83 min; *m/z* (ES+) 475.3 (M + H$^+$); ^{1}H NMR (600 MHz, DMSO-d_6): 13.89 (s, 1H), 8.74−8.73 (m, 2H), 8.07−8.06 (m, 2H), 7.63−7.47 (m, 9H), 5.15 (bs, 1H), 4.17−4.11 (m, 4H), 3.95−3.88 (m, 2H), 3.32−3.30 (m, 1H), 1.63−1.43 (m, 4H); ^{13}C NMR (151 MHz, DMSO-d_6): 173.6, 167.1, 157.2, 151.1, 145.1, 141.3, 130.7, 129.0, 128.5, 126.1, 124.5, 123.9, 63.7, 55.1, 43.2, 26.3, 24.9; HRMS (ESI+) calcd for $C_{25}H_{27}N_6O_2S$ (M + H)$^+$ 475.1916, found 475.1913.

*4.1.5.27. (2S)-2-{Bis[(pyridin-3-yl)methyl]amino}-5-(3-phenyl-5-sulfanylidene-4,5-dihydro-1H-1,2,4-triazol-4-yl)pentanoic Acid (**27**).* Purification by RP-HPLC (0.1% TFA in water/MeCN, 95:5 to 65:35 in 30 min). White powder, 53 mg (14%); UPLC-MS t_R: 1.55 min; *m/z* (ES+) 475.3 (M + H$^+$); ^{1}H NMR (500 MHz, DMSO-d_6): 13.97 (s, 1H), 12.82 (bs, 1H), 8.62−8.60 (m, 4H), 8.07−8.06 (m, 2H), 7.66−7.48 (m, 7H), 4.06−3.94 (m, 2H), 3.87−3.76 (m, 4H), 3.17−3.14 (m, 1H), 1.74−1.51 (m, 4H); ^{13}C NMR (126 MHz, DMSO-d_6): 173.3, 167.1, 151.2, 145.2, 144.2, 137.3, 130.8, 129.1, 128.6, 126.8, 126.2, 125.3, 61.9, 51.8, 43.4, 25.9, 24.8; HRMS (ESI+) calcd for $C_{25}H_{27}N_6O_2S$ (M + H)$^+$ 475.1916, found 475.1920.

*4.1.5.28. (2S)-2-{Bis[(pyrazin-2-yl)methyl]amino}-5-(3-phenyl-5-sulfanylidene-4,5-dihydro-1H-1,2,4-triazol-4-yl)pentanoic Acid (**28**).* Purification by RP-HPLC (0.1% TFA in water/MeCN, 80:20 to 50:50 in 30 min). White powder, 29 mg (25%); UPLC-MS t_R: 1.16 min; *m/z* (ES+) 477.2 (M + H$^+$); ^{1}H NMR (500 MHz, DMSO-d_6): 13.94 (s, 1H), 12.60 (bs, 1H), 8.50−8.42 (m, 6H), 7.62−7.46 (m, 9H), 4.07−3.97 (m, 2H), 3.96−3.87 (m, 4H), 3.29−3.26 (m, 1H), 1.81−1.53 (m, 4H); ^{13}C NMR (126 MHz, DMSO-d_6): 173.7, 167.2, 154.7, 151.2, 144.8, 143.8, 143.1, 130.8, 129.1, 128.5, 126.2, 63.1, 55.0, 43.4, 26.2, 24.9; HRMS (ESI+) calcd for $C_{23}H_{24}N_8O_2S$ (M + H)$^+$ 477.1821, found 477.1822.

*4.1.5.29. (2S)-2-{Bis[(1,3-thiazol-4-yl)methyl]amino}-5-(3-phenyl-5-sulfanylidene-4,5-dihydro-1H-1,2,4-triazol-4-yl)pentanoic Acid (**29**).* Purification by RP-HPLC (0.1% TFA in water/MeCN, 90:10 to 60:40 in 30 min). White powder, 68 mg (26%); UPLC-MS t_R: 2.16 min; *m/z* (ES+) 487.1 (M + H$^+$); ^{1}H NMR (500 MHz, DMSO-d_6): 13.96 (s, 1H), 9.05 (s, 2H), 7.61−7.49 (m, 7H), 4.10−3.89 (m, 6H), 3.37 (bs, 1H), 1.69−1.58 (m, 4H); ^{13}C NMR (126 MHz, DMSO-d_6): 172.8, 167.1, 154.5, 153.1, 151.3, 130.8, 129.1, 128.6, 126.2, 118.1, 61.9, 50.3, 43.4, 25.7, 24.9; HRMS (ESI+) calcd for $C_{21}H_{23}N_6O_2S_3$ (M + H)$^+$ 487.1039, found 487.1041.

*4.1.5.30. (2S)-2-{Bis[(1,3-thiazol-5-yl)methyl]amino}-5-(3-phenyl-5-sulfanylidene-4,5-dihydro-1H-1,2,4-triazol-4-yl)pentanoic Acid (**30**).* Purification by RP-HPLC (0.1% TFA in water/MeCN, 95:5 to 65:35 in 30 min). White powder, 82 mg (73%); UPLC-MS t_R: 2.31 min; *m/z* (ES+) 487.0 (M + H$^+$); ^{1}H NMR (500 MHz, DMSO-d_6): 13.96 (s, 1H), 12.58 (bs, 1H), 9.02 (s, 2H), 7.74 (s, 2H), 7.64−7.51

https://doi.org/10.1021/acs.jmedchem.2c01257
J. Med. Chem. XXXX, XXX, XXX−XXX

(m, 5H), 4.06−4.00 (m, 2H), 3.97 (d, J = 15.1 Hz, 2H), 3.83 97 (d, J = 15.0 Hz, 2H), 3.07 (t, J = 7.4 Hz, 1H), 1.71−1.61 (m, 1H), 1.52 (dd, J = 15.3, 7.6 Hz, 2H), 1.47−1.35 (m, 1H); ^{13}C NMR (126 MHz, DMSO-d_6): 173.3, 167.2, 154.7, 151.2, 141.3, 138.4, 130.9, 129.2, 128.2, 126.2, 60.6, 46.1, 43.3, 26.0, 25.2; HRMS (ESI+) calcd for $C_{21}H_{23}N_6O_2S_3$ (M + H)$^+$ 487.1039, found 487.1030.

*4.1.5.31. (2S)-2-{[(1H-Imidazol-4-yl)methyl][(5-methyl-1H-imidazol-4-yl)methyl]amino}-5-(3-phenyl-5-sulfanylidene-4,5-dihydro-1H-1,2,4-triazol-4-yl)pentanoic Acid (**31**).* Purification by RP-HPLC (0.1% TFA in water/MeCN, 100:0 to 70:30 in 30 min). White powder, 109 mg (97%); UPLC-MS t_R: 1.34 min; m/z (ES+) 467.2 (M + H$^+$); ^{1}H NMR (500 MHz, DMSO-d_6): 14.34 (bs, 2H), 13.97 (s, 1H), 12.87 (bs, 1H), 9.00 (s, 1H), 8.93 (s, 1H), 7.63−7.48 (m, 6H), 4.00−3.91 (m, 2H), 3.81−3.67 (m, 4H), 3.11−3.08 (m, 1H), 2.13 (s, 3H), 1.61−1.41 (m, 4H); ^{13}C NMR (126 MHz, DMSO-d_6): 173.3, 167.2, 151.2, 134.3, 133.1, 131.3, 130.8, 129.1, 128.5, 127.2, 126.2, 125.0, 117.1, 60.9, 44.2, 44.0, 43.1, 25.7, 24.7, 8.7; HRMS (ESI+) calcd for $C_{22}H_{27}N_8O_2S$ (M + H)$^+$ 467.1972, found 467.1992.

*4.1.5.32. (2S)-2-{[(1H-Imidazol-4-yl)methyl][(3-methyl-imidazol-4-yl)methyl]amino}-5-(3-phenyl-5-sulfanylidene-4,5-dihydro-1H-1,2,4-triazol-4-yl)pentanoic Acid (**32**).* Purification by RP-HPLC (0.1% TFA in water/MeCN, 100:0 to 70:30 in 30 min). White powder, 48 mg (82%); UPLC-MS t_R: 1.35 min; m/z (ES+) 467.2 (M + H$^+$); ^{1}H NMR (500 MHz, DMSO-d_6): 14.49 (bs, 1H), 13.99 (s, 1H), 12.91 (bs, 1H), 8.99 (s, 2H), 7.64−7.48 (m, 7H), 4.02−3.80 (m, 2H), 3.77−3.72 (m, 4H), 3.67 (s, 3H), 3.21−3.18 (m, 1H), 1.69−1.58 (m, 4H); ^{13}C NMR (126 MHz, DMSO-d_6): 173.1, 167.1, 151.2, 136.4, 134.6, 131.2, 130.8, 130.5, 129.1, 128.6, 126.2, 119.1, 118.0, 61.7, 44.5, 43.8, 43.3, 33.3, 25.8, 24.9; HRMS (ESI+) calcd for $C_{22}H_{27}N_8O_2S$ (M + H)$^+$ 467.1972, found 467.1969.

*4.1.5.33. (2S)-2-{[(1H-Imidazol-2-yl)methyl][(1H-imidazol-4-yl)-methyl]amino}-5-(3-phenyl-5-sulfanylidene-4,5-dihydro-1H-1,2,4-triazol-4-yl)pentanoic Acid (**33**).* Purification by RP-HPLC (0.1% TFA in water/MeCN, 91:9 to 61:39 in 30 min). White powder, 59 mg (58%); UPLC-MS t_R: 1.83 min; m/z (ES+) 453.2 (M + H$^+$); ^{1}H NMR (500 MHz, DMSO-d_6): 14.27 (bs, 2H), 13.97 (s, 1H), 8.99 (s, 1H), 7.62−7.47 (m, 8H), 4.15−4.07 (m, 2H), 4.04−3.93 (m, 2H), 3.89−3.81 (m, 2H), 3.22−3.19 (m, 1H), 1.68−1.53 (m, 4H); ^{13}C NMR (126 MHz, DMSO-d_6): 173.3, 167.1, 151.2, 145.3, 134.6, 130.8, 130.5, 129.1, 128.5, 126.2, 119.3, 117.6, 62.2, 45.7, 45.5, 43.3, 26.2, 24.8; HRMS (ESI+) calcd for $C_{21}H_{25}N_8O_2S$ (M + H)$^+$ 453.1816, found 453.1828.

*4.1.5.34. (2S)-2-{[(1H-Imidazol-4-yl)methyl][(1H-pyrazol-4-yl)-methyl]amino}-5-(3-phenyl-5-sulfanylidene-4,5-dihydro-1H-1,2,4-triazol-4-yl)pentanoic Acid (**34**).* Purification by RP-HPLC (0.1% TFA in water/MeCN, 95:5 to 65:35 in 30 min). White powder, 57 mg (52%); UPLC-MS t_R: 1.54 min; m/z (ES+) 453.1 (M + H$^+$); ^{1}H NMR (500 MHz, DMSO-d_6): 14.22 (bs, 1H), 13.98 (s, 1H), 9.05 (s, 1H), 7.64−7.50 (m, 8H), 4.06−3.95 (m, 2H), 3.85−3.77 (m, 2H), 3.65−3.57 (m, 2H), 3.20−3.18 (m, 1H), 1.74−1.49 (m, 4H); ^{13}C NMR (126 MHz, DMSO-d_6): 173.6, 167.1, 151.3, 134.3, 133.6, 131.9, 130.8, 129.1, 128.6, 126.2, 117.2 (2C), 116.7, 60.7, 44.7, 44.1, 43.5, 26.0, 24.8; HRMS (ESI+) calcd for $C_{21}H_{25}N_8O_2S$ (M + H)$^+$ 453.1816, found 453.1801.

*4.1.5.35. (2S)-2-{Benzyl[(1H-imidazol-4-yl)methyl]amino}-5-(3-phenyl-5-sulfanylidene-4,5-dihydro-1H-1,2,4-triazol-4-yl)pentanoic Acid (**35**).* Purification by RP-HPLC (0.1% TFA in water/MeCN, 90:10 to 60:40 in 30 min). White powder, 26 mg (34%); UPLC-MS t_R: 2.16 min; m/z (ES+) 463.0 (M + H$^+$); ^{1}H NMR (500 MHz, DMSO-d_6): 14.13 (bs, 1H), 13.97 (s, 1H), 12.70 (bs, 1H), 8.97 (s, 1H), 7.61−7.21 (m, 10H), 4.02−3.92 (m, 2H), 7.78−3.70 (m, 4H), 3.08−3.06 (m, 1H), 1.74−1.46 (m, 4H); ^{13}C NMR (126 MHz, DMSO-d_6): 173.4, 167.1, 151.3, 138.7, 134.3, 131.5, 130.8, 129.1, 128.6, 128.5, 128.3, 127.1, 126.2, 117.4, 61.2, 54.6, 44.6, 43.4, 26.1, 24.9; HRMS (ESI+) calcd for $C_{24}H_{27}N_6O_2S$ (M + H)$^+$ 463.1911, found 463.1888.

*4.1.5.36. (2S)-2-{[(1H-Imidazol-4-yl)methyl][(pyridin-2-yl)-methyl]amino}-5-(3-phenyl-5-sulfanylidene-4,5-dihydro-1H-1,2,4-triazol-4-yl)pentanoic Acid (**36**).* Purification by RP-HPLC (0.1% TFA in water/MeCN, 95:5 to 65:35 in 30 min). White powder, 44 mg (58%); UPLC-MS t_R: 1.49 min; m/z (ES+) 464.4 (M + H$^+$); ^{1}H NMR (500 MHz, DMSO-d_6): 14.07 (bs, 1H), 13.96 (s, 1H), 8.97 (s, 1H), 8.51−8.50 (m, 1H), 7.83 (s, 1H), 7.62−7.45 (m, 7H), 7.36 (s, 1H), 4.02−3.80 (m, 6H), 3.21−3.19 (m, 1H), 1.71−1.52 (m, 4H); ^{13}C NMR (126 MHz, DMSO-d_6): 173.6, 167.1, 158.2, 158.0, 151.1, 134.3, 131.2, 130.8, 129.1, 128.5, 126.2, 123.2, 122.9, 117.5, 62.3, 55.3, 45.4, 43.4, 26.3, 24.9; HRMS (ESI+) calcd for $C_{23}H_{26}N_7O_2S$ (M + H)$^+$ 464.1869, found 464.1870.

*4.1.5.37. (2S)-2-{[(1H-Imidazol-4-yl)methyl][(pyridin-3-yl)-methyl]amino}-5-(3-phenyl-5-sulfanylidene-4,5-dihydro-1H-1,2,4-triazol-4-yl)pentanoic Acid (**37**).* Purification by RP-HPLC (0.1% TFA in water/MeCN, 95:5 to 65:35 in 30 min). White powder, 24 mg (24%); UPLC-MS t_R: 1.45 min; m/z (ES+) 464.4 (M + H$^+$); ^{1}H NMR (500 MHz, DMSO-d_6): 14.33 (bs, 1H), 13.98 (s, 1H), 12.84 (bs, 1H), 8.97 (s, 1H), 8.63−8.62 (m, 2H), 7.63−7.60 (m, 1H), 7.56−7.46 (m, 7H), 4.04−3.94 (m, 2H), 3.87−3.72 (m, 4H), 3.17−3.14 (m, 1H), 1.74−1.51 (m, 4H); ^{13}C NMR (126 MHz, DMSO-d_6): 173.3, 167.1, 151.2, 145.7, 144.8, 140.4, 134.4, 131.0, 130.8, 129.1, 128.5, 126.8, 126.2, 124.1, 117.7, 61.7, 51.8, 44.9, 43.4, 26.1, 24.8; HRMS (ESI+) calcd for $C_{23}H_{26}N_7O_2S$ (M + H)$^+$ 464.1869, found 464.1870.

*4.1.5.38. (2S)-2-{[(1H-Imidazol-4-yl)methyl][(pyrazin-2-yl)-methyl]amino}-5-(3-phenyl-5-sulfanylidene-4,5-dihydro-1H-1,2,4-triazol-4-yl)pentanoic Acid (**38**).* Purification by RP-HPLC (0.1% TFA in water/MeCN, 90:10 to 60:40 in 30 min). White powder, 27 mg (32%); UPLC-MS t_R: 1.71 min; m/z (ES+) 465.3 (M + H$^+$); ^{1}H NMR (600 MHz, DMSO-d_6): 14.09 (bs, 1H), 13.92 (s, 1H), 12.69 (bs, 1H), 8.93 (s, 1H), 8.60 (s, 1H), 8.47 (s, 2H), 7.63−7.47(m, 5H), 7.44 (s, 1H), 4.04−3.79 (m, 6H), 3.24−3.22 (m, 1H), 1.75−1.52 (m, 4H); ^{13}C NMR (151 MHz, DMSO-d_6): 173.4, 167.1, 154.5, 151.1, 144.5, 143.6, 143.1, 134.3, 131.1, 130.7, 129.0, 128.5, 126.1, 117.6, 62.5, 54.4, 45.8, 43.4, 26.2, 24.8; HRMS (ESI+) calcd for $C_{22}H_{24}N_8O_2S$ (M + H)$^+$ 465.1816, found 465.1809.

*4.1.5.39. (2S)-2-{[(1H-Imidazol-4-yl)methyl][(1,3-thiazol-4-yl)-methyl]amino}-5-(3-phenyl-5-sulfanylidene-4,5-dihydro-1H-1,2,4-triazol-4-yl)pentanoic Acid (**39**).* Purification by RP-HPLC (0.1% TFA in water/MeCN, 90:10 to 60:40 in 30 min). White powder, 33 mg (36%); UPLC-MS t_R: 1.83 min; m/z (ES+) 470.2 (M + H$^+$); ^{1}H NMR (500 MHz, DMSO-d_6): 14.07 (bs, 1H), 13.96 (s, 1H), 12.64 (bs, 1H), 9.00−8.98 (m, 2H), 7.62−7.54 (m, 3H), 7.49−7.45 (m, 4H), 4.03−3.90 (m, 4H), 3.84 (s, 2H), 3.20 (t, J = 7.1, 14.3 Hz, 1H), 1.73−1.48 (m, 4H); ^{13}C NMR (126 MHz, DMSO-d_6): 173.7, 167.1, 155.00, 154.0, 151.2, 134.3, 131.7, 130.8, 129.1, 128.6, 126.2, 117.2, 116.4, 61.8, 50.4, 45.0, 43.4, 26.2, 24.9; HRMS (ESI+) calcd for $C_{21}H_{24}N_7O_2S_2$ (M + H)$^+$ 470.1427, found 470.1442.

*4.1.5.40. (2S)-2-{[(1H-Imidazol-4-yl)methyl][(1,3-thiazol-5-yl)-methyl]amino}-5-(3-phenyl-5-sulfanylidene-4,5-dihydro-1H-1,2,4-triazol-4-yl)pentanoic Acid (**40**).* Purification by RP-HPLC (0.1% TFA in water/MeCN, 90:10 to 60:40 in 30 min). White powder, 20 mg (17%); UPLC-MS t_R: 1.77 min; m/z (ES+) 470.1 (M + H$^+$); ^{1}H NMR (500 MHz, DMSO-d_6): 14.13 (bs, 1H), 13.97 (s, 1H), 12.75 (bs, 1H), 8.98−8.96 (m, 2H), 7.71 (s, 1H), 7.71−7.50 (m, 5H), 7.40 (s, 1H), 4.07−3.88 (m, 4H), 3.78 (s, 2H), 3.19 (t, J = 7.2, 14.3 Hz, 1H), 1.72−1.49 (m, 4H); ^{13}C NMR (126 MHz, DMSO-d_6): 173.5, 167.1, 154.3, 151.3, 141.6, 137.9, 134.3, 131.2, 130.8, 129.1, 128.6, 126.2, 117.4, 61.9, 46.5, 44.8, 43.4, 26.2, 25.0; HRMS (ESI+) calcd for $C_{21}H_{24}N_7O_2S_2$ (M + H)$^+$ 470.1427, found 470.1438.

*4.1.5.41. (2S)-5-(3-{[1,1′-Biphenyl]-3-yl}--5-sulfanylidene-4,5-dihydro-1H-1,2,4-triazol-4-yl)-2-{bis[(1H-imidazol-4-yl)methyl]-amino}pentanoic Acid (**41**).* Purification by RP-HPLC (0.1% TFA in water/MeCN, 95:5 to 55:45 in 35 min). White powder, 41 mg (55%); UPLC-MS t_R: 1.88 min; m/z (ES+) 529.2 (M + H$^+$); ^{1}H NMR (500 MHz, DMSO-d_6): 14.30 (bs, 2H), 14.04 (s, 1H), 12.84 (bs, 1H), 9.00 (s, 2H), 7.95−7.87 (m, 2H), 7.72−7.41 (m, 9H), 4.07−4.01 (m, 2H), 3.79 (s, 4H), 3.25−3.22 (m, 1H), 1.78−1.51 (m, 4H); ^{13}C NMR (126 MHz, DMSO-d_6): 173.4, 167.2, 151.1, 141.0, 139.0, 134.4, 131.0, 129.7, 129.1, 129.0, 128.1, 127.5, 126.9, 126.7, 117.5, 61.3, 44.6, 43.4, 26.0, 24.8; HRMS (ESI+) calcd for $C_{27}H_{29}N_8O_2S$ (M + H)$^+$ 529.2129, found 529.2115.

*4.1.5.42. (2S)-2-{Bis[(1H-imidazol-4-yl)methyl]amino}-5-[3-(naphthalen-2-yl)-5-sulfanylidene-4,5-dihydro-1H-1,2,4-triazol-4-yl]pentanoic Acid (**42**).* Purification by RP-HPLC (0.1% TFA in

https://doi.org/10.1021/acs.jmedchem.2c01257
J. Med. Chem. XXXX, XXX, XXX−XXX

water/MeCN, 90:10 to 60:40 in 30 min). White powder, 94 mg (26%); UPLC-MS t_R: 1.68 min; m/z (ES+) 503.2 (M + H$^+$); ^{1}H NMR (500 MHz, DMSO-d_6): 14.39 (bs, 2H), 14.06 (s, 1H), 12.86 (bs, 1H), 8.97 (s, 2H), 8.26 (s, 1H), 8.03−7.97 (m, 3H), 7.74−7.60 (m, 3H), 7.49 (s, 2H), 4.17−4.06 (m, 2H), 3.75 (s, 4H), 3.22−3.19 (m, 1H), 1.74−1.50 (m, 4H); ^{13}C NMR (126 MHz, DMSO-d_6): 173.4, 167.3, 151.1, 134.4, 133.4, 132.4, 130.9, 128.8, 128.5, 128.4, 127.9, 127.8, 127.2, 125.0, 123.5, 117.5, 61.3, 44.5, 43.4, 26.1, 24.8; HRMS (ESI+) calcd for $C_{25}H_{27}N_8O_2S$ (M + H)$^+$ 503.1972, found 503.1967.

*4.1.5.43. (2S)-5-(3-Benzyl-5-sulfanylidene-4,5-dihydro-1H-1,2,4-triazol-4-yl)-2-{bis[(1H-imidazol-4-yl)methyl]amino}pentanoic Acid (**43**).* Purification by RP-HPLC (0.1% TFA in water/MeCN, 90:10 to 60:40 in 30 min). White powder, 100 mg (29%); UPLC-MS t_R: 0.88 min; m/z (ES+) 467.3 (M + H$^+$); ^{1}H NMR (500 MHz, DMSO-d_6): 14.42 (bs, 2H), 13.64 (s, 1H), 12.93 (bs, 1H), 9.06 (s, 2H), 7.60 (s, 2H), 7.32−7.18 (m, 5H), 4.08 (s, 2H), 3.91−3.76 (m, 6H), 3.11−3.08 (m, 1H), 1.65−1.18 (m, 4H); ^{13}C NMR (126 MHz, DMSO-d_6): 171.7, 164.9, 149.5, 133.4, 132.7, 129.3, 127.0, 125.3, 115.9, 59.8, 43.0, 41.1, 29.1, 24.5, 22.9; HRMS (ESI+) calcd for $C_{22}H_{27}N_8O_2S$ (M + H)$^+$ 467.1972, found 467.1975.

*4.1.5.44. (2S)-2-{Bis[(1H-imidazol-4-yl)methyl]amino}-5-{[3-[(naphthalen-2-yl)methyl]-5-sulfanylidene-4,5-dihydro-1H-1,2,4-triazol-4-yl}pentanoic Acid (**44**).* Purification by RP-HPLC (0.1% TFA in water/MeCN, 90:10 to 60:40 in 30 min). White powder, 120 mg (64%); UPLC-MS t_R: 1.00 min; m/z (ES+) 517.2 (M + H$^+$); ^{1}H NMR (500 MHz, DMSO-d_6): 14.34 (bs, 2H), 13.65 (s, 1H), 12.83 (bs, 1H), 9.02 (s, 2H), 7.87−7.83 (m, 2H), 7.78 (s, 1H), 7.54 (s, 2H), 7.49−7.47 (m, 2H), 7.37−7.35 (m, 1H), 4.24 (s, 2H), 3.86−3.76 (m, 6H), 3.07−3.04 (m, 1H), 1.67−1.28 (m, 4H); ^{13}C NMR (126 MHz, DMSO-d_6): 173.4, 166.7, 151.2, 134.4, 132.9, 132.6, 132.0, 131.0, 128.3, 127.5, 127.3, 127.0, 126.4, 126.0, 117.5, 61.5, 44.6, 42.9, 31.0, 26.1, 24.7; HRMS (ESI+) calcd for $C_{26}H_{29}N_8O_2S$ (M + H)$^+$ 517.2129, found 517.2139.

*4.1.5.45. (2S)-2-{Bis[(1H-imidazol-4-yl)methyl]amino}-5-(3-cyclohexyl-5-sulfanylidene-4,5-dihydro-1H-1,2,4-triazol-4-yl)pentanoic Acid (**45**).* Purification by RP-HPLC (0.1% TFA in water/MeCN, 95:5 to 65:35 in 30 min). White powder, 37 mg (46%); UPLC-MS t_R: 1.56 min; m/z (ES+) 459.2 (M + H$^+$); ^{1}H NMR (500 MHz, DMSO-d_6): 14.32 (bs, 2H), 13.54 (s, 1H), 9.04 (s, 2H), 7.60 (s, 2H), 3.95−3.80 (m, 6H), 3.32−3.29 (m, 1H), 2.64−2.60 (m, 1H), 1.78−1.22 (m, 14H); ^{13}C NMR (126 MHz, DMSO-d_6): 173.0, 165.9, 156.0, 134.5, 131.2, 117.5, 61.7, 44.8, 42.4, 33.9, 30.9, 26.3, 25.4, 25.3, 25.2; HRMS (ESI+) calcd for $C_{21}H_{31}N_8O_2S$ (M + H)$^+$ 459.2285, found 459.2283.

4.2. Metallo-β-Lactamase Inhibition Assays. The inhibition potency of the compounds toward VIM-type enzymes, NDM-1 and IMP-1 has been assessed with a reporter substrate method and specifically by measuring the rate of hydrolysis of the reporter substrate (such as 150 μM imipenem, 150 μM meropenem, 120 μM cefotaxime or 100 μM nitrocefin) at 30 °C in 50 mM HEPES buffer (pH 7.5) in the absence and presence of several concentrations of the inhibitor (final concentration, 0.5−1000 μM).

The reaction rate was measured as the variation of absorbance observed upon substrate hydrolysis in a UV−visible spectrophotometer or microplate reader at a wavelength of 300 nm (imipenem, meropenem), 260 nm (cefotaxime), or 482 nm (nitrocefin) and in the presence of a purified MBL enzyme (such as VIM-1, VIM-2, VIM-4, NDM-1, and IMP-1, at a final concentration ranging from 1 to 70 nM).

The inhibition constants (K_i) were determined on the basis of a model of competitive inhibition by analyzing the dependence of the ratio v_0/v_i (v_0, hydrolysis velocity in the absence of inhibitor; v_i, hydrolysis velocity in the presence of inhibitor) as a function of [I] as already described.[61] The slope of the plot of v_0/v_i *vs* [I], which corresponds to $K_m^S/(K_m^S + [S])K_i$ (where K_m^S is the K_m value of the reporter substrate and [S] its concentration in the reaction mixture) and allowed the calculation of the K_i value. Alternatively, a Dixon plot analysis was carried out by measuring the initial hydrolysis rates in the presence of variable concentrations of inhibitor and substrate. This allowed K_i values to be determined and supported the hypothesis that the various compounds behaved as competitive inhibitors of the various tested enzymes. The assays were performed in triplicate.

4.3. Microbiological Assays. The minimum inhibitory concentrations (MICs) of meropenem (MEM) were determined in triplicate using cation-supplemented Mueller−Hinton broth and a bacterial inoculum of 5 × 10^4 CFU/well, as recommended by the CLSI,[62] in both the absence and presence of a fixed concentration (32 μg/mL) of an inhibitor. MDR VIM-1- or VIM-4-producing *K. pneumoniae*, VIM-2-producing *P. aeruginosa*, and NDM-1-producing *E. coli* clinical isolates present in our collection (respectively, 7023, VA-416/02, VA-182/00, and SI-004) were used. Compound **8** activity was also evaluated on additional strains from the MicrobiH$_2$Omme Collection in Montpellier: the clinical VIM-1-producing *P. aeruginosa* ARS243 and the environmental VIM-4-producing *P. aeruginosa* FAPLB64 isolated from an urban river (Font d'Aurelle) in Montpellier (France). The chequerboard analysis and the determination of the average fractional inhibitory concentration (FIC) index were carried out and interpreted as previously described.[63,64]

4.4. Cell Toxicity: Membrane Integrity Assay. The potential cytotoxic activity of compounds was evaluated using the commercially available integrity assay (CytoTox 96 nonradioactive cytotoxicity assay, Promega). The compounds were tested for their ability to induce the lysis of HeLa cells by measuring the release of lactate dehydrogenase (LDH) after incubating the HeLa cell cultures (20,000 cells/well) for 24 h (37 °C, 5% CO_2) in Dulbecco's modified Eagle's medium (DMEM) supplemented with 10% fetal bovine serum, 4.5 mg/mL glucose, and 2 mM L-glutamine in the absence and presence of varying concentrations of the compounds (up to 250 μM). Further controls included samples containing the medium only or in which cell lysis was induced by the addition of 9% Triton X-100 (maximum LDH release control). The percentage of cytotoxicity was computed as 100 × (sample LDH release)/(maximum LDH release). The variation of the percentage of cytotoxicity allowed us to compute an IC_{50} value (compound concentration inducing 50% cytotoxicity).

4.5. Equilibrium Dialysis and Native State Electrospray Ionization Mass Spectrometry. These studies have been performed on compounds **8**, **26**, **27**, and **30** following published procedures.[53] Recombinant VIM-2 and NDM-1 used in these experiments were prepared as described in the Supporting Information.

4.5.1. Metal Analyses and Equilibrium Dialysis. Previously published procedures were used for the metal analyses and equilibrium dialysis experiments.[53] In brief, the Zn^{II} content of purified VIM-2 and NDM-1 was determined using an atomic absorption spectrometer (AA, PerkinElmer PinAAcle 500). The emission wavelength was set to 213.86 nm.[65] The VIM-2 and NDM-1 samples were diluted to 3 μM with 50 mM HEPES, pH 7.5, and dialyzed overnight against 50 mM HEPES, pH 7.5, containing 2 mM Tris (2-carboxyethyl) phosphine hydrochloride (TCEP) and 6 μM $ZnCl_2$. A calibration curve was generated using serial dilutions of the Fisherbrand zinc metal standard.

VIM-2 and NDM-1 (final concentration 3 μM), in 5 mL of 50 mM HEPES, pH 7.5, were mixed with the compound of interest at concentrations from 0 to 48 μM. The samples were incubated on ice for 1 h and then dialyzed separately versus 500 mL of 50 mM HEPES, pH 7.5, at 4 °C overnight (dialysis tubing MWCO 12,000−14,000, Fisherbrand). The Zn(II) content in the mixtures was determined using AA as described above.

4.5.2. Native State Electrospray Ionization Mass Spectrometry (Native MS). NanoESI-MS analysis was used to confirm the mechanism of inhibition of selected inhibitors following a previously published procedure.[53] TCEP (final concentration 2 mM) and 2 equiv $ZnCl_2$ (from a 0.1 M $ZnCl_2$ stock) were added to purified VIM-2 and NDM-1 (150 μM). The samples were incubated for 1 h and dialyzed overnight against 100 mM ammonium acetate, pH 7.5. To analyze samples, a nano-electrospray ionization (n-ESI) probe (Thermo Fisher Scientific, San Jose, CA) with positive mode protein detection was used on a Thermo Scientific LTQ Orbitrap XL hybrid

https://doi.org/10.1021/acs.jmedchem.2c01257
J. Med. Chem. XXXX, XXX, XXX−XXX

ion trap-orbitrap mass spectrometer. The following were the major parameters used: capillary temperature, 180 °C; sheath gas, 0; auxiliary gas, 0; sweep gas, 0; spray voltage, 1.1−1.9 kV; tube-lens, 150 V; capillary voltage, 35 V; full scan ranging 1000−4000 (m/z); and resolution set to 30,000. The automated gain control was set as follows: full scan, 3×10^4; selected ion monitoring (SIM), 1×10^4; and MS^n, 1×10^4. The zoom for the ion trap was set as follows: full scan, 3×10^6; SIM, 1×10^5; and MS^n, 1×10^5 for Fourier transform. The nESI source was equipped with an offline unit (Cat# ES260), which was constructed based on previously published work.[52] To construct the source, a platinum wire (0.25 mm diameter) was inserted into the center of the offline unit. The glass capillaries (inner tip diameter 0.8 mm, outer tip diameter 1.5 mm) were produced in-house using a micropipette puller (model P-87 Flaming/Brown Micropipette Puller, Sutter Instrument, Inc.) (inner tip diameter after pulling ∼1 μm). Using an infusion syringe (Thermo Scientific), a 5 μL sample was loaded into the pulled glass capillary. The platinum wire was then inserted into the center of the capillary, and the capillary position was adjusted to approximately 3 mm away from the MS inlet.

4.6. Isothermal Calorimetry (ITC) of Compound Binding to VIM-2 and NDM-1. ITC titrations were performed as previously described[41] on a MicroCal ITC200 (GE-Malvern) equipped with a 200 μL Hastelloy sample cell and an automated 40 μL glass syringe rotating at 1000 rpm. VIM-2 and NDM-1 in 10 mM HEPES−NaOH, 0.15 M NaCl, pH 7.5 were diluted to the desired concentration with the same buffer and were brought to DMSO concentration identical to that of the injected compound. The tested compounds were solubilized in DMSO at 20 mM concentration and were diluted to 200 μM with the enzyme buffer, resulting in a final DMSO concentration of 1%.

In a standard experiment, VIM-2 or NDM-1 (19 μM) was titrated by one initiating injection (0.5 μL) followed by 19 injections (2 μL) of compound **8** or **26** (200 μM) at an interval of 150 s. Dilution heat of compound injections into buffer, at the corresponding DMSO concentration, was subtracted from raw data. The data so obtained were fitted via the nonlinear least-squares minimization method to determine binding stoichiometry (n), association constant (K_a), and change in enthalpy of binding (ΔH°_b) using ORIGIN 7 software v.7 (OriginLab). In the fitting procedure, the compound concentration was lowered to provide n around 1 and to take compound solubility into account under ITC conditions. The Gibbs free energy of binding, ΔG°_b, was calculated from K_a ($\Delta G^\circ_b = -RT \ln K_a$) and the entropic term, $T\Delta S^\circ_b$, was derived from the Gibbs−Helmholtz equation using the experimental ΔH°_b value ($\Delta G^\circ_b = \Delta H^\circ_b - T\Delta S^\circ_b$).

4.7. X-ray Crystallography with VIM-2. VIM-2 β-lactamase was expressed and purified following established protocols.[61,66] Crystals of the enzyme were obtained using the sitting-drop vapor diffusion method[67] at room temperature as described elsewhere.[61,66,68] The complex with compound **8** was obtained by the soaking technique,[67] by adding 1 μL of compound solution (5 mM, solubilized in a 1:9 molar ratio DMSO/PEG400 mixture), in the crystallization drop. Crystals were flash-frozen in liquid nitrogen after 15 min exposure. Diffraction data were collected at 100 K using synchrotron radiation at the Diamond Light Source (DLS, Oxfordshire, U.K.) beamline I04, equipped with an Eiger2 XE 16M detector. Reflections were integrated using XDS[69] and scaled with Scala[70] from the CCP4 suite.[71] The structure was solved by the molecular replacement technique as implemented in MOLREP[72] and the structure of VIM-2 (PDB code 7OVF[37]) was used as search model (excluding nonprotein atoms and solvent molecules). The model was refined using REFMAC5[73] from the CCP4 suite. The molecular graphic software Coot[74] was used for visual inspection and manual rebuilding of missing atoms in the protein model. The inspection of the Fourier difference map clearly evidenced the presence of **8** inside the catalytic cavity of the enzyme that was modeled accordingly. The occupancy of zinc ions and exogenous ligands (inhibitor and acetate anions) was adjusted and refined to values resulting in atomic displacement parameters close to those of neighboring protein atoms in fully occupied sites. The final model was manually inspected and validated with Coot and Procheck.[75] Structural figures were generated using the molecular graphic software CCP4mg.[76] Data collection, processing, and model refinement statistics are summarized in Table S1 in the Supporting Information. Final coordinates and structure factors for the VIM-2/**8** complex were deposited in the Protein Data Bank (https://www.rcsb.org/) under the code 8A4M.

4.8. X-ray Crystallography with NDM-1. *4.8.1. NDM-1 Production, Purification, and Crystallization in Complex with Inhibitors.* NDM-1 protein without signal peptide (28−270, UniProtKB C7C422) was recombinantly produced and purified as previously described.[77] For crystallization purposes, a final size exclusion chromatography purification step has been introduced (Superdex 75 26/60, Cytiva, in 20 mM HEPES, 100 mM NaCl, pH 7.0).

Purified NDM-1 was concentrated to 60 mg/mL and submitted to sitting-drop isothermal vapor diffusion crystallization at 293 K; 1.2 μL drops were incubated by mixing an equal volume of protein and precipitant buffer (0.1 M HEPES, 0.1 M Mops, pH 7.5, 0.03 M $MgCl_2 \cdot 6H_2O$, 0.03 M $CaCl_2 \cdot 2H_2O$, 12.5% v/v MPD, 12.5% PEG 1000, 12.5% w/v PEG 3350) and optimized by microseeding.

NDM-1 crystals were soaked for 24−72 h in 5 mM solutions of inhibitors **8** (JMV7061) and **26** (JMV7475), dissolved in 0.1 M HEPES, 0.1 M Mops, pH 7.5, 0.05 M NaCl, 5% v/v DMSO, 12.5% v/v MPD, 12.5% PEG 1000, 12.5% w/v PEG 3350. Crystals were cryo-protected adding 20% v/v ethylene glycol to the precipitant solution before freezing in liquid nitrogen.

4.8.2. Structure Building and Refinement. X-ray diffraction data were collected at the European Synchrotron Radiation Facility (ESRF, Grenoble, France) and analyzed by the available automated processing pipelines for space group determination and reflection indexing. Data reduction was performed by Aimless (CCP4i2 interface[70]). Molecular replacement was carried out by Molrep, using PDB 6TGD as a template. Initial model has been adjusted both by manual and automated structure refinement, the latter carried out either by Refmac5 or Refine software (CCP4i2 and Phenix interface[73,78]). The presence of metal ions has been verified by anomalous maps. Two strong peaks in the catalytic pocket at values higher than 20 sigma were evidenced in the maps of the complex between NDM-1 and **26**, confirming the presence of the two catalytic and highly conserved Zn atoms in both chains of the asymmetric unit (a.s.u.). Satellite weaker peaks were observed in correspondence to side sites, previously characterized as calcium sites[77] and most likely due to crystallization conditions. On the contrary, no significant peaks were identified in the maps of NDM-1 crystals treated with **8**, as a consequence of metal stripping by the compound.

Compound **26** was detected by difference maps, and its stereochemical description was built by AceDRG.[79] No ligand was detectable in the maps of NDM-1 complexes incubated with compound **8**, in agreement with the metal chelating activity of the latter.

■ ASSOCIATED CONTENT

Supporting Information

The Supporting Information is available free of charge at https://pubs.acs.org/doi/10.1021/acs.jmedchem.2c01257.

General synthesis of hydrazide compounds; production of VIM-2 and NDM-1 and their native MS analysis in the absence and presence of compounds **8**, **26**, and **30** (Figures S1−S5); ITC data (Figures S6 and S7); assays for determination of ADME parameters; inhibition assays for human metalloenzymes; data collection and refinement statistics for VIM-2/**8** and NDM-1/**26** complexes (Table S1); superimposition of VIM-2/**8** structure with VIM-2/hydrolyzed faropenem and VIM-2/hydrolyzed biapenem (Figure S8); NDM-1 3D structures after treatment with compounds **8** and **26** (Figure S9); and ^1H and ^{13}C NMR spectra for all compounds and representative RP-HPLC traces (PDF)

https://doi.org/10.1021/acs.jmedchem.2c01257
J. Med. Chem. XXXX, XXX, XXX−XXX

Molecular formula string (CSV)

Accession Codes

PDB code for VIM-2 bound to compound **8** is 8A4M. PDB code for NDM-1 bound to compound **26** is 8A76. The authors will release the atomic coordinates and experimental data upon article publication.

AUTHOR INFORMATION

Corresponding Authors

Jean-François Hernandez − *IBMM, CNRS, Univ Montpellier, ENSCM, 34000 Montpellier, France*; Email: jean-francois.hernandez@umontpellier.fr

Laurent Gavara − *IBMM, CNRS, Univ Montpellier, ENSCM, 34000 Montpellier, France*; Email: laurent.gavara@umontpellier.fr

Jean-Denis Docquier − *Dipartimento di Biotecnologie Mediche, Università di Siena, 53100 Siena, Italy; Centre d'Ingénierie des Protéines-InBioS, Université de Liège, B-4000 Liège, Belgium*; orcid.org/0000-0001-9483-4476; Email: jddocquier@unisi.it

Authors

Alice Legru − *IBMM, CNRS, Univ Montpellier, ENSCM, 34000 Montpellier, France*

Federica Verdirosa − *Dipartimento di Biotecnologie Mediche, Università di Siena, 53100 Siena, Italy*; orcid.org/0000-0003-3560-9361

Yen Vo-Hoang − *IBMM, CNRS, Univ Montpellier, ENSCM, 34000 Montpellier, France*

Giusy Tassone − *Dipartimento di Biotecnologie, Chimica e Farmacia, Università di Siena, 53100 Siena, Italy*; orcid.org/0000-0002-2575-5528

Filippo Vascon − *Laboratory of Structural Biology, Department of Biology, University of Padua, 35121 Padova, Italy*

Caitlyn A. Thomas − *Department of Chemistry and Biochemistry, Miami University, Oxford, Ohio 45056, United States*

Filomena Sannio − *Dipartimento di Biotecnologie Mediche, Università di Siena, 53100 Siena, Italy*; orcid.org/0000-0003-3001-8159

Giuseppina Corsica − *Dipartimento di Biotecnologie Mediche, Università di Siena, 53100 Siena, Italy*

Manuela Benvenuti − *Dipartimento di Biotecnologie, Chimica e Farmacia, Università di Siena, 53100 Siena, Italy*; orcid.org/0000-0003-0709-2537

Georges Feller − *Laboratoire de Biochimie, Centre d'Ingénierie des Protéines-InBioS, Université de Liège, B-4000 Liège, Belgium*

Rémi Coulon − *IBMM, CNRS, Univ Montpellier, ENSCM, 34000 Montpellier, France*

Francesca Marcoccia − *Dipartimento di Biotecnologie Mediche, Università di Siena, 53100 Siena, Italy*

Savannah Rowane Devente − *Dipartimento di Biotecnologie Mediche, Università di Siena, 53100 Siena, Italy*

Ezeddine Bouajila − *IBMM, CNRS, Univ Montpellier, ENSCM, 34000 Montpellier, France*

Catherine Piveteau − *Drugs and Molecules for Living System, U1177, Inserm, Université de Lille, Faculté de Pharmacie, 59006 Lille, France*

Florence Leroux − *Drugs and Molecules for Living System, U1177, Inserm, Université de Lille, Faculté de Pharmacie, 59006 Lille, France*

Rebecca Deprez-Poulain − *Drugs and Molecules for Living System, U1177, Inserm, Université de Lille, Faculté de Pharmacie, 59006 Lille, France*; orcid.org/0000-0002-3318-5297

Benoît Deprez − *Drugs and Molecules for Living System, U1177, Inserm, Université de Lille, Faculté de Pharmacie, 59006 Lille, France*

Patricia Licznar-Fajardo − *HydroSciences Montpellier, UMR5151, Univ Montpellier, CNRS, IRD, CHU Montpellier, 34000 Montpellier, France*

Michael W. Crowder − *Department of Chemistry and Biochemistry, Miami University, Oxford, Ohio 45056, United States*; orcid.org/0000-0002-3138-0283

Laura Cendron − *Laboratory of Structural Biology, Department of Biology, University of Padua, 35121 Padova, Italy*

Cecilia Pozzi − *Dipartimento di Biotecnologie, Chimica e Farmacia, Università di Siena, 53100 Siena, Italy*; orcid.org/0000-0003-2574-3911

Stefano Mangani − *Dipartimento di Biotecnologie, Chimica e Farmacia, Università di Siena, 53100 Siena, Italy*; orcid.org/0000-0003-4824-7478

Complete contact information is available at: https://pubs.acs.org/10.1021/acs.jmedchem.2c01257

Author Contributions

[¶]A.L. and F.V. contributed equally.

Author Contributions

[#]J.-F.H., J.-D.D., and L.G. are co-last authors.

Notes

The authors declare no competing financial interest.

ACKNOWLEDGMENTS

Part of this work was supported by *SATT AxLR* (RESIST—655, 19/0162). The authors thank Pierre Sanchez for mass spectrometry analyses; Sandrine Warenghem and Alexandre Biela for performing the selectivity profile and the ADME study, respectively, on the ARIADNE platforms of the French national infrastructure ChemBioFrance; and Diamond Light Source for providing us beamtime (BAG proposal MX21741) and the staff of beamline I04 for their assistance with crystal testing and data collection. The authors are grateful to the European Synchrotron Radiation Facility (ESRF, Grenoble, France) and its staff for providing them beamtime and assistance in using beamline ID23−1 (proposal MX-2363). The Dipartimento di Biotecnologie Mediche and the Dipartimento di Biotecnologie, Chimica e Farmacia, University of Siena, were both awarded "Department of Excellence 2018−2022" by the Italian Ministry of Education, University and Research (MIUR, L. 232/2016).

DEDICATION

This paper is dedicated to the memory of Dr. Otto Dideberg who passed away on March 2, 2022. Otto worked as a crystallographer at the Institut de Biologie Structurale (Grenoble, France) and he was a pioneer in the resolution of crystallographic structures of MBLs (see Carfi A. et al. *EMBO J.* **1995**, 14, 4914−4921). Our work on 1,2,4-triazole-3-thiones as MBL inhibitors was initiated after his group identified the original binding mode of these compounds to a dizinc MBL (see ref 31).

https://doi.org/10.1021/acs.jmedchem.2c01257
J. Med. Chem. XXXX, XXX, XXX−XXX

■ ABBREVIATIONS USED

ADME, absorption, distribution, metabolism, excretion; AMR, antimicrobial resistance; Boc, *tert*-butyloxycarbonyl; CFU, colony-forming unit; CLSI, Clinical and Laboratory Standards Institute; DMF, dimethylformamide; DMSO, dimethylsulfoxide; DPT, di(2-pyridyl) thionocarbonate; ESBL, extended-spectrum β-lactamase; HEPES, 4-(2-hydroxyethyl)-1-piperazine-ethanesulfonic acid; HeLa, tumoral cells from Henrietta Lacks; Im, imidazole; IMP, imipenemase; ITC, isothermal calorimetry; KPC, *Klebsiella pneumoniae* Carbapenemase; LC-MS, liquid chromatography coupled to mass spectrometry; LDH, lactate dehydrogenase; MBL, metallo-β-lactamase; MDR, multidrug resistant; MEM, meropenem; MIC, minimum inhibitory concentration; Mops, 4-Morpholinopropane sulfonate; NDM, New Delhi metallo-β-lactamase; OXA, oxacillinase; PDB, Protein Data Bank; Pyr, pyridine; RP-HPLC, reversed-phase High-Pressure Liquid Chromatography; SBL, serine-β-lactamase; TCEP, tris (2-carboxyethyl) phosphine; TFA, trifluoroacetic acid; VIM, Verona integron-borne metallo-β-lactamase; WHO, World Health Organization; XDR, extremely drug resistant

■ REFERENCES

(1) Venter, H. Reversing resistance to counter antimicrobial resistance in the World Health Organisation's critical priority of most dangerous pathogens. *Biosci. Rep.* **2019**, *39*, No. BSR20180474.

(2) O'Neill, J. Review on antimicrobial resistance. Tackling drug-resistant infections globally: Final report and recommendations. May 2016 https://amr-review.org.

(3) Cassini, A.; Högberg, L. D.; Plachouras, D.; Quattrocchi, A.; Hoxha, A.; Simonsen, G. S.; Colomb-Cotinat, M.; Kretzschmar, M.; Devleesschauwer, B.; Cecchini, M.; Ouakrim, D. A.; Oliveira, T. C.; Struelens, M. J.; Suetens, C.; Monnet, D. L.; Burden of AMR Collaborative Group. Attributable deaths and disability-adjusted life-years caused by infections with antibiotic-resistant bacteria in the EU and the European Economic Area in 2015: a population-level modelling analysis. *Lancet Infect. Dis.* **2019**, *19*, 56−66.

(4) Teillant, A.; Gandra, S.; Barter, D.; Morgan, D. J.; Laxminarayan, R. Potential burden of antibiotic resistance on surgery and cancer chemotherapy antibiotic prophylaxis in the USA: a literature review and modelling study. *Lancet Infect. Dis.* **2015**, *15*, 1429−1437.

(5) Nordmann, P.; Naas, T.; Poirel, L. Global spread of carbapenemase-producing *Enterobacteriaceae*. *Emerg. Infect. Dis.* **2011**, *17*, 1791−1798.

(6) Walsh, T. R.; Toleman, M. A. The emergence of pan-resistant Gram-negative pathogens merits a rapid global political response. *J. Antimicrob. Chemother.* **2012**, *67*, 1−3.

(7) World Health Organization. Global priority list of antibiotic-resistant bacteria to guide research, discovery and development of new antibiotics. 27 February 2017.

(8) Exner, M.; Bhattacharya, S.; Christiansen, B.; Gebel, J.; Goroncy-Bermes, P.; Hartemann, P.; Heeg, P.; Ilschner, C.; Kramer, A.; Larson, E.; Merkens, W.; Mielke, M.; Oltmanns, P.; Ross, B.; Rotter, M.; Schmithausen, R. M.; Sonntag, H.-G.; Trautmann, M. Antibiotic resistance: What is so special about multidrug-resistant Gram-negative bacteria? *GMS Hyg. Infect. Control.* **2017**, *12*, No. Doc05.

(9) Fernandes, R.; Amador, P.; Prudêncio, C. β-Lactams: chemical structure, mode of action and mechanisms of resistance. *Rev. Med. Microbiol.* **2013**, *24*, 7−17.

(10) Bush, K. The ABCD's of β-lactamase nomenclature. *J. Infect. Chemother.* **2013**, *19*, 549−559.

(11) Bush, K. Past and present perspectives on β-lactamases. *Antimicrob. Agents Chemother.* **2018**, *62*, No. e01076-18.

(12) Salahuddin, P.; Kumar, A.; Khan, A. U. Structure, function of serine and metallo-β-lactamases and their inhibitors. *Curr. Protein Pept. Sci.* **2017**, *19*, 130−144.

(13) Tehrani, K. H. M. E.; Martin, N. I. β-Lactam/β-lactamase inhibitor combinations: an update. *Med. Chem. Commun.* **2018**, *9*, 1439−1456.

(14) Docquier, J.-D.; Mangani, S. An update on β-lactamase inhibitor discovery and development. *Drug Resist. Updates* **2018**, *36*, 13−29.

(15) Bush, K.; Bradford, P. A. Interplay between β-lactamases and new β-lactamase inhibitors. *Nat. Rev. Microbiol.* **2019**, *17*, 295−306.

(16) Bahr, G.; Gonzalez, L. J.; Vila, A. J. Metallo-β-lactamases in the age of multidrug resistance: from structure and mechanism to evolution, dissemination, and inhibitor design. *Chem. Rev.* **2021**, *121*, 7957−8094.

(17) Naas, T.; Oueslati, S.; Bonnin, R. A.; Dabos, M. L.; Zavala, A.; Dortet, L.; Retailleau, P.; Iorga, B. I. Beta-lactamase database (BLDB) - structure and function. *J. Enzyme Inhib. Med. Chem.* **2017**, *32*, 917−919.

(18) Boyd, S. E.; Livermore, D. M.; Hooper, D. C.; Hope, W. W. Metallo-β-lactamases: structure, function, epidemiology, treatment options, and the development pipeline. *Antimicrob. Agents Chemother.* **2020**, *64*, No. e00397-20.

(19) Linciano, P.; Cendron, L.; Gianquinto, E.; Spyrakis, F.; Tondi, D. Ten years with New Delhi Metallo-β-lactamase-1 (NDM-1): From structural insights to inhibitor design. *ACS Infect. Dis.* **2019**, *5*, 9−34.

(20) Stewart, A. C.; Bethel, C. R.; VanPelt, J.; Bergstrom, A.; Cheng, Z.; Miller, C. G.; Williams, C.; Poth, R.; Morris, M.; Lahey, O.; Nix, J. C.; Tierney, D. L.; Page, R. C.; Crowder, M. W.; Bonomo, R. A.; Fast, W. Clinical variants of New Delhi Metallo-β-Lactamase are evolving to overcome zinc scarcity. *ACS Infect. Dis.* **2017**, *3*, 927−940.

(21) Cheng, Z.; Thomas, P. W.; Ju, L.; Bergstrom, A.; Mason, K.; Clayton, D.; Miller, C.; Bethel, C. R.; VanPelt, J.; Tierney, D. L.; Page, R. C.; Bonomo, R. A.; Fast, W.; Crowder, M. W. Evolution of New Delhi Metallo-β-Lactamase (NDM) in the clinic: effects of NDM mutations on stability, zinc affinity, and mono-zinc activity. *J. Biol. Chem.* **2018**, *293*, 12606−12618.

(22) Bahr, G.; Gonzalez, L. J.; Vila, A. J. Metallo-β-lactamases and a tug-of-war for the available zinc at the host-pathogen interface. *Curr. Opin. Chem. Biol.* **2022**, *66*, No. 102103.

(23) Mojica, M. F.; Rossi, M.-A.; Vila, A. J.; Bonomo, R. A. The urgent need for metallo-β-lactamase inhibitors: an unattended global threat. *Lancet Infect. Dis.* **2022**, *22*, e28−e34.

(24) Krajnc, A.; Lang, P. A.; Panduwawala, T. D.; Brem, J.; Schofield, C. J. Will morphing boron-based inhibitors beat the β-lactamases? *Curr. Opin. Chem. Biol.* **2019**, *50*, 101−110.

(25) Chen, C.; Oelschlaeger, P.; Wang, D.; Xu, H.; Wang, Q.; Wang, C.; Zhao, A.; Yang, K. W. Structure and mechanism-guided design of dual serine/metallo-carbapenemase inhibitors. *J. Med. Chem.* **2022**, *65*, 5954−5974.

(26) Burns, C. J.; Daigle, D.; Liu, B.; McGarry, D.; Pevear, D. C.; Trout, R. E. β-Lactamase inhibitors. WO2014/089365A1.

(27) Liu, B.; Trout, R. E. L.; Chu, G. H.; McGarry, D.; Jackson, R. W.; Hamrick, J. C.; Daigle, D. M.; Cusick, S. M.; Pozzi, C.; De Luca, F.; Benvenuti, M.; Mangani, S.; Docquier, J.-D.; Weis, W. J.; Pevear, D. C.; Xerri, L.; Burns, C. J. Discovery of Taniborbactam (VNRX-5133): a broad spectrum serine- and metallo-β-lactamase inhibitor for carbapenem-resistant bacterial infections. *J. Med. Chem.* **2020**, *63*, 2789−2801.

(28) Hecker, S. J.; Reddy, K. R.; Lomovskaya, O.; Griffith, D. C.; Rubio-Aparicio, D.; Nelson, K.; Tsivkovski, R.; Sun, D.; Sabet, M.; Tarazi, Z.; Parkinson, J.; Totrov, M.; Boyer, S. H.; Glinka, T. W.; Pemberton, O. A.; Chen, Y.; Dudley, M. N. Discovery of cyclic boronic acid QPX7728, an ultrabroad- spectrum inhibitor of serine and metallo-β-lactamases. *J. Med. Chem.* **2020**, *63*, 7491−7507.

(29) Davies, D. T.; Leiris, S.; Sprynski, N.; Castandet, J.; Lozano, C.; Bousquet, J.; Zalacain, M.; Vasa, S.; Dasari, P. K.; Pattipati, R.; Vempala, N.; Gujjewar, S.; Godi, S.; Jallala, R.; Sathyap, R. R.; Darshanoju, N. A.; Ravu, V. R.; Juventhala, R. R.; Pottabathini, N.; Sharma, S.; Pothukanuri, S.; Holden, K.; Warn, P.; Marcoccia, F.; Benvenuti, M.; Pozzi, C.; Mangani, S.; Docquier, J.-D.; Lemonnier, M.; Everett, M. ANT2681: SAR studies leading to the identification of

https://doi.org/10.1021/acs.jmedchem.2c01257
J. Med. Chem. XXXX, XXX, XXX−XXX

a metallo-lactamase inhibitor with potential for clinical use in combination with meropenem for the treatment of infections caused by NDM-producing *Enterobacteriaceae*. *ACS Infect. Dis.* **2020**, *6*, 2419−2430.
(30) Olsen, L.; Jost, S.; Adolph, H. W.; Pettersson, I.; Hemmingsen, L.; Jørgensen, F. S. New leads of metallo-β-lactamase inhibitors from structure-based pharmacophore design. *Bioorg. Med. Chem.* **2006**, *14*, 2627−2635.
(31) Nauton, L.; Kahn, R.; Garau, G.; Hernandez, J.-F.; Dideberg, O. Structural insights into the design of inhibitiors of the L1 metallo-β-lactamase from *Stenotrophomonas maltophilia*. *J. Mol. Biol.* **2008**, *375*, 257−269.
(32) Vella, P.; Hussein, W. M.; Leung, E. W.; Clayton, D.; Ollis, D. L.; Mitić, N.; Schenk, G.; McGeary, R. P. The identification of new metallo-β-lactamase inhibitor leads from fragment-based screening. *Bioorg. Med. Chem. Lett.* **2011**, *21*, 3282−3285.
(33) Christopeit, T.; Carlsen, T. J.; Helland, R.; Leiros, H. K. Discovery of novel inhibitor scaffolds against the metallo-β-lactamase VIM-2 by surface plasmon resonance (SPR) based fragment screening. *J. Med. Chem.* **2015**, *58*, 8671−8682.
(34) Spyrakis, F.; Celenza, G.; Marcoccia, F.; Santucci, M.; Cross, S.; Bellio, P.; Cendron, L.; Perilli, M.; Tondi, D. Structure-based virtual screening for the discovery of novel inhibitors of New Delhi Metallo-β-lactamase-1. *ACS Med. Chem. Lett.* **2018**, *9*, 45−50.
(35) Gavara, L.; Sevaille, L.; De Luca, F.; Mercuri, P.; Bebrone, C.; Feller, G.; Legru, A.; Cerboni, G.; Tanfoni, S.; Baud, D.; Cutolo, G.; Bestgen, B.; Chelini, G.; Verdirosa, F.; Sannio, F.; Pozzi, C.; Benvenuti, M.; Kwapien, K.; Fischer, M.; Becker, K.; Frère, J.-M.; Mangani, S.; Gresh, N.; Berthomieu, D.; Galleni, M.; Docquier, J.-D.; Hernandez, J.-F. 4-Amino-1,2,4-triazole-3-thione-derived Schiff bases as metallo-β-lactamase inhibitors. *Eur. J. Med. Chem.* **2020**, *208*, No. 112720.
(36) Spyrakis, F.; Santucci, M.; Maso, L.; Cross, S.; Gianquinto, E.; Sannio, F.; Verdirosa, F.; De Luca, F.; Docquier, J.-D.; Cendron, L.; Tondi, D.; Venturelli, A.; Cruciani, G.; Costi, M. P. Virtual screening identifies broad-spectrum β-lactamase inhibitors with activity on clinically relevant serine- and metallo-carbapenemases. *Sci. Rep.* **2020**, *10*, No. 12763.
(37) Legru, A.; Verdirosa, F.; Hernandez, J.-F.; Tassone, G.; Sannio, F.; Benvenuti, M.; Conde, P.-A.; Bossis, G.; Thomas, C. A.; Crowder, M. W.; Dillenberger, M.; Becker, K.; Pozzi, C.; Mangani, S.; Docquier, J.-D.; Gavara, L. 1,2,4-Triazole-3-thione compounds with a 4-ethyl alkyl/aryl sulfide substituent are broad-spectrum metallo-β-lactamase inhibitors with re-sensitization activity. *Eur. J. Med. Chem.* **2021**, *226*, No. 113873.
(38) Verdirosa, F.; Gavara, L.; Sevaille, L.; Tassone, G.; Corsica, G.; Legru, A.; Feller, G.; Chelini, G.; Mercuri, P. S.; Tanfoni, S.; Sannio, F.; Benvenuti, M.; Cerboni, G.; De Luca, F.; Bouajila, E.; Vo Hoang, Y.; Licznar-Fajardo, P.; Galleni, M.; Pozzi, C.; Mangani, S.; Docquier, J.-D.; Hernandez, J.-F. 1,2,4-Triazole-3-thione analogues with a 2-ethylbenzoic acid at position 4 as VIM-type metallo-β-lactamase inhibitors. *ChemMedChem* **2022**, *17*, No. e202100699.
(39) Sevaille, L.; Gavara, L.; Bebrone, C.; De Luca, F.; Nauton, L.; Achard, M.; Mercuri, P. S.; Tanfoni, S.; Borgianni, L.; Guyon, C.; Lonjon, P.; Turan-Zitouni, G.; Dzieciolowski, J.; Becker, K.; Bénard, L.; Condon, C.; Maillard, L.; Martinez, J.; Frère, J.-M.; Dideberg, O.; Galleni, M.; Docquier, J.-D.; Hernandez, J.-F. 1,2,4-Triazole-3-thione compounds as inhibitors of dizinc metallo-β-lactamase. *ChemMedChem* **2017**, *12*, 972−985.
(40) Gavara, L.; Verdirosa, F.; Legru, A.; Mercuri, P. S.; Nauton, L.; Sevaille, L.; Feller, G.; Berthomieu, D.; Sannio, F.; Marcoccia, F.; Tanfoni, S.; De Luca, F.; Gresh, N.; Galleni, M.; Docquier, J.-D.; Hernandez, J.-F. 4-(*N*-Alkyl- and -acyl-amino)-1,2,4-triazole-3-thione analogs as metallo-β-lactamase inhibitors: impact of 4-linker on potency and spectrum of inhibition. *Biomolecules* **2020**, *10*, 1094.
(41) Gavara, L.; Legru, A.; Verdirosa, F.; Sevaille, L.; Nauton, L.; Corsica, G.; Mercuri, P. S.; Sannio, F.; Feller, G.; Coulon, R.; De Luca, F.; Cerboni, G.; Tanfoni, S.; Chelini, G.; Galleni, M.; Docquier, J.-D.; Hernandez, J.-F. 4-Alkyl-1,2,4-triazole-3-thione analogues as metallo-β-lactamase inhibitors. *Bioorg Chem.* **2021**, *113*, No. 105024.
(42) Gavara, L.; Verdirosa, F.; Sevaille, L.; Legru, A.; Corsica, G.; Nauton, L.; Mercuri, P. S.; Sannio, F.; De Luca, F.; Hadjadj, M.; Cerboni, G.; Vo Hoang, Y.; Licznar-Fajardo, P.; Galleni, M.; Docquier, J.-D.; Hernandez, J.-F. 1,2,4-Triazole-3-thione analogues with an arylakyl group at position 4 as metallo-β-lactamase inhibitors. *Bioorg. Med. Chem.* **2022**, *72*, No. 116964.
(43) Deprez-Poulain, R. F.; Charton, J.; Leroux, V.; Deprez, B. P. Convenient synthesis of 4*H*-1,2,4-triazole-3-thiols using di-2-pyridylthionocarbonate. *Tetrahedron Lett.* **2007**, *48*, 8157−8162.
(44) Hernandez, J.-F.; Gavara, L.; Docquier, J.-D.; Sevaille, L.; Legru, A. Inhibitors of Metallo-β-Lactamases. WO2020/099645.
(45) Baran, P.; Richter, J. Essentials of Heterocyclic Chemistry-I. https://www.scripps.edu/baran/heterocycles/Essentials1-2009.pdf.
(46) Gasque, L.; Lopez-Rosales, A.; Bernès, S.; Mendoza-Diaz, G. Bioinspired Co(II) and Zn(II) complexes with an imidazole derived tripodal ligand. Structural models for astacins and MnSOD. *Polyhedron* **2017**, *127*, 167−175.
(47) Hevroni, B. L.; Jantz, T.; Gottlieb, H. E.; Fischer, B. (Aminomethylene)phosphonate analogues as Zn^{II} chelators: synthesis and characterization. *Eur. J. Inorg. Chem.* **2017**, *2017*, 2955−2967.
(48) Azumah, R.; Dutta, J.; Somboro, A. M.; Ramtahal, M.; Chonco, L.; Parboosing, R.; Bester, L. A.; Kruger, H. G.; Naicker, T.; Essack, S. Y.; Govender, T. *In vitro* evaluation of metal chelators as potential metallo-β-lactamase inhibitors. *J. Appl. Microbiol.* **2016**, *120*, 860−867.
(49) Kildahl-Andersen, G.; Schnaars, C.; Prandina, A.; Radix, S.; Le Borgne, M.; Jordheim, L. P.; Gjøen, T.; Andresen, A. M. S.; Lauksund, S.; Fröhlich, C.; Samuelsen, Ø.; Rongved, P.; Åstrand, O. A. H. Synthesis and biological evaluation of zinc chelating compounds as metallo-β-lactamase inhibitors. *MedChemComm* **2019**, *10*, 528−537.
(50) Chen, F.; Bai, M.; Liu, W.; Kong, H.; Zhang, T.; Yao, H.; Zhang, E.; Du, J.; Qin, S. H_2dpa derivatives containing pentadentate ligands: An acyclic adjuvant potentiates meropenem activity *in vitro* and *in vivo* against metallo-β-lactamase-producing Enterobacterales. *Eur. J. Med. Chem.* **2021**, *224*, No. 113702.
(51) Jin, W. B.; Xu, C.; Qi, X. L.; Zeng, P.; Gao, W.; Lai, K. H.; Chiou, J.; Chan, E. W. C.; Leung, Y.-C.; Chan, T. H.; Wong, K.-Y.; Chen, S.; Chan, K.-F. Synthesis of 1,3,4-trisubstituted pyrrolidines as meropenem adjuvants targeting New Delhi metallo-β-lactamase. *New J. Chem.* **2021**, *45*, 3515−3534.
(52) Chen, A. Y.; Thomas, P. W.; Stewart, A. C.; Bergstrom, A.; Cheng, Z.; Miller, C.; Bethel, C. R.; Marshall, S. H.; Credille, C. V.; Riley, C. L.; Page, R. C.; Bonomo, R. A.; Crowder, M. W.; Tierney, D. L.; Fast, W.; Cohen, S. M. Dipicolinic acid derivatives as inhibitors of New Delhi Metallo-β-lactamase-1. *J. Med. Chem.* **2017**, *60*, 7267−7283.
(53) Thomas, C. A.; Cheng, Z.; Yang, K.; Hellwarth, E.; Yurkiewicz, C. J.; Baxter, F. M.; Fullington, S. A.; Klinsky, S. A.; Otto, J. L.; Chen, A. Y.; Cohen, S. M.; Crowder, M. W. Probing the mechanisms of inhibition for various inhibitors of metallo-β-lactamases VIM-2 and NDM-1. *J. Inorg. Biochem.* **2020**, *210*, No. 111123.
(54) Chen, A. Y.; Thomas, P. W.; Cheng, Z.; Xu, N. Y.; Tierney, D. L.; Crowder, M. W.; Fast, W.; Cohen, S. M. Investigation of dipicolinic acid isosteres for the inhibition of metallo-β-lactamases. *ChemMedChem* **2019**, *14*, 1271−1282.
(55) Yamaguchi, Y.; Jin, W.; Matsunaga, K.; Ikemizu, S.; Yamagata, Y.; Wachino, J.; Shibata, N.; Arakawa, Y.; Kurosaki, H. Crystallographic investigation of the inhibition mode of a VIM-2 metallo-β-lactamase from *Pseudomonas aeruginosa* by a mercaptocarboxylate inhibitor. *J. Med. Chem.* **2007**, *50*, 6647−6653.
(56) Lucic, A.; Hinchliffe, P.; Malla, T. R.; Tooke, C. L.; Brem, J.; Calvopiña, K.; Lohans, C. T.; Rabe, P.; McDonough, M. A.; Armistead, T.; Orville, A. M.; Spencer, J.; Schofield, C. J. Faropenem reacts with serine and metallo-β-lactamases to give multiple products. *Eur. J. Med. Chem.* **2021**, *215*, No. 113257.
(57) Lucic, A.; Malla, T. R.; Calvopiña, K.; Tooke, C. L.; Brem, J.; McDonough, M. A.; Spencer, J.; Schofield, C. J. Studies on the

https://doi.org/10.1021/acs.jmedchem.2c01257
J. Med. Chem. XXXX, XXX, XXX−XXX

reactions of biapenem with VIM metallo β-lactamases and the serine β-lactamase KPC-2. *Antibiotics* **2022**, *11*, 396.
(58) Kim, Y.; Tesar, C.; Mire, J.; Jedrzejczak, R.; Binkowski, A.; Babnigg, G.; Sacchettini, J.; Joachimiak, A. Structure of apo- and monometalated forms of NDM-1, a highly potent carbapenem-hydrolyzing metallo-β-lactamase. *PLoS One* **2011**, *6*, No. e24621.
(59) Hammer-Dedet, F.; Jumas-Bilak, E.; Licznar-Fajardo, P. The hydric environment: A hub for clinically relevant carbapenemase encoding genes. *Antibiotics* **2020**, *9*, 699.
(60) Cheng, Z.; Bethel, C. R.; Thomas, P. W.; Shurina, B. A.; Alao, J. P.; Thomas, C. A.; Yang, K.; Marshall, S. H.; Zhang, H.; Sturgill, A. M.; Kravats, A. N.; Page, R. C.; Fast, W.; Bonomo, R. A.; Crowder, M. W. Carbapenem use is driving the evolution of imipenemase 1 variants. *Antimicrob. Agents Chemother.* **2021**, *65*, No. e01714-20.
(61) Docquier, J.-D.; Lamotte-Brasseur, J.; Galleni, M.; Amicosante, G.; Frère, J.-M.; Rossolini, G. M. On functional and structural heterogeneity of VIM-type metallo-β-lactamases. *J. Antimicrob. Chemother.* **2003**, *51*, 257−266.
(62) Clinical Laboratory Standard Institute. Methods for dilution antimicrobial susceptibility tests for bacteria that grow aerobically, Document M07-A10, 2015, Twelfth ed. Wayne, PA, USA.
(63) European Comittee for Antimicrobial Susceptibility Testing (EUCAST) of the ESCMID. Terminology relating to methods for the determination of susceptibility of bacteria to antimicrobial agents. *Clin. Microbiol. Infect.* **2000**, *6*, 503−508.
(64) Hall, M. J.; Middleton, R. F.; Westmacott, D. The fractional inhibitory concentration (FIC) index as a measure of synergy. *J. Antimicrob. Chemother.* **1983**, *11*, 427−433.
(65) Smith, J. C., Jr.; Butrimovitz, G. P.; Purdy, W. C. Direct measurement of zinc in plasma by atomic absorption spectroscopy. *Clin. Chem.* **1979**, *25*, 1487−1491.
(66) Garcia-Saez, I.; Docquier, J.-D.; Rossolini, G. M.; Dideberg, O. The three-dimensional structure of VIM-2, a Zn-β-lactamase from *Pseudomonas aeruginosa* in its reduced and oxidised form. *J. Mol. Biol.* **2008**, *375*, 604−611.
(67) Benvenuti, M.; Mangani, S. Crystallization of soluble proteins in vapor diffusion for X-ray crystallography. *Nat. Protoc.* **2007**, *2*, 1633−1651.
(68) Leiris, S.; Coelho, A.; Castandet, J.; Bayet, M.; Lozano, C.; Bougnon, J.; Bousquet, J.; Everett, M.; Lemonnier, M.; Sprynski, N.; Zalacain, M.; Pallin, T. D.; Cramp, M. C.; Jennings, N.; Raphy, G.; Jones, M. W.; Pattipati, R.; Shankar, B.; Sivasubrahmanyam, R.; Soodhagani, A. K.; Juventhala, R. R.; Pottabathini, N.; Pothukanuri, S.; Benvenuti, M.; Pozzi, C.; Mangani, S.; De Luca, F.; Cerboni, G.; Docquier, J.-D.; Davies, D. T. SAR Studies leading to the identification of a novel series of metallo-β-lactamase inhibitors for the treatment of carbapenem-resistant *Enterobacteriaceae* infections that display efficacy in an animal infection model. *ACS Infect. Dis.* **2019**, *5*, 131−140.
(69) Kabsch, K. XDS. *Acta Crystallogr., Sect. D: Biol. Crystallogr.* **2010**, *66*, 125−132.
(70) Evans, P. R. An introduction to data reduction: space-group determination, scaling and intensity statistics. *Acta Crystallogr., Sect. D: Biol. Crystallogr.* **2011**, *67*, 282−292.
(71) Winn, M. D.; Ballard, C. C.; Cowtan, K. D.; Dodson, E. J.; Emsley, P.; Evans, P. R.; Keegan, R. M.; Krissinel, E. B.; Leslie, A. G.; McCoy, A.; McNicholas, S. J.; Murshudov, G. N.; Pannu, N. S.; Potterton, E. A.; Powell, H. R.; Read, R. J.; Vagin, A.; Wilson, K. S. Overview of the CCP4 suite and current developments. *Acta Crystallogr., Sect. D: Biol. Crystallogr.* **2011**, *67*, 235−242.
(72) Vagin, A.; Teplyakov, A. Molecular replacement with MOLREP. *Acta Crystallogr., Sect. D: Biol. Crystallogr.* **2010**, *66*, 22−25.
(73) Murshudov, G. N.; Skubák, P.; Lebedev, A. A.; Pannu, N. S.; Steiner, R. A.; Nicholls, R. A.; Winn, M. D.; Long, F.; Vagin, A. A. REFMAC5 for the refinement of macromolecular crystal structures. *Acta Crystallogr., Sect. D: Struct. Biol.* **2011**, *67*, 355−367.
(74) Emsley, P.; Lohkamp, B.; Scott, W. G.; Cowtan, K. Features and development of Coot. *Acta Crystallogr., Sect. D: Biol. Crystallogr.* **2010**, *66*, 486−501.
(75) Laskowski, R. A.; MacArthur, M. W.; Moss, D. S.; Thornton, J. M. PROCHECK: a program to check the stereochemical quality of protein structures. *J. Appl. Crystallogr.* **1993**, *26*, 283−291.
(76) McNicholas, S.; Potterton, E.; Wilson, K. S.; Noble, M. E. M. Presenting your structures: the CCP4mg molecular-graphics software. *Acta Crystallogr., Sect. D: Biol. Crystallogr.* **2011**, *67*, 386−394.
(77) Cendron, L.; Quotadamo, A.; Maso, L.; Bellio, P.; Montanari, M.; Celenza, G.; Venturelli, A.; Costi, M. P.; Tondi, D. X-ray Crystallography deciphers the activity of broad-spectrum boronic acid β-lactamase inhibitors. *ACS Med. Chem. Lett.* **2019**, *10*, 650−655.
(78) Afonine, P. V.; Grosse-Kunstleve, R. W.; Echols, N.; Headd, J. J.; Moriarty, N. W.; Mustyakimov, M.; Terwilliger, T. C.; Urzhumtsev, A.; Zwart, P. H.; Adams, P. D. Towards automated crystallographic structure refinement with phenix.refine. *Acta Crystallogr., Sect. D: Biol. Crystallogr.* **2012**, *68*, 352−367.
(79) Long, F.; Nicholls, R. A.; Emsley, P.; Graæulis, S.; Merkys, A.; Vaitkus, A.; Murshudov, G. N. AceDRG: a stereochemical description generator for ligands. *Acta Crystallogr., Sect. D: Struct. Biol.* **2017**, *73*, 112−122.

https://doi.org/10.1021/acs.jmedchem.2c01257
J. Med. Chem. XXXX, XXX, XXX−XXX